Engineered Biofilms for Materials Production and Patterning

Engineered biofilms for materials production and patterning

A dissertation presented
by

Yuyin Chen

to

The Committee on Higher Degrees in Biophysics

in partial fulfillment of the requirements
for the degree of
Doctor of Philosophy
in the subject of

Biophysics

Harvard University
Cambridge, Massachusetts

Feburary 10, 2016

Prof. Timothy K. Lu Yuyin Chen

Engineered biofilms for materials production and patterning

Abstract

Natural materials, such as bone, integrate living cells composed of organic molecules together with inorganic components. This enables combinations of functionalities, such as mechanical strength and the ability to regenerate and remodel, which are not present in existing synthetic materials. Taking a cue from nature, we propose that engineered 'living functional materials' and 'living materials synthesis platforms' that incorporate both living systems and inorganic components could transform the performance and the manufacturing of materials[1]. As a proof-of-concept, we recently demonstrated that synthetic gene circuits in *Escherichia coli* enabled biofilms to be both a functional material in its own right and a materials-synthesis platform. To demonstrate the former, we engineered *E. coli* biofilms into a chemical-inducer-responsive electrical switch. To demonstrate the latter, we engineered *E. coli* biofilms to dynamically organize biotic-abiotic materials across multiple length scales, template gold nanorods, gold nanowires, and metal/semiconductor heterostructures, and synthesize semiconductor nanoparticles[1]. Thus, tools from synthetic biology, such as those for artificial gene regulation, can be used to engineer the spatiotemporal characteristics of living systems and to interface living systems with inorganic materials. Such hybrids can possess novel properties enabled by living cells while retaining desirable

functionalities of inorganic systems. These systems, as living functional materials and as living materials foundries, would provide a radically different paradigm of materials performance and synthesis – materials possessing multifunctional, self-healing, adaptable, and evolvable properties that are created and organized in a distributed, bottom-up, autonomously assembled, and environmentally sustainable manner.

Table of contents

Acknowledgements

The process of putting together this thesis provided an opportunity to reflect on the period of intellectual and personal growth that I was lucky enough to experience over the past few years.

It was my tremendously good fortune to have joined Prof. Tim Lu's lab just as it was getting off the ground, and to have a PI who facilitated my growth both character-wise and intellectually. Working with Tim inculcated in me greater decisiveness and better ability to prioritize, which will serve me well in all aspects of life going forward. Working in Tim's lab has also shaped the way I think about biological questions; learning the engineer's approach of measurement + quantitative modeling as a way to understand has given me a powerful set of tools with which to dissect biological systems that I study in the future.

I am very grateful to my collaborators, labmates, and classmates for their camaraderie: Nicole Billings, Zhengtao Deng, Eleonore Tham, Michelle Lu, Rob Citorik, Sam Perli, Allen Cheng, Nate Roquet, Chao Zhong, Urartu Seker, and others. Michele Jakoulov and Jim Hogle go to great lengths to make the Biophysics program a warm, connected place despite us students being spread out over three campuses.

I also wish to thank faculty who generously took time from their schedules to serve on my DAC and Thesis committees: Profs. Jim Hogle, Markus Buehler, George Whitesides, David Clarke, Shmuel Rubinstein, and Jennifer Lewis.

The Hertz Foundation, Office of Naval Research, and NIH supported me financially during graduate training. I am especially grateful to the Hertz Foundation

for creating a community of like-minded individuals who, by example of their blue-skies pursuits, provided reassurance that it is OK to take intellectual risks.

My parents, HuiHui and Jingke, my sister Anna, and my childhood friend Alex Flis have been a bedrock of support throughout my entire life. The greatest blessing of all during my graduate school years has been meeting my wife, Siting. She has made me a warmer, wiser, and livelier person, and I am overjoyed that we are embarking on a life together.

Chapter 1

Publication: this chapter is adapted from

Chen AY, Zhong C, Lu TK. Engineering living functional materials. *ACS Synth Biol.* 2015 Jan 16;4(1):8-11.

Contributions: AYC and TKL wrote main text, CZ provided input, AYC made figures.

An overarching goal of synthetic biology is to design biological systems for useful applications. In exploring the space of possibilities, one logical approach is to consider the characteristic properties of living systems, how they may be useful, and how synthetic biology tools can engineer them. Three such properties are evolvability, self-organization, and responsiveness to environment. We propose that: 1) these properties of living systems have been productively applied in synthetic biology, 2) these characteristics are useful to materials science by enabling new functionalities and synthesis capabilities, and 3) synthetic biology is well-positioned to harness these features to create novel living functional materials and materials foundries (Figure 1).

Protein engineering and heterologous expression have allowed protein domains to be borrowed from nature and modified or fused in various combinations to generate useful products, such as soft materials. For example, pH and temperature-sensitive leucine zipper domains fused to hydrophilic domains have led to polymers that reversibly form a hydrogel in response to their environment[1] . Spider silk protein has also been recombinantly expressed and spun into fibers, with processing of this aggregation-prone protein facilitated by extracellular secretion[2].

Traditionally, when engineered proteins are used as building blocks for materials, only the first step in creating the materials (i.e., heterologous expression of subunits) is performed by cells. Assembly of subunits into higher-order structures is performed *in vitro* after subunit purification. However, living systems are capable of much more than heterologous protein expression. As a result of advances in synthetic biology, there is the opportunity to evolve or design materials subunits and to engineer cells to assemble subunits in-

to higher-order materials, rather than depend solely on *in vitro* assembly[3]. Having cells perform assembly, or even be incorporated as part of the final material, would open up many new capabilities for novel materials, such as self-healing, remodeling, hierarchical organization, and other properties characteristic of living systems. Furthermore, such materials could be grown in bottom-up, energy efficient processes, thus enabling distributed manufacturing. We envision that these living functional materials could revolutionize the fundamental ways in which our world makes and uses materials.

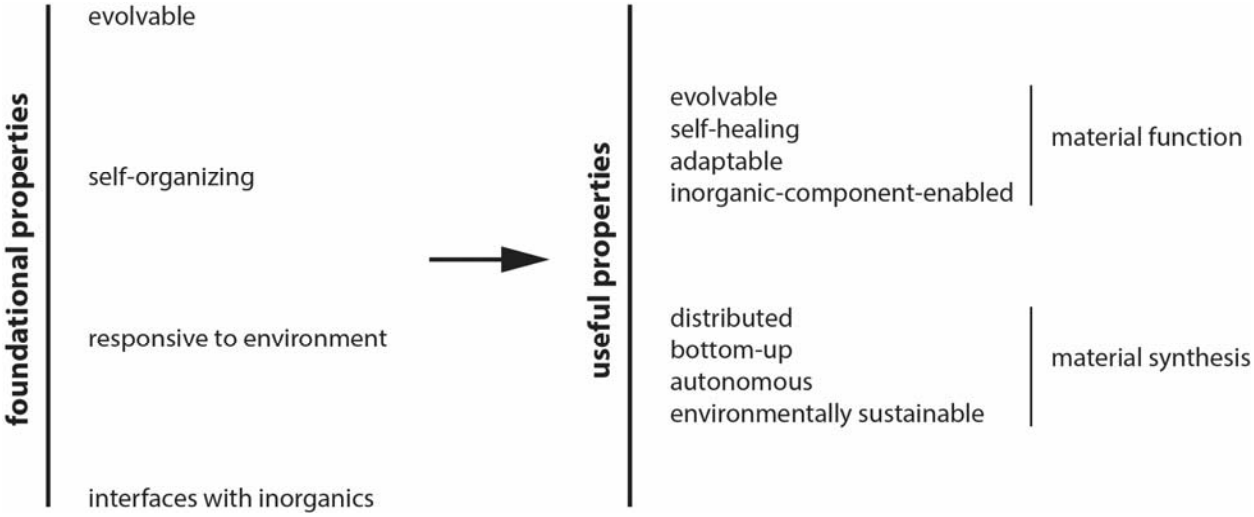

Figure 1-1 | Foundational properties of living systems give rise to useful properties for materials function and synthesis. Integrating non-living and living systems enables the creation of 'living functional materials'.

Evolvability

Living systems are able to generate heritable diversity in the form of genetic variation that manifests as phenotypes that can be acted upon by selective pressures. This property has been applied in synthetic biology to create directed evolution platforms[4] that have been used to optimize metabolic pathways, create novel enzymes, and evolve protein domains with useful binding properties.

An early directed evolution platform, phage display, has proven useful to materials science as a way to select for peptides that bind and nucleate inorganic materials. This approach eventually allowed fabrication of genetically engineered batteries[5] and other devices. New directed evolution platforms leveraging cells could be adapted to optimize pathways for assembling materials. Such a platform could allow tuning of not only the peptide sequence and subunit composition of materials such as collagen, polyesters, and polysaccharides, but also how the subunits are assembled – an important determinant of material properties.

Self-organization

Living systems can perform impressive feats of self-organization that are hierarchical and coordinated in space and time, a prime example being embryogenesis. This property has been studied using synthetic-biology approaches, as well as applied broadly for patterning based on intercellular communication and motility[6,7], for synchronization of cell populations, and for intracellular organization to achieve cell polarization.

Nature's solutions for creating hierarchal self-organized structures[8] (biomolecules→ biomolecular assemblies → organelles → cells → tissues → organs → organisms)

may be mapped onto the problems that materials scientists face in fabricating multi-scale patterned materials. Self-organization in biology is carried out by genetic programs and aided by physical forces; one-dimensional strings of letters in DNA, encoding genes and regulatory elements, can somehow direct the fabrication of complex three-dimensional structures in cells and organisms.

Understanding and modifying these programs through synthetic biology may allow us to harness them for making materials that assemble autonomously. Early steps have been taken in this direction at various scales. Work in biomolecular self-assembly uses the physical components that store and carry out genetic programs to create nanoscale materials. Intricate static and dynamic structures may be precisely assembled by using DNA as a structural material as well as the carrier of instructions for its own assembly[9]; similar feats may be achieved with designer RNA and proteins. Self-organization at larger scales has also been harnessed to create materials, some examples being: active self-assembled matter based on microtubules and kinesin[10], self-organized tissues[11] and organoids[12], and self-organized robot swarms[13] (inspired by social insects) that create user-defined structures.

Responsiveness to environment

Living systems sense inputs from the environment, integrate them, and respond with appropriate outputs. Environmental responsiveness is a property that is one of the building blocks of evolvability and self-organization, and is useful in its own right. The sense-and-respond property of living systems has been applied broadly in synthetic biology[14,15], some examples being optogenetic control of cell behavior, light-dark boundary de-

tection, sensing-and-destruction of pathogenic microbes via detection of quorum sensing molecules, sensing-and-destruction of cancer cells via detection of microRNA signatures, sensing-and-amelioration of high uric acid levels, and multi-cellular computation in which cells implementing simple logic gates are wired together by chemical signaling. Cells have also been incorporated into materials as sense-and-respond modules that, for example, produce urate oxidase in response to uric acid or produce insulin upon activation by light.

Living sense-and-respond systems can be useful as "smart" environmentally responsive factories for materials or "smart" environmentally-responsive materials (if cells themselves are incorporated as part of the material and endow it with function). A specific example of a responsive material would be one that senses damage and autonomously self-heals. Such a system would be capable of sensing and repairing more diverse types of damage compared to current non-living self-healing materials, which largely respond to mechanical and thermal damage with relatively simple fixes[16].

Bridging the function gap with inorganic materials

While living matter made of organic molecules offers exciting prospects for novel functional materials, it can be deficient in certain useful properties, such as the ability to conduct electrons and the ability to interact with magnetic fields. This gap can be bridged by incorporating inorganic components that possess such properties, creating multi-functional materials that combine the capabilities of living systems with those of inorganic materials. An example from nature is magnetotactic bacteria, which are able to navigate magnetic field lines based on their ability to biomineralize ferromagnetic crystals and or-

ganize them into chains (magnetosome chains). In a synthetic context, interfacing biology with inorganic materials can be accomplished via biomineralization, which may be engineered with synthetic biology, or via bioconjugate chemistry. As an example of the former, gene clusters encoding the biosynthetic pathway for magnetosome chains in *M. gryphiswaldense* have been transferred to a foreign microbial host to form functional, heterologous magnetosomes. As an example of the latter, semiconductor devices were incorporated into the extracellular matrix of engineered tissues to give hybrid, or "cyborg" tissues[17].

A platform for engineering living functional materials

As described above, a large body of literature has developed around engineering living systems that evolve, self-organize, and compute. A complementary literature has developed around engineering inorganic nanomaterials with diverse, tunable properties. Leveraging these capabilities, we recently presented a novel platform for integrating living cells with inorganic components into living functional materials[18] (Figure 2). We engineered *E. coli* biofilms with artificial gene circuits to control the synthesis of extracellular curli amyloid nanofibers. These nanofibers were functionalized with peptide domains to interface them with inorganic materials. This platform enables multiple novel materials properties derived from the combination of synthetic biology and materials science. Specifically, these engineered *E. coli* biofoundries can be used to manufacture materials with controllable nanoscale-to-microscale structure and composition by controlling either the timing or magnitude (e.g., frequency modulation or amplitude modulation, respectively) of external induc-

er inputs. Furthermore, by using cell-cell communication circuits, the synthetic biofilms generated materials whose nanoscale-to-microscale composition and structure were varied in a dynamic and autonomous fashion, with no requisite user input.

Moreover, by incorporating synthetic gene circuits with other forms of patterning, such as spatial inducer gradients and protein engineering, we were able to achieve self-organization of materials across multiple length scales with biofilms. The ability to hierarchically organize materials across multiple length scales is a major challenge for materials science, but is one that can be readily addressed with biological systems. Specifically, by combining synthetic gene circuits with spatial inducer gradients to control curli nanofiber production, engineered biofilms were able to implement nanoscale-to-millimeter-scale patterning. By integrating synthetic gene circuits with protein engineering of the curli amyloid subunits themselves, the artificial biofilms were able to more finely control the nanoscale-to-microscale patterning of the curli nanofibers. With further integration of top-down patterning strategies (such as inputs of patterned light or 3D printing) with bottom-up organization (such as rational design of protein self-assembly or directed evolution to achieve desired morphologies) and synthetic gene circuits, the precise, dynamic, and autonomous control of multi-scale structure should be achievable by living functional materials.

We also demonstrated that living functional materials and living materials-synthesis platforms based on biofilms can organize and synthesize biotic-abiotic hybrid structures with novel functions. For example, gold nanorods, nanowires, and chains were templated on biofilm-synthesized curli nanofibers. This allowed the implementation of electrically conductive biofilm switches whose conductivity could be toggled on with the addition of

external chemical signals. In addition, semiconductor quantum dots were synthesized or organized on biofilm-fabricated curli nanofibers, and co-assembled with metal nanoparticles. The resulting metal/semiconductor heterostructures exhibited modulated fluorescence properties. Thus, we have shown that biofilm-based living functional materials can be used to synthesize and organize biotic-abiotic systems, as well as modulate their properties. Since biofilms are robust and abundant living systems that are easy to grow and scale up, they are promising substrates for the distributed, environmentally-friendly manufacturing of materials and devices. We envision that related platforms could enable the creation of cell-synthesized batteries and solar cells, self-healing living-cell glues, self-regenerating catalytic membranes and filters, enzymatic scaffolds for tunable reaction rates, and dynamic extracellular matrices for tissue engineering.

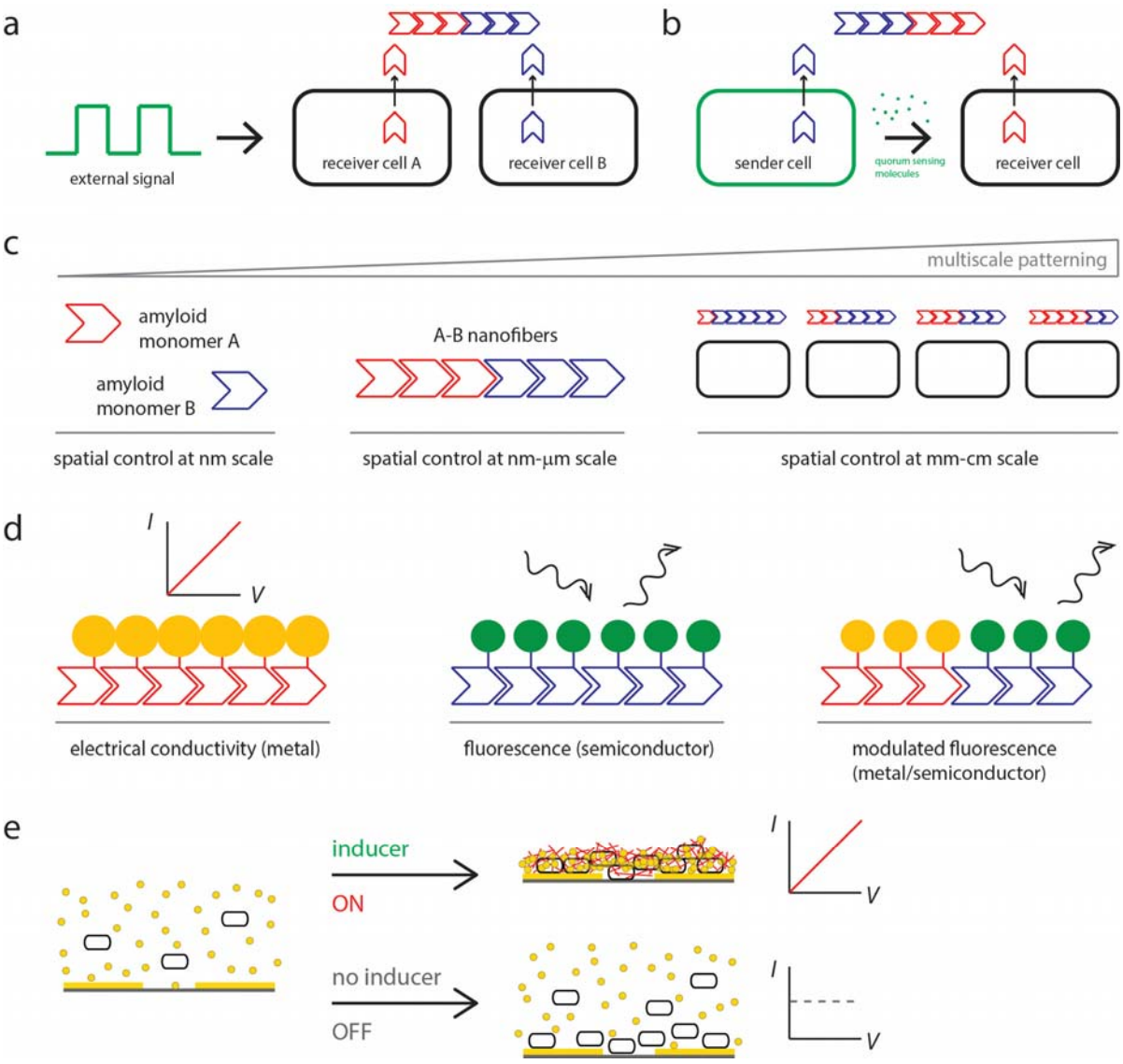

Figure 1-2 | A living materials-synthesis platform and living functional material based on *E. coli* biofilms (Figure adapted from Chen *et al.*[18]). This strategy is able to a) pattern materials in response to external inputs, b) organize materials autonomously via cell-to-cell communication, c) pattern materials across multiple length scales, d) interface with inorganic components to enable electrical conductivity and modulated fluorescence, and e) implement a chemically-responsive electrical switch based on biofilms.

Outlook

Living system properties of evolvability, self-organization, and responsiveness to the environment, in conjunction with tools to interface cells with inorganic components, constitute a foundation for synthesizing materials with novel functionalities. Our recent work with engineered biofilms[18] establishes a proof-of-concept that living cellular systems can act not only as foundries for new materials, but can also be incorporated into hybrid materials systems. Man-made materials are often made by centralized, top-down, energy-intensive processes, and are limited in their ability to respond and adapt. The integration of engineered living systems with inorganic components to create 'living materials-synthesis platforms' and 'living functional materials' has the potential to dramatically change the fabrication and use of materials.

References

1 Petka, W. A., Harden, J. L., McGrath, K. P., Wirtz, D. & Tirrell, D. A. Reversible hydrogels from self-assembling artificial proteins. *Science* **281**, 389-392, doi:DOI 10.1126/science.281.5375.389 (1998).

2 Widmaier, D. M. *et al.* Engineering the Salmonella type III secretion system to export spider silk monomers. *Molecular systems biology* **5**, 309, doi:10.1038/msb.2009.62 (2009).

3 Rice, M. K. & Ruder, W. C. Creating biological nanomaterials using synthetic biology. *Science and Technology of Advanced Materials* **15**, 014401 (2014).

4 Wang, H. H. *et al.* Programming cells by multiplex genome engineering and accelerated evolution. *Nature* **460**, 894-898, doi:10.1038/nature08187 (2009).

5 Lee, Y. J. *et al.* Fabricating genetically engineered high-power lithium-ion batteries using multiple virus genes. *Science* **324**, 1051-1055, doi:10.1126/science.1171541 (2009).

6 Basu, S., Gerchman, Y., Collins, C. H., Arnold, F. H. & Weiss, R. A synthetic multicellular system for programmed pattern formation. *Nature* **434**, 1130-1134, doi:10.1038/nature03461 (2005).

7 Payne, S. *et al.* Temporal control of self-organized pattern formation without morphogen gradients in bacteria. *Molecular systems biology* **9**, 697, doi:10.1038/msb.2013.55 (2013).

8 Weiner, S. & Wagner, H. D. The material bone: Structure mechanical function relations. *Annu Rev Mater Sci* **28**, 271-298, doi:DOI 10.1146/annurev.matsci.28.1.271 (1998).

9 Seeman, N. C. Nanomaterials Based on DNA. *Annu Rev Biochem* **79**, 65-87, doi:DOI 10.1146/annurev-biochem-060308-102244 (2010).

10 Sanchez, T., Chen, D. T., DeCamp, S. J., Heymann, M. & Dogic, Z. Spontaneous motion in hierarchically assembled active matter. *Nature* **491**, 431-434, doi:10.1038/nature11591 (2012).

11 Liu, J. S. & Gartner, Z. J. Directing the assembly of spatially organized multicomponent tissues from the bottom up. *Trends in cell biology* **22**, 683-691, doi:10.1016/j.tcb.2012.09.004 (2012).

12 Lancaster, M. A. *et al.* Cerebral organoids model human brain development and microcephaly. *Nature* **501**, 373-379, doi:10.1038/nature12517 (2013).

13 Werfel, J., Petersen, K. & Nagpal, R. Designing Collective Behavior in a Termite-Inspired Robot Construction Team. *Science* **343**, 754-758, doi:10.1126/science.1245842 (2014).

14 Benenson, Y. Biomolecular computing systems: principles, progress and potential. *Nature reviews. Genetics* **13**, 455-468, doi:10.1038/nrg3197 (2012).

15 Brophy, J. A. & Voigt, C. A. Principles of genetic circuit design. *Nature methods* **11**, 508-520, doi:10.1038/nmeth.2926 (2014).

16 Wool, R. P. Self-healing materials: a review. *Soft Matter* **4**, 400-418, doi:10.1039/b711716g (2008).

17 Tian, B. *et al.* Macroporous nanowire nanoelectronic scaffolds for synthetic tissues. *Nat Mater* **11**, 986-994, doi:10.1038/nmat3404 (2012).

18 Chen, A. Y. *et al.* Synthesis and patterning of tunable multiscale materials with engineered cells. *Nat Mater* **13**, 515-523 (2014).

Chapter 2

Publication: this chapter is adapted from

Chen AY, Deng Z, Billings AN, Seker UO, Lu MY, Citorik RJ, Zakeri B, Lu TK. Synthesis and patterning of tunable multiscale materials with engineered cells. *Nat Mater.* 2014 May;13(5):515-23.

Contributions: TKL and AYC conceived the experiments. AYC planned all experiments and executed the majority of the experiments, ZD performed quantum dot synthesis and aided in HRTEM imaging for Fig 6, ANB performed microfluidic experiments and fluorescence microscopy for Fig 1, MYL aided in cloning, and RJC aided in strain construction, AYC, ZD, ANB and TKL analyzed the data and discussed results. AYC wrote the manuscript and made figures with input from TKL.

Natural multicellular assemblies such as biofilms, shells, and skeletal tissues have distinctive characteristics that would be useful for materials production and patterning[1-9]. They can detect external signals and respond via remodelling, implement patterning across different length scales, and organize inorganic compounds to create organic-inorganic composites. In this work, such systems provide inspiration for the design of environmentally responsive systems that can integrate biotic and abiotic materials via hierarchical self-assembly. To achieve these capabilities, we engineered artificial gene circuits and self-assembling amyloid fibrils together with synthetic cellular consortia[10-16] and abiotic materials.

Our model system is curli, an extracellular amyloid material produced by *E. coli* that forms fibrils based on the self-assembly of the secreted major curli subunit CsgA[17]. Secreted CsgA monomers are templated on CsgB, which is anchored to the cell surface, to form curli fibrils; moreover, CsgA secreted from one cell can interact with CsgB on other cells[17]. Using synthetic riboregulators[18], we implemented inducible transcriptional and translational control over the expression of CsgA subunits engineered to display various peptide tags, which can interface with inorganic materials. We transformed our synthetic circuits into an *E. coli* MG1655 *PRO csgA ompR234* host strain (see Supplementary Table 3 and Supplementary Fig. 20), which has the endogenous *csgA* gene deleted. The *ompR234* mutation enables curli production in liquid media at 30°C by enhancing the expression of genes from the native curli operon, including *csgB*[19,20]. We first introduced histidine-tagged CsgA ($CsgA_{His}$) expression under tight regulation by an anhydrotetracycline (aTc) inducer-responsive riboregulator[18] (Fig. 1a). $CsgA_{His}$ contained two histidine tags, one inserted before the first repeat domain and one inserted after the last repeat domain in CsgA

(Supplementary Table 1). The resulting cell strain was designated $aTc_{Receiver}/CsgA_{His}$. Immuno-gold labelling experiments with anti-CsgA antibodies (M. Chapman, University of Michigan[21,22]) showed that curli fibrils were only produced in the presence of aTc (Fig. 1b and Supplementary Fig. 1). Using confocal microscopy, we characterized biofilms formed by $aTc_{Receiver}/CsgA_{His}$ cells augmented with an mCherry-expressing plasmid for convenient visualization. This strain formed biofilms only when induced by aTc, both under static culture conditions (Fig. 1c and Supplementary Fig. 2a) and when cultured in microfluidic flow cells (Fig. 1d and Supplementary Fig. 2b). Biofilm growth was confirmed with a standard crystal-violet (CV) assay (Supplementary Fig. 3). We also quantified curli production with dot blots and found a yield of 63±5.8 (s.e.m.) mg/cm^3 of biofilm after 24h (Supplementary Fig. 22).

To create engineered cellular consortia for materials patterning, we built three additional strains: one with CsgA under regulation by an acyl-homoserine lactone (AHL)-inducible riboregulator ($AHL_{Receiver}/CsgA$), one with CsgA under regulation by an aTc-inducible riboregulator ($aTc_{Receiver}/CsgA$), and one with $CsgA_{His}$ under regulation by an AHL-inducible riboregulator ($AHL_{Receiver}/CsgA_{His}$). These strains only produced curli fibrils in the presence of the cognate inducer, demonstrating tight and orthogonal regulation of *csgA* and $csgA_{His}$ expression (Supplementary Fig. 8). Moreover, insertion of heterologous histidine tags did not interfere with curli fibril formation based on Congo Red assays and TEM imaging (Supplementary Fig. 4 and 5).

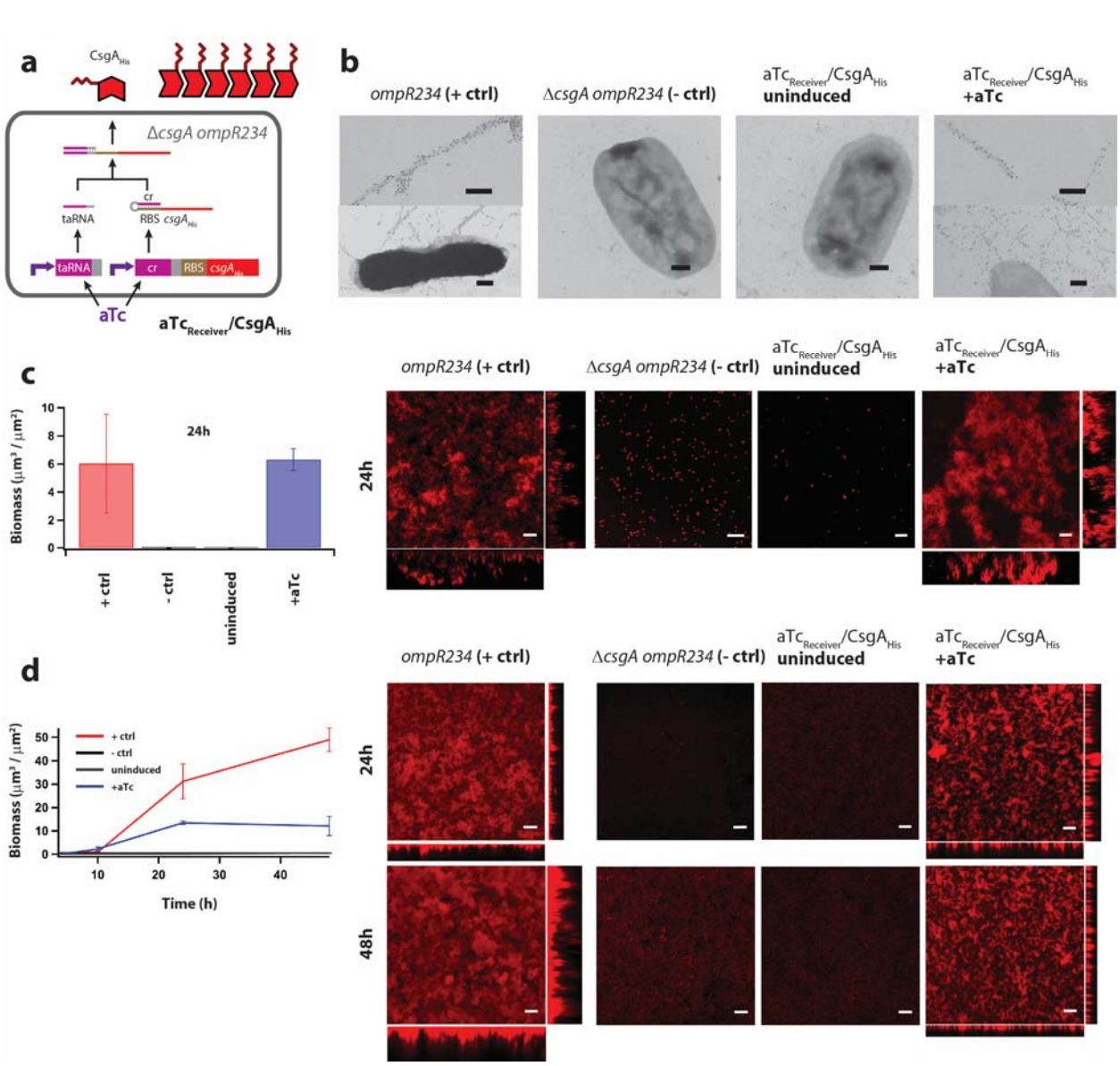

Figure 2-1 | Inducible production of engineered curli fibrils and biofilms. a, Riboregulator circuits tightly regulate expression of curli subunits, such as $CsgA_{His}$. Production of $CsgA_{His}$ requires the expression of *trans*-activating RNA (taRNA). The taRNA prevents the *cis*-repressive (cr) sequence from blocking the ribosome-binding sequence (RBS) controlling translation of the mRNA transcript. In the absence of inducer, mRNA and taRNA levels are low, thus leading to significant repression of gene expression. The

Figure 2-1 (Continued)

addition of aTc induces transcription of both *csgA*$_{His}$ mRNA and taRNA, thus enabling CsgA$_{His}$ production. Tight regulation of curli expression is useful for controlling patterning (Supplementary Fig. 19). **b,** Immuno-labelling of curli fibrils with rabbit anti-CsgA antibodies and gold-conjugated goat anti-rabbit antibodies. Positive-control ("+ ctrl") MG1655 *ompR234* cells ("*ompR234*", see Supplementary Table 3), which have an intact endogenous *csgA* gene, produce curli fibrils that were labelled by anti-CsgA antibodies and are attached to cells. However, negative-control ("− ctrl") cells with the *csgA* gene knocked out and no *csgA*-expressing circuits ("Δ*csgA ompR234*", see Supplementary Table 3), as well as aTc$_{Receiver}$/CsgA$_{His}$ cells in the absence of aTc, did not produce curli fibrils. Inducing aTc$_{Receiver}$/CsgA$_{His}$ cells with aTc enabled the synthesis of curli fibrils that were labelled by anti-CsgA antibodies and attached to cells. Scale bars are 200nm. **c,** Confocal microscopy and biomass quantification revealed that under static culture conditions, *E. coli ompR234* cells formed thick adherent biofilms. However, *E. coli* Δ*csgA ompR234* cells, as well as aTc$_{Receiver}$/CsgA$_{His}$ cells in the absence of aTc, did not form biofilms. Inducing aTc$_{Receiver}$/CsgA$_{His}$ cells with aTc led to the formation of thick adherent biofilms. **d,** Confocal microscopy and biomass quantification revealed similar biofilm-forming capabilities by *E. coli ompR234* and induced aTc$_{Receiver}$/CsgA$_{His}$ cells when grown in flow cells. To enable visualization, we transformed a constitutive mCherry-expressing plasmid into all strains (see Supplementary Methods). Cells were grown in liquid M63 media with glucose; the corresponding experiments for other media conditions are shown in Supplementary Figure 1 and 2. Scale bars in c) and d) are 50μm, and orthogonal XZ and YZ views are maximum-intensity projections.

Externally controllable patterning

We engineered consortia composed of $AHL_{Receiver}$/CsgA and $aTc_{Receiver}$/$CsgA_{His}$ cells to produce two-component protein fibrils composed of CsgA and $CsgA_{His}$ (Fig. 2). By tuning the pulse lengths and pulse amplitudes of AHL and/or aTc, fibrils with different structures and compositions were formed. For example, we mixed equal numbers of $AHL_{Receiver}$/CsgA and $aTc_{Receiver}$/$CsgA_{His}$ cells together and induced this mixed-cell population first with AHL, followed by aTc (Fig. 2a). In analogy to block co-polymers, this produced block "co-fibrils" consisting of blocks of CsgA (unlabelled fibril segments) and blocks of $CsgA_{His}$ (fibril segments labelled by nickel nitrilotriacetic acid-conjugated gold particles (NiNTA-AuNPs). NiNTA-AuNPs specifically labelled $CsgA_{His}$-based curli fibrils but not CsgA-based curli fibrils (Supplementary Fig. 9).

We tuned the length distribution of the CsgA and $CsgA_{His}$ blocks, as well as the relative proportions of CsgA and $CsgA_{His}$, by changing the relative lengths of AHL pulses versus aTc pulses. As AHL induction time increased, non-NiNTA-AuNP-labelled fibril segments increased in length, indicating longer CsgA blocks (Fig. 2b and Supplementary Fig. 6a). At the same time, the proportion of fibril length labelled with NiNTA-AuNP decreased, indicating a higher relative proportion of CsgA in the fibrils (Fig. 2b). With temporal separation in expression, the distinct CsgA and $CsgA_{His}$ segments within the block co-fibrils were longer than those in co-fibrils assembled when CsgA and $CsgA_{His}$ were secreted simultaneously with no temporal separation, even though the overall CsgA to $CsgA_{His}$ ratios were similar (Supplementary Fig. 6a). Thus, engineered cells can translate

the temporal interval length of input signals into different nanoscale structures and compositions of materials.

We also tuned the length distributions of the two types of blocks, as well as their relative proportions, by inducing simultaneous expression of the CsgA variants with different concentrations of AHL and aTc (Fig. 2c). With AHL-only induction, fibrils were almost uniformly unlabelled; with increasing aTc concentration, the population as well as lengths of unlabelled fibril segments decreased while those of labelled fibril segments increased (Fig. 2d, Supplementary Fig. 6b). With aTc-only induction, fibrils were almost uniformly labelled by NiNTA-AuNPs; with increasing AHL concentration, the population as well as lengths of unlabelled segments increased (Supplementary Fig. 7). Thus, engineered cells can translate the amplitudes of input signals, such as inducer concentrations, into different nanoscale structures and compositions of materials.

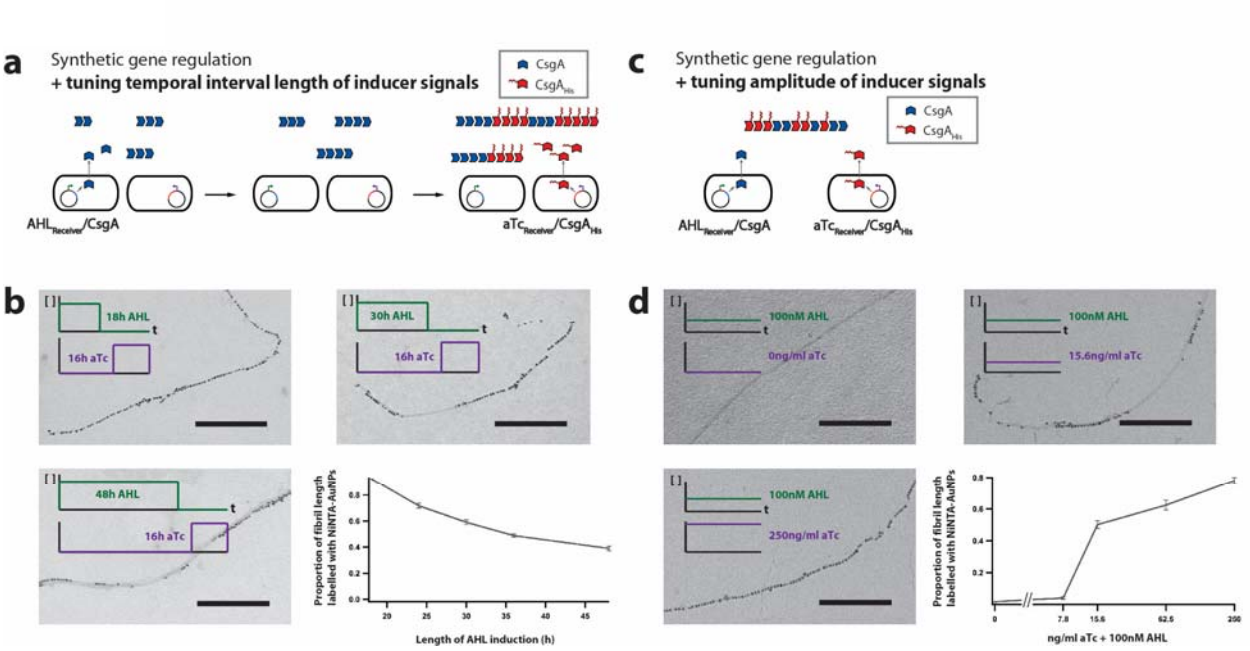

Figure 2-2 | Conversion of timing and amplitude of chemical inducer signals into material structure and composition. a, Inducible synthetic gene circuits couple curli subunit secretion to external chemical inducers. Engineered cells containing these circuits can translate induction pulse length into nanoscale structure and composition of block co-fibrils. **b,** We first used AHL to induce secretion of CsgA from AHL$_{Receiver}$/CsgA and then used aTc to induce secretion of CsgA$_{His}$ from aTc$_{Receiver}$/CsgA$_{His}$. We tuned the relative block lengths and proportions of CsgA and CsgA$_{His}$ (plot of the proportion of fibril length labelled by NiNTA-AuNP, solid grey line) by changing the relative lengths of AHL versus aTc induction times. Scale bars are 200nm. **c,** Synthetic genetic regulatory circuits that couple curli subunit secretion to external inducer signals can translate inducer concentration into nanoscale structure and composition of block co-fibrils. **d,** Engineered cells AHL induced secretion of CsgA from AHL$_{Receiver}$/CsgA, while at the same time, aTc induced secretion of CsgA$_{His}$ from aTc$_{Receiver}$/CsgA$_{His}$. We tuned the relative block lengths and proportions of

Figure 2-2 (Continued)

CsgA and $CsgA_{His}$ by changing the relative concentrations of AHL and aTc inducers applied simultaneously. The solid grey line indicates the proportion of fibril length labelled by NiNTA-AuNP with varying concentrations of aTc and constant 100nM AHL. Detailed histograms can be found in Supplementary Figure 6. Scale bars are 200nm.

Autonomous patterning

Cellular communities containing synthetic cellular communication circuits[23-26] can autonomously produce dynamic materials whose structure and composition changes with time (Fig. 3). Since *E. coli* does not normally produce AHL, we first engineered an *E. coli* strain that constitutively produces AHL and inducibly produces CsgA in the presence of aTc (AHL_{Sender}+$aTc_{Receiver}$/CsgA). This strain communicated with $AHL_{Receiver}$/$CsgA_{His}$ cells via the diffusible cellular communication signal, AHL. We then combined AHL_{Sender}+$aTc_{Receiver}$/CsgA and $AHL_{Receiver}$/$CsgA_{His}$ cells in varying ratios (Fig. 3a). Induction of this mixed-cell population by aTc resulted in CsgA secretion. Over time, AHL accumulation led to increasing secretion of $CsgA_{His}$, thus generating an increased population and lengths of $CsgA_{His}$ blocks, and a higher relative proportion of $CsgA_{His}$ in material composition (Fig. 3b and Supplementary Fig. 10). The temporal dynamics of changes in material composition was tunable by the initial seeding ratio of AHL_{Sender}+$aTc_{Receiver}$/CsgA to $AHL_{Receiver}$/$CsgA_{His}$ cells (Fig. 3b). When only AHL_{Sender}+$aTc_{Receiver}$/CsgA cells were present, fibrils were almost

uniformly unlabelled; when only $AHL_{Receiver}/CsgA_{His}$ cells were present, no fibrils were formed (Fig. 3b).

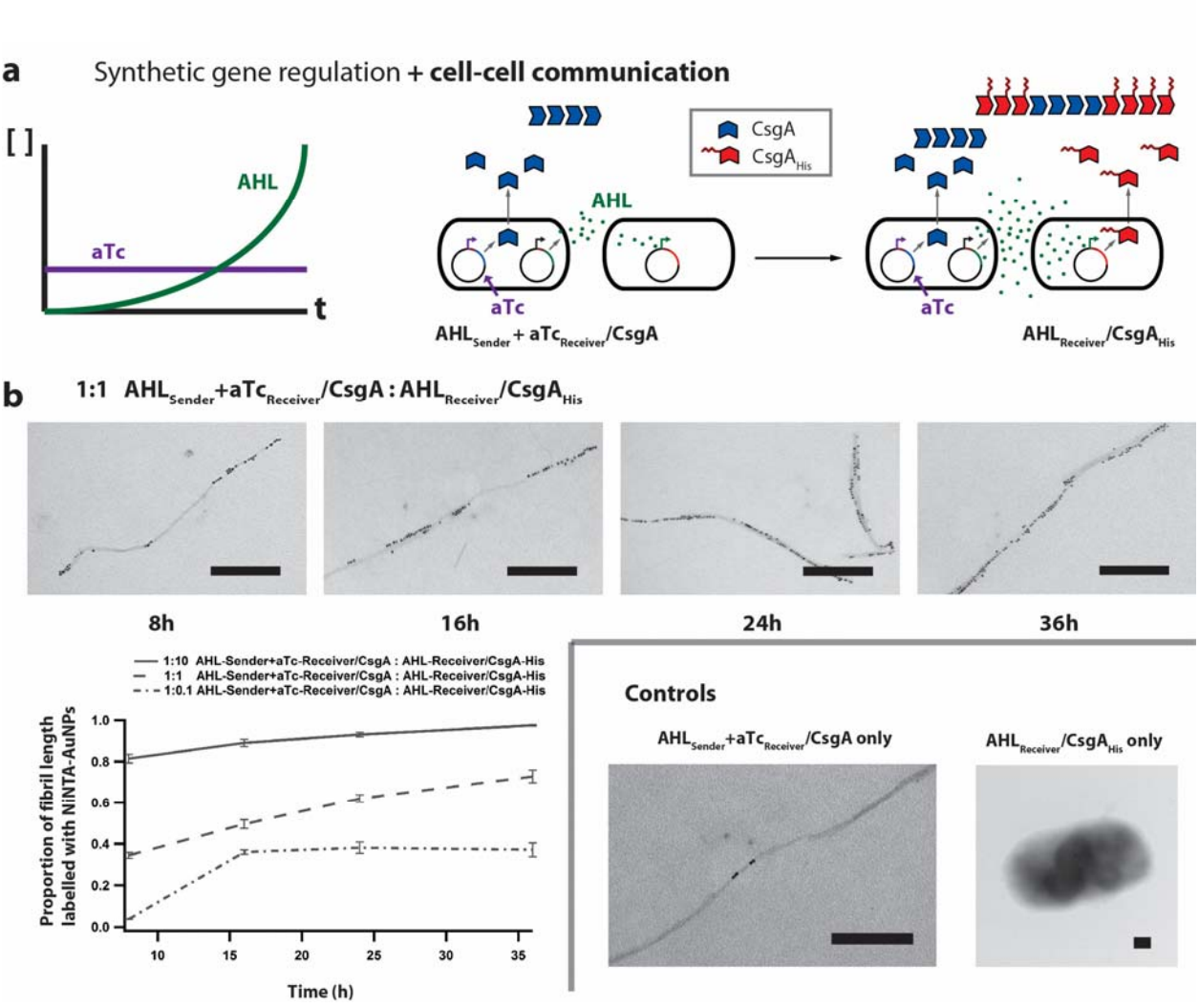

Figure 2-3 | Synthetic cellular communication for dynamic, autonomous material production and patterning. a, Synthetic gene circuits that couple curli subunit secretion to external inducer signals, when combined with synthetic cellular communication circuits, allow for the production of materials whose structure and composition changes autonomously with time. AHL_{Sender}+$aTc_{Receiver}$/CsgA secreted both CsgA and AHL. As AHL signal accumulated, $AHL_{Receiver}/CsgA_{His}$ secreted increasing levels of $CsgA_{His}$. **b,** Using the

Figure 2-3 (Continued)

autonomous cellular communication system, the length of $CsgA_{His}$ blocks and the proportion of $CsgA_{His}$ increased with time (plot of the proportion of fibril length labelled by NiNTA-AuNP, grey lines). This behavior could be tuned by the ratio of the seeding density of AHL_{Sender}+$aTc_{Receiver}$/CsgA cells to $AHL_{Receiver}$/$CsgA_{His}$ cells. When only AHL_{Sender}+$aTc_{Receiver}$/CsgA cells were present, the resulting fibrils were almost uniformly unlabelled; when only $AHL_{Receiver}$/$CsgA_{His}$ cells were present, no curli fibrils were formed (Controls). Detailed histograms can be found in Supplementary Fig. 10. Scale bars are 200nm.

Multiscale patterning

In addition, engineered cellular consortia can achieve spatial control over multiple length scales. Genetic regulation of subunit expression allows fibril patterning from tens of nanometres to micrometres, while spatial control at the macroscale can be achieved via spatially varying inducer concentrations. These two methods of control can be combined to create materials patterned across multiple length scales (Fig. 4). To demonstrate this, we created agar plates with opposing concentration gradients of AHL and aTc and overlaid bacterial populations consisting of equal numbers of four cell strains: $AHL_{Receiver}$/CsgA, $aTc_{Receiver}$/$CsgA_{His}$, $AHL_{Receiver}$/GFP, and $aTc_{Receiver}$/mCherry. The $AHL_{Receiver}$/GFP and $aTc_{Receiver}$/mCherry cells enabled visualization of inducer concentration gradients (Fig. 4b and Supplementary Fig. 12). $AHL_{Receiver}$/CsgA and $aTc_{Reciever}$/$CsgA_{His}$ cells secreted different

levels of CsgA and $CsgA_{His}$, depending on their positions on the concentration gradient, to generate a spatial gradient of changing fibril structures (Fig. 4a). This multiscale material was patterned at the nanoscale as block co-fibrils and at the millimetre scale with position-dependent fibril structure (Fig. 4b and Supplementary Fig. 11a). Agar plates without inducer concentration gradients did not generate fibril structures that varied along the plate (Supplementary Fig. 11a).

Protein engineering can also control the structure of cell-produced biomaterials at the nanoscale. We hypothesized that fusing tandem repeats of CsgA together would increase the distance between equivalent positions on adjacent monomers where functional domains can be displayed. Concatenating eight tandem repeats of CsgA and adding a histidine tag to the C-terminus ($8XCsgA_{His}$) resulted in fibrils that were labelled by a syncopated pattern of NiNTA-AuNP, with clusters of particles separated by 33.3±27.1 (s.e.m.) nm (Fig. 4c and Supplementary Fig. 11b). Using this finding, we demonstrated a second example of multiscale assembly. Specifically, we combined equal numbers of $AHL_{Receiver}/8XCsgA_{His}$ and $aTc_{Receiver}/CsgA_{His}$ cells. We induced this mixed-cell population sequentially with AHL followed by aTc (Fig. 4d) to generate block co-fibrils consisting of $8XCsgA_{His}$ segments and $CsgA_{His}$ segments patterned across the nanometre to micrometre scales (Fig. 4d and Supplementary Fig. 11c).

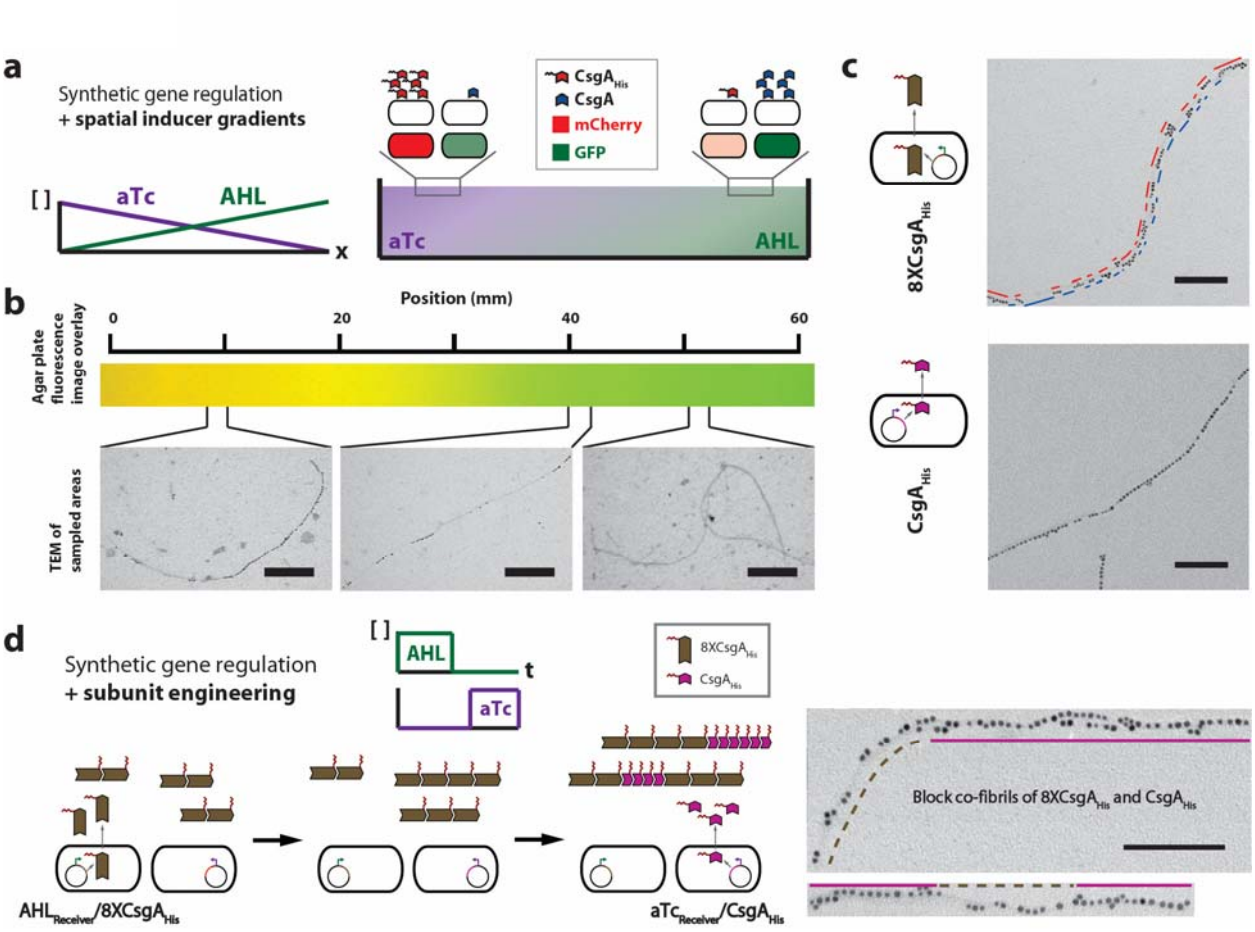

Figure 2-4 | Multiscale patterning with cellular consortia via synthetic gene regulation combined with inducer gradients and subunit engineering. a, Synthetic gene circuits that couple curli subunit secretion to external inducer signals, when combined with a spatial inducer gradient, enable patterning across multiple length scales. We used an agar plate with opposing concentration gradients of AHL and aTc to achieve control at the macroscale (Supplementary Fig. 12). This was combined with regulation of nanoscale patterning to achieve multiscale patterning. Embedded in top agar were equal numbers of $AHL_{Receiver}$/CsgA, $aTc_{Receiver}$/$CsgA_{His}$, $AHL_{Receiver}$/GFP, and $aTc_{Receiver}$/mCherry cells. **b,** By combining synthetic gene regulation with spatial inducer gradients, we created a change in the nanoscale structure of fibrils across a distance of millimetres. This

Figure 2-4 (Continued)

nanoscale and macroscale patterning was shown by changes in segment lengths of unlabelled and NiNTA-AuNP-labelled fibril segments at different locations across the agar plate. Inducer concentration gradients were demonstrated by overlaid GFP and mCherry fluorescence images of embedded $AHL_{Receiver}$/GFP and and $aTc_{Receiver}$/mCherry reporter cells. Scale bars are 200nm. **c,** We also achieved patterning at the nanoscale by protein engineering of curli subunits. Concatenating eight tandem repeats of CsgA and adding one histidine tag to the C-terminus ($8XCsgA_{His}$) resulted in fibrils that were labelled by a syncopated pattern of NiNTA-AuNPs, with clusters of particles separated by 33.3±27.1 (s.e.m.) nm. Scale bars are 100nm. **d,** Synthetic gene circuits that couple curli subunit secretion to external inducer signals, when combined with subunit engineering, enable patterning across multiple length scales (nanometres to micrometres). We used AHL to induce production of $8XCsgA_{His}$ from $AHL_{Receiver}$/$8XCsgA_{His}$ and then used aTc to induce production of $CsgA_{His}$ from $aTc_{Receiver}$/$CsgA_{His}$. In the TEM images, dashed brown lines refer to syncopated $8XCsgA_{His}$ segments while the solid amethyst lines indicate $CsgA_{His}$ segments. Detailed histograms for data shown here can be found in Supplementary Figure 11. Scale bars are 100nm.

Interfaces with inorganic materials

Our living cell system can be used to create functional materials, such as environmentally switchable conductive biofilms. We hypothesized that aTc-inducible

production of $CsgA_{His}$ monomers by $aTc_{Receiver}/CsgA_{His}$ cells would generate extracellular amyloid fibrils that organize NiNTA-AuNPs into chains and form a conductive biofilm network. As shown in Figure 1, the expression of extracellular curli fibrils enables surface adherence by multicellular bacterial communities, resulting in biofilm formation. Engineered biofilms were grown on interdigitated electrodes deposited on Thermanox coverslips, with $aTc_{Receiver}/CsgA_{His}$ cells cultured in the presence of NiNTA-AuNPs and in the presence or absence of aTc inducer (Fig. 5a). We showed by confocal microscopy that biofilms were formed in an aTc-dependent manner (Supplementary Fig. 14). Scanning electron microscopy (SEM), scanning electron microscopy/energy dispersive X-ray spectroscopy (SEM/EDS), and transmission electron microscopy (TEM) were performed to further characterize biofilm samples (Fig. 5b). In the presence of aTc, biofilms formed, spanned electrodes (as shown by SEM imaging), and contained networks of gold that connected electrodes (as shown by SEM/EDS elemental mapping). In contrast, SEM imaging of cells grown in the absence of induction showed only scattered bacteria in the gaps between electrodes, and SEM/EDS showed no gold networks. TEM imaging revealed that aTc-induced biofilms organized gold particles into dense networks (Fig. 5b and Supplementary Fig. 16), while samples with cells in the absence of aTc showed only scattered, isolated gold particles (Fig. 5b). Biofilms formed in the presence of aTc had 0.82±0.17 (s.e.m.) nanosiemens conductance, whereas samples with cells in the absence of aTc had no measureable conductance (Supplementary Fig. 15). Biofilms formed with $aTc_{Receiver}/CsgA_{His}$ cells induced by aTc, but grown in the absence of NiNTA-AuNPs, had electrical conductance that was two orders of magnitude lower than those formed in presence of NiNTA-AuNPs (Supplementary Fig. 17a). Samples containing

$AHL_{Receiver}$/$CsgA_{His}$ cells grown in the presence of NiNTA-AuNPs and aTc had no measureable conductance (Supplementary Fig. 17b).

We extended cell-based gold-particle patterning to create nanowires and nanorods via additional gold deposition. When $aTc_{Receiver}$/$CsgA_{His}$ and $AHL_{Receiver}$/CsgA cells were induced with only aTc, the resulting curli fibrils templated gold nanowires. When the cells were induced with both aTc and AHL, the resulting co-fibrils contained $CsgA_{His}$ and CsgA which templated consecutive gold nanorods (Fig. 5c). Gold nanorods have been studied for a range of applications because of their more broadly tunable absorption spectra compared to nanoparticles, which allows for peak absorption in the near-IR window used for *in vivo* imaging and photothermal ablation[27]. Moreover, via conjugation with targeting ligands and drug molecules, they can also act as targeted drug delivery vehicles for therapeutic and diagnostic applications[28,29].

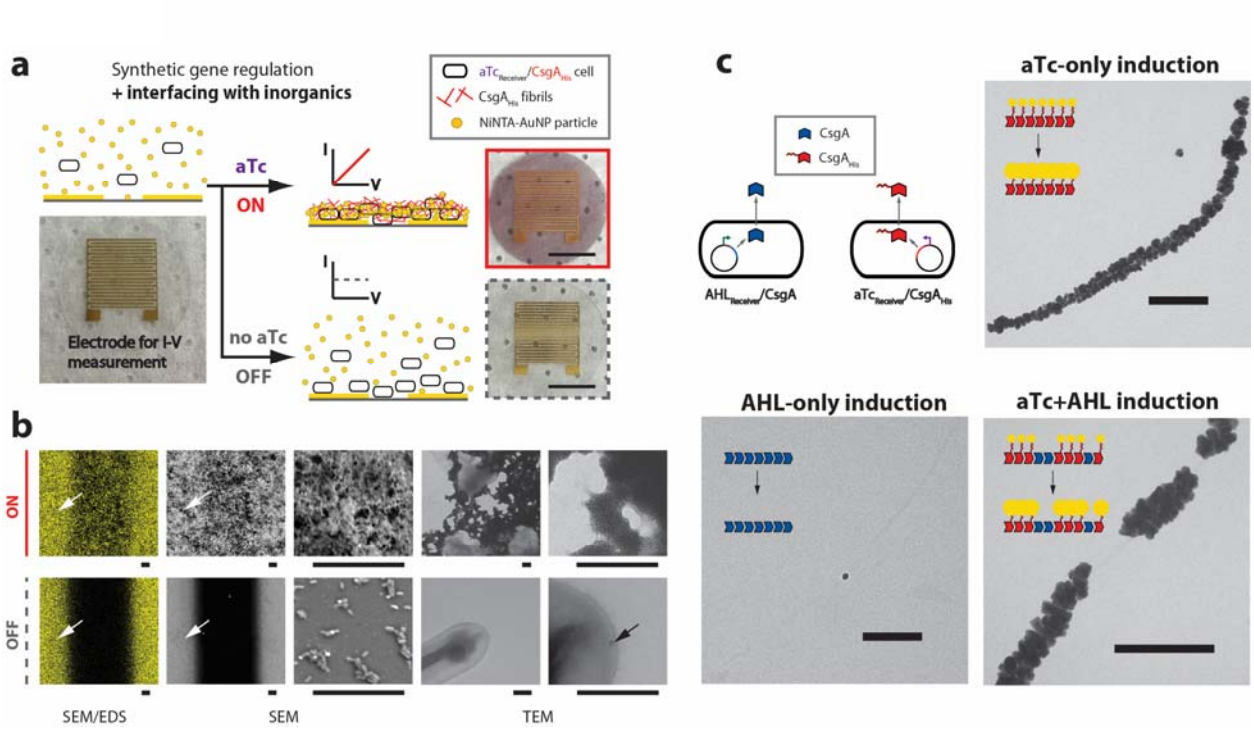

Figure 2-5 | Environmentally switchable conductive biofilms and cell-based synthesis of curli-templated nanowires and nanorods. a, We used $aTc_{Receiver}/CsgA_{His}$ cells to form amyloid fibrils composed of $CsgA_{His}$ in response to aTc. When combined with NiNTA-AuNPs, we created conductive biofilms that can be externally controlled as electrical switches. When aTc was added to $aTc_{Receiver}/CsgA_{His}$ cells grown in the presence of NiNTA-AuNPs, it triggered the formation of conductive biofilms on electrodes, with embedded 5nm gold particles giving biofilms a red colour ('ON', solid red box). However, in the absence of aTc, few cells adhered to the electrodes ('OFF', dashed grey box). Scale bars are 5mm. **b,** SEM/EDS elemental mapping of the aTc-induced 'ON' state for $aTc_{Receiver}/CsgA_{His}$ biofilms showed that networks of gold in the biofilms connected the electrodes (white arrows). SEM imaging showed that the biofilms bridged electrodes. TEM imaging showed networks of aggregated gold particles. In contrast, SEM/EDS mapping of

Figure 2-5 (Continued)

the 'OFF' state showed no gold networks, SEM imaging showed only scattered cells in the gap between electrodes, and TEM imaging showed only scattered and isolated gold particles (black arrow). Scale bars of scanning electron micrographs are 20 · m and scale bars of transmission electron micrographs are 200nm. **c,** A mixed population of $aTc_{Receiver}$/$CsgA_{His}$ and $AHL_{Receiver}$/CsgA cells produced curli templates for organizing either gold nanowires or gold nanorods when they were induced with aTc only or both aTc and AHL, respectively. NiNTA-AuNPs were patterned on $CsgA_{His}$ subunits within curli fibrils and then gold enhanced. Scale bars are 200nm.

We also used cellular biofabrication to create co-fibrils that assembled CdTe/CdS quantum dots (QDs) with gold nanoparticles, resulting in the modulation of QD fluorescence (Fig. 6). We leveraged interactions between the SpyCatcher protein and the SpyTag peptide tag[30], which results in the formation of covalent bonds, to dock QDs to fibrils displaying SpyTag. We used an orthogonal interaction between anti-FLAG antibodies and the FLAG affinity tag to dock 40nm gold particles to fibrils displaying the FLAG tag. $CsgA_{SpyTag}$ fibrils were specifically bound by SpyCatcher-conjugated CdTe/CdS QDs (QD-SpyCatcher, Supplementary Fig. 21), while $CsgA_{FLAG}$ fibrils were specifically bound by anti-FLAG antibodies which were in turn bound by 40nm gold particles conjugated with secondary antibodies (Fig. 6a). $AHL_{Receiver}$/$CsgA_{SpyTag}$ and $aTc_{Receiver}$/$CsgA_{FLAG}$ strains were co-cultured in the presence of AHL, aTc, or both AHL and aTc. In the presence of AHL, fibrils

produced by the cellular consortia only bound QD-SpyCatcher, whereas in the presence of aTc, the resulting fibrils only bound antibody-conjugated 40nm gold particles (Fig. 6b and Supplementary Fig. 18). When both inducers were present, the fibrils co-assembled QDs with gold nanoparticles (Fig. 6b). Characterization with fluorescence-lifetime imaging microscopy (FLIM) revealed that co-assemblies of QDs and gold nanoparticles had altered fluorescence lifetimes and intensities compared to assemblies of QDs alone (Fig. 6c).

These results demonstrate that the behaviour of stimuli-responsive materials can be modulated by curli fibrils patterned with engineered cells. AuNP-QD heterostructures are of interest because plasmon-exciton interactions between plasmonic AuNPs and fluorescent QDs allow for tailoring of photon emission properties. By selecting appropriate materials and architectures, one can potentially tune emission intensity, directionality, and spectral profile for a range of applications[31-34].

In addition to organizing pre-formed nanomaterials, cell-fabricated curli fibrils can be used to grow inorganic materials. To demonstrate this, we engineered a strain that produced curli fibrils displaying a ZnS-nucleating peptide ($CsgA_{ZnS\ peptide}$, Supplementary Table 1)[35]. The resulting fibrils nucleated ~5nm particles (Fig. 6d), whereas control fibrils composed of wild-type CsgA nucleated few such particles (Fig. 6e). HRTEM images revealed that the nucleated particles had a cubic zinc blende ZnS (111) structure with a typical crystalline spacing of 0.31nm (Fig. 6d). EDS analysis of elemental composition showed an approximately 1:1 ratio of zinc and sulphur (Fig. 6d). These data indicate that the particles are ZnS nanocrystals. The nanocrystals were fluorescent, with an emission peak at 490nm when excited at 405nm (Fig. 6d).

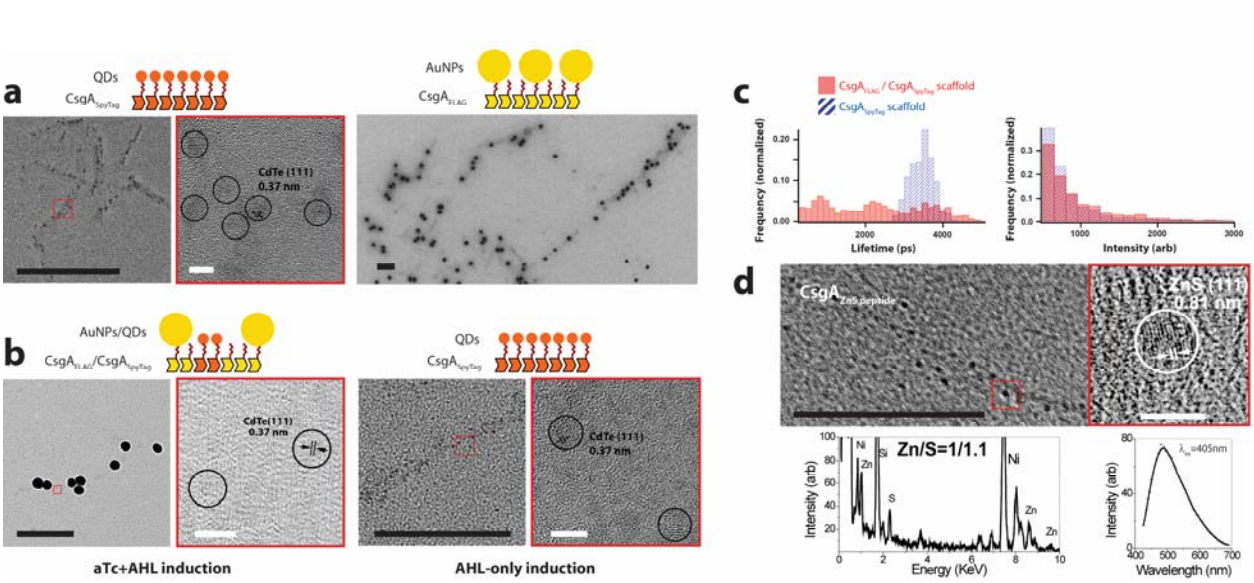

Figure 2-6 | Assembly and tuning of functional AuNP-QD heterostructures and nucleation of fluorescent ZnS QDs on cell-synthesized curli fibrils. a, $CsgA_{SpyTag}$ fibrils specifically bind CdTe/CdS QDs conjugated to the SpyCatcher protein; the CdTe cores of QDs are seen under HRTEM. $CsgA_{FLAG}$ fibrils are specifically bound by anti-FLAG antibodies which are in turn bound by 40nm AuNPs conjugated to secondary antibodies. **b,** A mixed population of $aTc_{Receiver}/CsgA_{FLAG}$ and $AHL_{Receiver}/CsgA_{SpyTag}$ cells produced curli templates for either AuNP-QD heterostructures (co-fibrils of $CsgA_{FLAG}$ and $CsgA_{SpyTag}$) or QD-only assemblies ($CsgA_{SpyTag}$ fibrils) depending on whether they were induced by both aTc and AHL, or AHL only, respectively. **c,** Cell-patterned curli fibrils enable the tuning of stimuli-responsive inorganic-organic materials. AuNP-QD assemblies patterned on $CsgA_{FLAG}/CsgA_{SpyTag}$ scaffolds (solid red bars) exhibited different fluorescence lifetime and intensity properties than QD-only assemblies patterned on $CsgA_{SpyTag}$ scaffolds (hashed blue bars). **d,** $CsgA_{ZnS\ peptide}$ fibrils nucleated ~5nm nanoparticles with a cubic zinc blende ZnS (111) structure and approximately 1:1 ratio of zinc and sulphur. The particles were

Figure 2-6 (Continued)

fluorescent, with an emission peak at 490nm when excited at 405nm. **e,** Control CsgA fibrils nucleated few such particles. In a), b), d), and e) black scale bars are 200nm and white scale bars are 5nm; the images outlined by red boxes are zoomed-in versions of the inset red boxes.

Outlook

We have shown that protein-based amyloid fibrils produced by living cells can be interfaced with different inorganic materials via a range of strategies. Beyond being a convenient model system with which to explore the applications of living systems to materials science, protein materials are of practical interest because they constitute a major class of biomaterials[36]. Protein materials can have programmable structures[37] and diverse functionalities, such as responsiveness to physicochemical stimuli[38], the ability to interact with living systems[39], and the ability to organize abiotic materials for expanded functionalities[35,40-42]. Amyloid fibrils can provide beneficial materials properties such as resistance to degradation and mechanical strength comparable to that of steel[43]. As we have shown here, amyloid fibrils assembled by cells constitute a versatile scaffold that can co-organize and synthesize fluorescent QDs as well as gold nanowires, nanorods, and nanoparticles. This approach could be generalized to include multiple CsgA variants with different functional properties and abilities to interact with various inorganic materials. In addition, curli fibrils with tunable structure and composition could be used as patterned

scaffolds for multi-enzyme systems by displaying orthogonal affinity tags on curli fibers which interact with different enzymes.

Most existing examples of protein biomaterials are assembled *in vitro* from chemically synthesized peptides or purified subunits and do not take full advantage of the fact that the materials' constituent subunits can be integrated into living cell communities. Living cells are natural platforms for engineering multiscale patterned materials because biology is organized in a hierarchical manner, from macromolecules (e.g. proteins, nucleic acids, carbohydrates, lipids) to macromolecular assemblies (synthetic variants of which are used as nanomaterials[37,44-46]) to organelles to cells and to tissues. In fact, natural biological materials such as bone are hierarchically organized to fulfil varied functional requirements[1,9]. Thus, we have demonstrated an engineered cellular platform that synthesizes and patterns self-assembling materials with controllable functionality, structure, and composition.

Using gene circuits within engineered biofilms for multiscale patterning of materials is a novel application area for synthetic biology. This work applies useful characteristics of multicellular communities to materials fabrication and builds upon previous efforts to engineer biofilms with synthetic circuits[10-16]. This strategy can be expanded to other cellular and biomaterials contexts for applications ranging from biointegrated electronic and optical devices[47-49] to tissue engineering scaffolds[50]. For example, cells designed to compute and integrate complex signals could be used to assemble functional materials in response to their environment[18,19]. These "smart" living materials could be composed of specialized cellular consortia that coordinate with each other for multi-functional materials

synthesis. Mammalian cells capable of tunable, environmentally responsive synthesis of multiscale materials could be used to mimic the dynamic microenvironment of *in vivo* extracellular matrices[51] for tissue engineering. Our demonstration of a gradient material patterned at the nanoscale and the millimetre scale could be used to biofabricate functionally graded materials[52]. Moreover, leveraging hierarchical organization from biology for multiscale patterning should complement other strategies for materials synthesis that require directed intervention[53], such as 3D printing[52]. Repeated materials-synthesis processes or environmentally switchable behaviours could be achieved by triggering biofilm disassembly[12,13,54].

In summary, by integrating synthetic gene networks in engineered cells with extracellular protein biomaterials, living materials with environmental responsiveness, tunable functionalities, multiscale patterning, and even the ability to self-heal and remodel could be realized. In such materials, there would be a division of labour between cells (providing functionalities of living systems)[55], extracellular protein materials (providing spatial patterning and structural integrity), and interfaced abiotic materials (providing functionalities of non-living systems). Thus, we envision that engineering artificial cellular consortia, such as biofilms, to synthesize and organize heterogeneous functional materials will enable the realization of smart composite materials that combine the properties of living and non-living systems.

Methods Summary

Culture conditions. Seed cultures were inoculated from glycerol stocks and grown in LB-Miller medium for 12h at 37°C. Experimental cultures were grown at 30°C in M63 minimal medium supplemented with 1mM $MgSO_4$ and with 0.2% w/v glucose or 0.2% w/v glycerol. For inducing conditions, anhydrotetracycline (Sigma) at concentrations of 1-250ng/ml and N-(β-ketocaproyl)-L-homoserine lactone (Sigma) at concentrations of 1-1000nM were used.

Anti-CsgA immuno-labelling. Rabbit anti-CsgA primary antibody (M. Chapman, University of Michigan) was used at 1:1000 dilution, goat anti-rabbit secondary antibody conjugated to 10nm gold particles (Sigma) was used at 1:10 dilution.

NiNTA-AuNP labelling. For specific binding of NiNTA-AuNP (Nanoprobes) to histidine tags displayed on curli fibrils, buffer consisting of 1X PBS with 0.487M NaCl, 80mM imidazole, and 0.2v/v% Tween20 was used.

Conductive biofilm conductance measurement. Interdigitated electrodes (IDEs) for measuring biofilm conductance were created by sputtering gold through custom shadowing masks (Tech-Etch) onto Thermanox coverslips (Nunc). IDEs were placed in 24-well plate wells and conductive biofilms grown by adding 100nM NiNTA-AuNP into culture medium. After biofilm culture, IDEs were washed by repeatedly immersing in ddH_2O, laid on a flat surface, and allowed to air dry for three days. A Keithley 4200 picoammeter with two-point probe was used to carry out a voltage sweep.

Gold nanowire and nanorod synthesis. Gold was specifically deposited on NiNTA-AuNP chains using GoldEnhance™ EM kit (Nanoprobes).

Specific binding of QD-SpyCatcher. For specific binding of CdTe/CdS-SpyCatcher to SpyTag peptide tags displayed on curli fibrils, buffer consisting of 1X PBS + 350mM NaCl + 0.3v/v% Tween20 was used.

Specific binding of antibody-conjugated 40nm AuNP. Rabbit anti-FLAG primary antibody (Sigma) was used at 1:250 dilution, goat anti-rabbit secondary antibody conjugated to 40nm AuNPs (Abcam) was used at 1:10 dilution.

Zinc sulphide nanocrystal synthesis. Fibril samples were incubated with 1μM $ZnCl_2$ at RT for 12h, followed by addition of 1μM Na_2S. Samples were then incubated at 0°C for 24h by packing in ice and placing in a 4°C room, and subsequently allowed to age for 12h at RT.

Transmission electron microscopy. Samples were deposited on 200-mesh formvar/carbon coated nickel TEM grids and stained with 2% uranyl acetate. TEM images were obtained on a FEI Tecnai Spirit transmission electron microscope operated at 80kV accelerating voltage. High-resolution transmission electron microscopy (HRTEM) and energy-dispersive X-ray spectroscopy (EDS) were performed on a JEOL 2010F electron microscope operating at 200 kV.

Scanning electron microscopy. Samples were imaged with a JEOL JSM-6010LA scanning electron microscope operated at 10kV accelerating voltage. Images were obtained in secondary electron imaging (SEI) mode, and elemental mapping was performed with energy-dispersive X-ray spectroscopy (EDS).

Fluorescence microscopy. Fluorescence-lifetime imaging microscopy (FLIM) was performed with a Zeiss 710 NLO multiphoton microscope with 20X objective and connected to a time-correlated single-photon counting system (Becker & Hickl). The excitation source was a 2-photon laser (Coherent Chameleon Vision II) tuned to 800nm, and emission was detected through a 590-650nm bandpass filter. Lambda scan analysis of fluorescent ZnS nanocrystals was performed with a Zeiss LSM 710 NLO Laser Scanning Confocal with 10X objective and 405nm excitation laser.

References

1 Fratzl, P. & Weinkamer, R. Nature's hierarchical materials. *Progress in Materials Science* **52**, 1263-1334, doi:http://dx.doi.org/10.1016/j.pmatsci.2007.06.001 (2007).

2 Kollmannsberger, P., Bidan, C. M., Dunlop, J. W. C. & Fratzl, P. The physics of tissue patterning and extracellular matrix organisation: how cells join forces. *Soft Matter* **7**, 9549-9560, doi:10.1039/c1sm05588g (2011).

3 Stevens, M. M. & George, J. H. Exploring and engineering the cell surface interface. *Science* **310**, 1135-1138, doi:10.1126/science.1106587 (2005).

4 O'Toole, G., Kaplan, H. B. & Kolter, R. Biofilm formation as microbial development. *Annu Rev Microbiol* **54**, 49-79, doi:10.1146/annurev.micro.54.1.4954/1/49 [pii] (2000).

5 Epstein, A. K., Pokroy, B., Seminara, A. & Aizenberg, J. Bacterial biofilm shows persistent resistance to liquid wetting and gas penetration. *Proc Natl Acad Sci U S A* **108**, 995-1000, doi:1011033108 [pii]10.1073/pnas.1011033108 (2011).

6 Belcher, A. M. *et al.* Control of crystal phase switching and orientation by soluble mollusc-shell proteins. *Nature* **381**, 56 - 58 (1996).

7 Su, X. W., Zhang, D. M. & Heuer, A. H. Tissue Regeneration in the Shell of the Giant Queen Conch, Strombus gigas. *Chem. Mater.* **16**, 581-593 (2004).

8 Aizenberg, J. *et al.* Skeleton of Euplectella sp.: structural hierarchy from the nanoscale to the macroscale. *Science* **309**, 275-278, doi:10.1126/science.1112255 (2005).

9 Weiner, S. & Wagner, H. D. The material bone: Structure mechanical function relations. *Annu. Rev. Mater. Sci.* **28**, 271-298, doi:10.1146/annurev.matsci.28.1.271 (1998).

10 Brenner, K. & Arnold, F. H. Self-organization, layered structure, and aggregation enhance persistence of a synthetic biofilm consortium. *PloS one* **6**, e16791, doi:10.1371/journal.pone.0016791 (2011).

11 Brenner, K., Karig, D. K., Weiss, R. & Arnold, F. H. Engineered bidirectional communication mediates a consensus in a microbial biofilm consortium. *Proceedings of the National Academy of Sciences of the United States of America* **104**, 17300-17304, doi:10.1073/pnas.0704256104 (2007).

12 Hong, S. H. *et al.* Synthetic quorum-sensing circuit to control consortial biofilm formation and dispersal in a microfluidic device. *Nature communications* **3**, 613, doi:10.1038/ncomms1616 (2012).

13 Ma, Q., Yang, Z., Pu, M., Peti, W. & Wood, T. K. Engineering a novel c-di-GMP-binding protein for biofilm dispersal. *Environmental microbiology* **13**, 631-642, doi:10.1111/j.1462-2920.2010.02368.x (2011).

14 Lee, J., Jayaraman, A. & Wood, T. K. Indole is an inter-species biofilm signal mediated by SdiA. *BMC microbiology* **7**, 42, doi:10.1186/1471-2180-7-42 (2007).

15 Payne, S. *et al.* Temporal control of self-organized pattern formation without morphogen gradients in bacteria. *Molecular systems biology* **9**, 697, doi:10.1038/msb.2013.55 (2013).

16 Payne, S. & You, L. Engineered Cell-Cell Communication and Its Applications. *Advances in biochemical engineering/biotechnology*, doi:10.1007/10_2013_249 (2013).

17 Barnhart, M. M. & Chapman, M. R. Curli biogenesis and function. *Annu Rev Microbiol* **60**, 131-147, doi:10.1146/annurev.micro.60.080805.142106 (2006).

18 Callura, J. M., Cantor, C. R. & Collins, J. J. Genetic switchboard for synthetic biology applications. *Proc Natl Acad Sci U S A* **109**, 5850-5855, doi:10.1073/pnas.1203808109 (2012).

19 Prigent-Combaret, C. *et al.* Developmental pathway for biofilm formation in curli-producing Escherichia coli strains: role of flagella, curli and colanic acid. *Environmental microbiology* **2**, 450-464 (2000).

20 Vidal, O. *et al.* Isolation of an Escherichia coli K-12 mutant strain able to form biofilms on inert surfaces: involvement of a new ompR allele that increases curli expression. *Journal of bacteriology* **180**, 2442-2449 (1998).

21 Hung, C. *et al.* Escherichia coli biofilms have an organized and complex extracellular matrix structure. *mBio* **4**, e00645-00613, doi:10.1128/mBio.00645-13 (2013).

22 Wang, X., Hammer, N. D. & Chapman, M. R. The molecular basis of functional bacterial amyloid polymerization and nucleation. *The Journal of biological chemistry* **283**, 21530-21539, doi:10.1074/jbc.M800466200 (2008).

23 Basu, S., Gerchman, Y., Collins, C. H., Arnold, F. H. & Weiss, R. A synthetic multicellular system for programmed pattern formation. *Nature* **434**, 1130-1134, doi:nature03461[pii]10.1038/nature03461 (2005).

24 Bacchus W, L. M., El-Baba MD, Weber W, Stelling J, Fussenegger M. Synthetic two-way communication between mammalian cells. *Nat Biotechnol.* **30**, 991-996 (2012).

25 Tabor, J. J. *et al.* A synthetic genetic edge detection program. *Cell* **137**, 1272-1281, doi:S0092-8674(09)00509-1 [pii]10.1016/j.cell.2009.04.048 (2009).

26 Liu, C. *et al.* Sequential establishment of stripe patterns in an expanding cell population. *Science* **334**, 238-241, doi:10.1126/science.1209042 (2011).

27 Jang, B., Park, J. Y., Tung, C. H., Kim, I. H. & Choi, Y. Gold nanorod-photosensitizer complex for near-infrared fluorescence imaging and photodynamic/photothermal therapy in vivo. *ACS nano* **5**, 1086-1094, doi:10.1021/nn102722z (2011).

28 Dreaden, E. C. *et al.* Small molecule-gold nanorod conjugates selectively target and induce macrophage cytotoxicity towards breast cancer cells. *Small* **8**, 2819-2822, doi:10.1002/smll.201200333 (2012).

29 Libutti, S. K. *et al.* Phase I and pharmacokinetic studies of CYT-6091, a novel PEGylated colloidal gold-rhTNF nanomedicine. *Clinical cancer research : an official journal of the American Association for Cancer Research* **16**, 6139-6149, doi:10.1158/1078-0432.CCR-10-0978 (2010).

30 Zakeri, B. *et al.* Peptide tag forming a rapid covalent bond to a protein, through engineering a bacterial adhesin. *Proceedings of the National Academy of Sciences of the United States of America* **109**, E690-697, doi:10.1073/pnas.1115485109 (2012).

31 Polman, A. & Atwater, H. A. Photonic design principles for ultrahigh-efficiency photovoltaics. *Nat Mater* **11**, 174-177, doi:Doi 10.1038/Nmat3263 (2012).

32 Reineck, P. *et al.* A Solid-State Plasmonic Solar Cell via Metal Nanoparticle Self-Assembly. *Adv Mater* **24**, 4750-4755, doi:DOI 10.1002/adma.201200994 (2012).

33 Curto, A. G. *et al.* Unidirectional Emission of a Quantum Dot Coupled to a Nanoantenna. *Science* **329**, 930-933, doi:DOI 10.1126/science.1191922 (2010).

34 Yuan, Z. L. *et al.* Electrically driven single-photon source. *Science* **295**, 102-105, doi:DOI 10.1126/science.1066790 (2002).

35 Mao, C. *et al.* Viral assembly of oriented quantum dot nanowires. *Proceedings of the National Academy of Sciences of the United States of America* **100**, 6946-6951, doi:10.1073/pnas.0832310100 (2003).

36 Zhang, S. G. Fabrication of novel biomaterials through molecular self-assembly. *Nature biotechnology* **21**, 1171-1178, doi:10.1038/nbt874 (2003).

37 King, N. P. *et al.* Computational design of self-assembling protein nanomaterials with atomic level accuracy. *Science* **336**, 1171-1174, doi:10.1126/science.1219364 (2012).

38 Mart, R. J., Osborne, R. D., Stevens, M. M. & Ulijn, R. V. Peptide-based stimuli-responsive biomaterials. *Soft Matter* **2**, 822-835, doi:10.1039/b607706d (2006).

39 Webber, M. J. *et al.* Supramolecular nanostructures that mimic VEGF as a strategy for ischemic tissue repair. *Proceedings of the National Academy of Sciences of the United States of America* **108**, 13438-13443, doi:10.1073/pnas.1016546108 (2011).

40 So, C. R., Tamerler, C. & Sarikaya, M. Adsorption, diffusion, and self-assembly of an engineered gold-binding peptide on Au(111) investigated by atomic force microscopy. *Angew Chem Int Ed Engl* **48**, 5174-5177, doi:10.1002/anie.200805259 (2009).

41 Channon, K. J., Devlin, G. L. & MacPhee, C. E. Efficient energy transfer within self-assembling peptide fibers: a route to light-harvesting nanomaterials. *Journal of the American Chemical Society* **131**, 12520-12521, doi:10.1021/ja902825j (2009).

42 Scheibel, T. *et al.* Conducting nanowires built by controlled self-assembly of amyloid fibers and selective metal deposition. *Proc Natl Acad Sci U S A* **100**, 4527-4532, doi:10.1073/pnas.0431081100 [pii] (2003).

43 Smith, J. F., Knowles, T. P., Dobson, C. M., Macphee, C. E. & Welland, M. E. Characterization of the nanoscale properties of individual amyloid fibrils. *Proc Natl Acad Sci U S A* **103**, 15806-15811, doi:0604035103 [pii]10.1073/pnas.0604035103 (2006).

44 Felgner, P. L. *et al.* Lipofection: a highly efficient, lipid-mediated DNA-transfection procedure. *Proceedings of the National Academy of Sciences of the United States of America* **84**, 7413-7417 (1987).

45 Winfree, E., Liu, F., Wenzler, L. A. & Seeman, N. C. Design and self-assembly of two-dimensional DNA crystals. *Nature* **394**, 539-544, doi:10.1038/28998 (1998).

46 Rothemund, P. W. Folding DNA to create nanoscale shapes and patterns. *Nature* **440**, 297-302, doi:10.1038/nature04586 (2006).

47 Tian, B. *et al.* Macroporous nanowire nanoelectronic scaffolds for synthetic tissues. *Nature materials* **11**, 986-994, doi:10.1038/nmat3404 (2012).

48 Hwang, S. W. *et al.* A physically transient form of silicon electronics. *Science* **337**, 1640-1644, doi:10.1126/science.1226325 (2012).

49 Amsden, J. J. *et al.* Rapid nanoimprinting of silk fibroin films for biophotonic applications. *Adv Mater* **22**, 1746-1749, doi:10.1002/adma.200903166 (2010).

50 Lutolf, M. P. & Hubbell, J. A. Synthetic biomaterials as instructive extracellular microenvironments for morphogenesis in tissue engineering. *Nature biotechnology* **23**, 47-55, doi:10.1038/nbt1055 (2005).

51 Prewitz, M. C. *et al.* Tightly anchored tissue-mimetic matrices as instructive stem cell microenvironments. *Nature methods* **10**, 788-794, doi:10.1038/nmeth.2523 (2013).

52 Chiu, W. K. & Yu, K. M. Direct digital manufacturing of three-dimensional functionally graded material objects. *Computer-Aided Design* **40**, 1080–1093 (2008).

53 Xia, Y., Rogers, J. A., Paul, K. E. & Whitesides, G. M. Unconventional Methods for Fabricating and Patterning Nanostructures. *Chemical reviews* **99**, 1823-1848 (1999).

54 Kolodkin-Gal, I. *et al.* D-amino acids trigger biofilm disassembly. *Science* **328**, 627-629, doi:10.1126/science.1188628 (2010).

55 Gubeli, R. J., Burger, K. & Weber, W. Synthetic biology for mammalian cell technology and materials sciences. *Biotechnology advances* **31**, 68-78, doi:10.1016/j.biotechadv.2012.01.007 (2013).

Appendix

Supplementary Figures

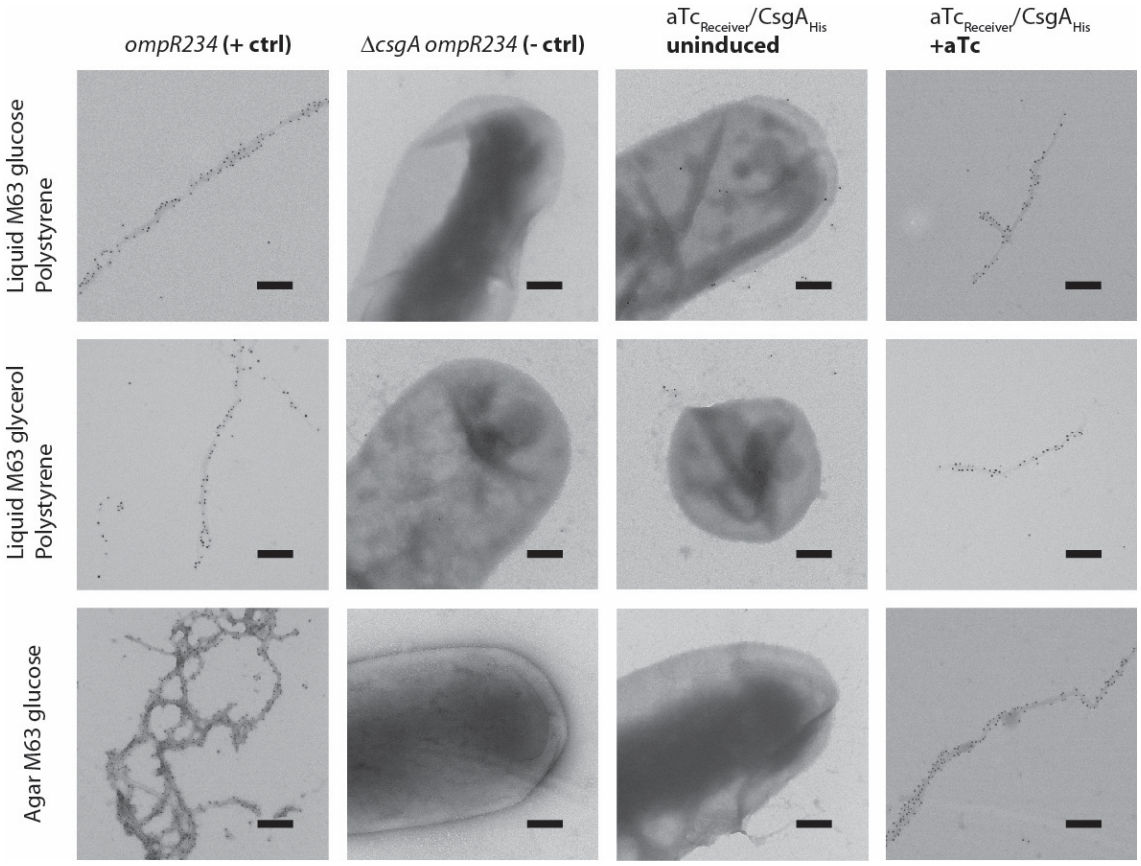

Supplementary Figure A-1 | Immuno-labelling of curli fibrils with rabbit anti-CsgA antibodies and gold-conjugated goat anti-rabbit antibodies. This data shows that *E. coli* MG1655 *ompR234* cells ("*ompR234*", see Supplementary Table 3), which have an intact endogenous *csgA* gene, produce curli fibrils that are labelled by anti-CsgA antibodies and attached to cells. However, cells with the *csgA* gene knocked out and no *csgA*-expressing circuits ("Δ*csgA ompR234*", see Supplementary Table 3), and $aTc_{Receiver}/CsgA_{His}$ cells in the absence of aTc, did not produce curli fibrils. Inducing $aTc_{Receiver}/CsgA_{His}$ cells with aTc enabled the production of curli fibrils that were labelled by anti-CsgA antibodies and attached to cells. This was the case for all culture conditions used (see Supplementary Methods): liquid M63 with glucose on Thermanox

Supplementary Figure A-1 (Continued)

(Fig. 1b), liquid M63 with glucose on polystyrene, liquid M63 with glycerol on polystyrene, and M63 with glucose in 0.7% agar. Scale bars are 200nm.

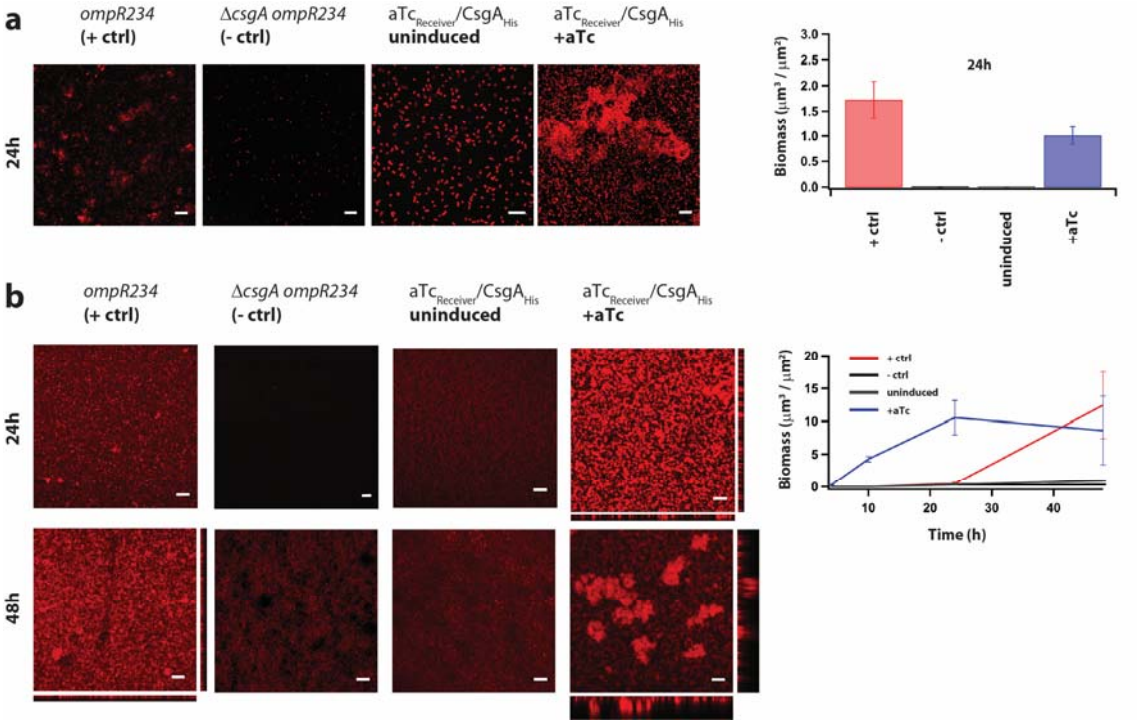

Supplementary Figure A-2 | a, Confocal microscopy and biomass quantification revealed that under static culture conditions with liquid M63 media containing glycerol, *E. coli* MG1655 *ompR234* ("*ompR234*"), which has an intact endogenous *csgA* gene, formed thick adherent biofilms. However, cells with the *csgA* gene knocked out and no *csgA*-expressing circuits ("Δ*csgA ompR234*"), and $aTc_{Receiver}/CsgA_{His}$ cells in the absence of aTc, did not form biofilms. In contrast, inducing $aTc_{Receiver}/CsgA_{His}$ cells with aTc resulted in the formation of thick adherent biofilms. **b,** Confocal microscopy and biomass quantification revealed similar biofilm-forming capabilities by MG1655 *ompR234* and induced $aTc_{Receiver}/CsgA_{His}$ cells when grown in flow cells with liquid M63 media containing glycerol. In this figure, a) and b) are complementary experiments to those shown in Fig. 1c and 1d, which used liquid M63 media with glucose; here, we used liquid M63 media with glycerol. To enable visualization, we transformed a constitutive mCherry-expressing plasmid into all strains (see Supplementary Methods). Orthogonal XZ and YZ views are maximum-intensity projections. Scale bars are 50μm.

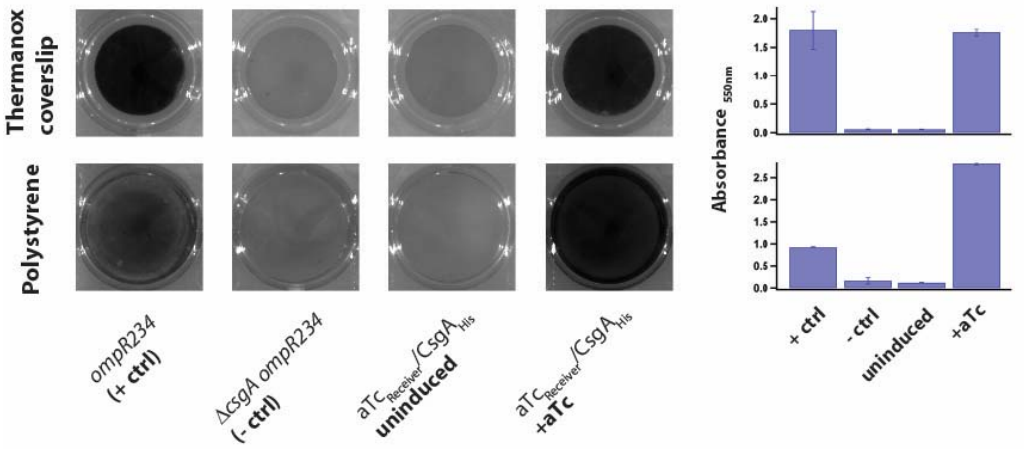

Supplementary Figure A-3 | Crystal Violet (CV) staining revealed that under static culture conditions with liquid M63 containing glucose, no biofilms were formed by $aTc_{Receiver}/CsgA_{His}$ cells in the absence of aTc, or by cells with the *csgA* gene knocked out (MG1655 *PRO* Δ*csgA ompR234*). In contrast, adherent biofilms are formed by $aTc_{Receiver}/CsgA_{His}$ cells in the presence of aTc, and by *E. coli* MG1655 *ompR234*. CV staining was quantified by absorbance at 550nm.

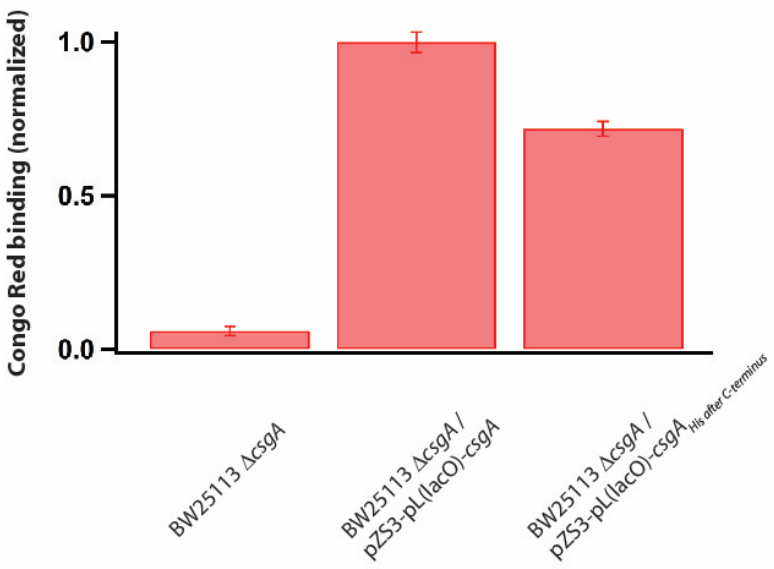

Supplementary Figure A-4 | Quantitative Congo Red (CR) binding assay of BW25113 Δ*csgA* cells, cells expressing CsgA (BW25113 Δ*csgA* / pZS3-pL(lacO)-*csgA*), and cells expressing CsgA with a His tag fused to the C-terminus (BW25113 Δ*csgA* / pZS3-pL(lacO)-*csgA*$_{His\ after\ C\text{-}terminus}$) shows that CsgA maintains ability to form amyloid fibrils after fusion of peptides to the C-terminus.

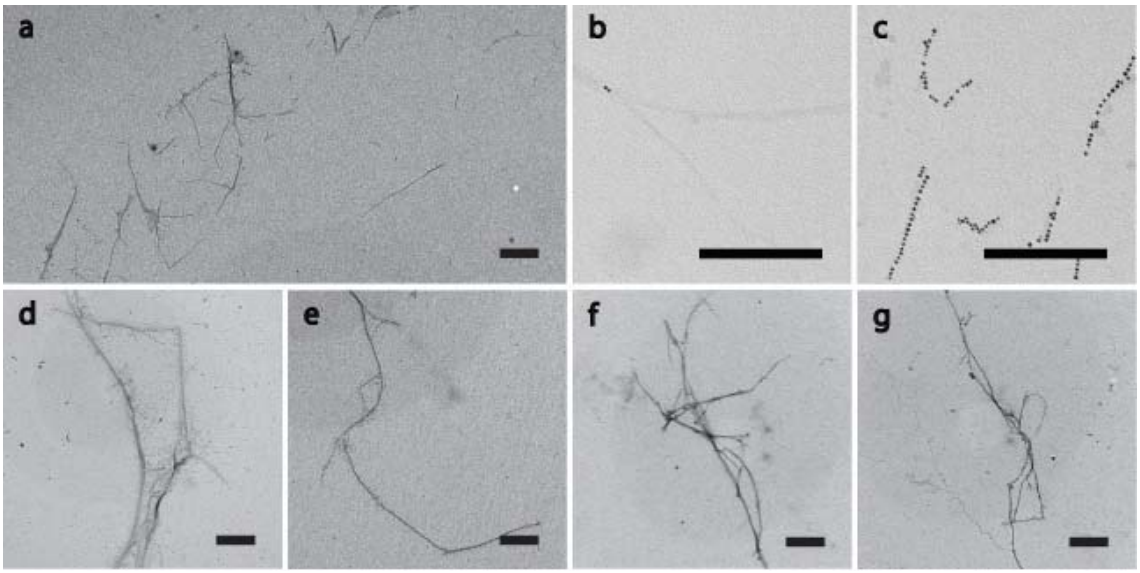

Supplementary Figure A-5 | Fibrils imaged with TEM are CsgA-based fibrils and histidine tag addition to CsgA does not interfere with fibril production. Histidine tags confer specific NiNTA gold particle (NiNTA-AuNP) binding functionality. Fibrils produced by engineered cell strains grown with chemical induction (**b-g**) have similar morphology to CsgA-based curli fibrils described in Chapman *et al.*[1] as well as **a,** curli fibrils produced by *E. coli* MG1655 *ompR234*. **b,** There was no specific labelling of CsgA fibrils with NiNTA-AuNPs in the absence of histidine tags on CsgA (fibrils produced by induced $aTc_{Receiver}$/CsgA cells). **c,** Curli fibrils were specifically labelled by NiNTA-AuNPs when histidine tags were added to CsgA (fibrils produced by induced $aTc_{Receiver}$/$CsgA_{His}$ cells). Furthermore, histidine tag addition to CsgA did not interfere with curli fibril production. **d,** Engineered cells expressing CsgA when induced by AHL ($AHL_{Receiver}$/CsgA) produced fibrils, as did **e,** engineered cells expressing $CsgA_{His}$ when

Supplementary Figure A-5 (Continued)

induced by AHL ($AHL_{Receiver}$/$CsgA_{His}$). **f,** Engineered cells expressing CsgA when induced by aTc ($aTc_{Receiver}$/CsgA) produced fibrils, as did **g,** engineered cells expressing $CsgA_{His}$ when induced by aTc ($aTc_{Receiver}$/$CsgA_{His}$). Scale bars are 200nm.

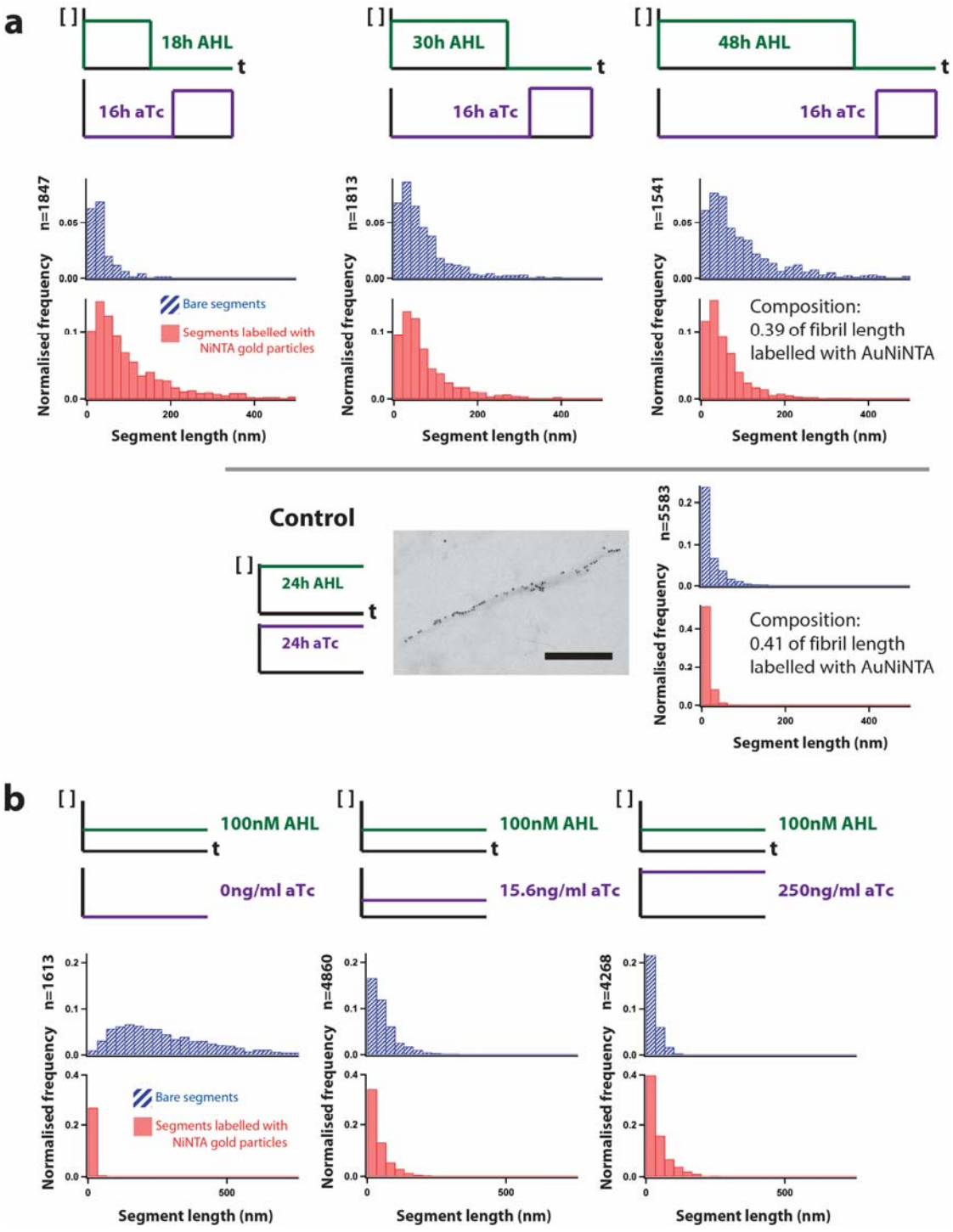

Supplementary Figure A-6 | Tuning the length distribution of CsgA and $CsgA_{His}$ blocks by changing temporal interval lengths and amplitudes of input signals. **a,** Histogram data corresponding to TEM images in Fig. 2b. The segments in block co-fibrils were longer than those in co-fibrils assembled when CsgA and $CsgA_{His}$ were secreted

Supplementary Figure A-6 (Continued)

simultaneously with no temporal separation (Control), even though both types of materials had similar ratios of CsgA to $CsgA_{His}$. Scale bar is 200nm. **b,** Histogram data corresponding to TEM images in Fig. 2d. Hashed blue bars indicate bare segments of amyloid fibrils that were unlabelled by NiNTA-AuNPs, while solid red bars indicate amyloid fibril segments labelled with NiNTA-AuNPs.

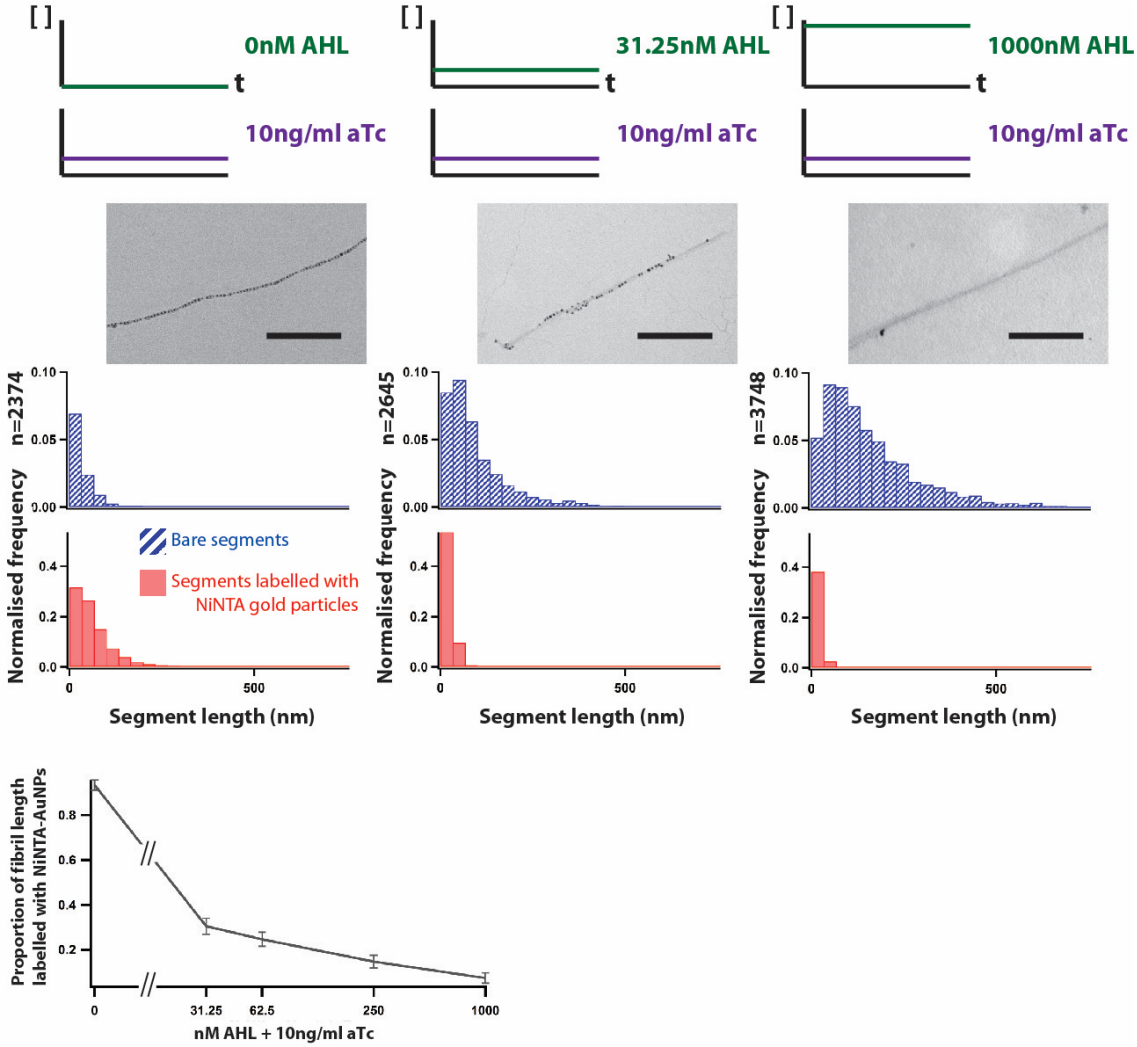

Supplementary Figure A-7 | Conversion of chemical inducer amplitude to material structure and composition. Complementary experiment to that described in Fig. 2d. With synthetic gene circuits, cells can translate the amplitude of input signals into nanoscale structure and composition of block co-fibrils. AHL induces secretion of CsgA from $AHL_{Receiver}$/CsgA, while at the same time, aTc induces secretion of $CsgA_{His}$ from $aTc_{Receiver}$/$CsgA_{His}$. We tuned the length distributions of the CsgA and $CsgA_{His}$ blocks, as well as the relative proportions of CsgA and $CsgA_{His}$, by changing the relative concentration of simultaneously applied AHL and aTc inducers. Hashed blue bars indicate bare segments of amyloid fibrils that were unlabelled, while solid red bars

Supplementary Figure A-7 (Continued)

indicate amyloid fibril segments labelled with NiNTA-AuNPs. Solid grey line indicates the proportion of fibril length labelled by NiNTA-AuNPs. Scale bars are 200nm.

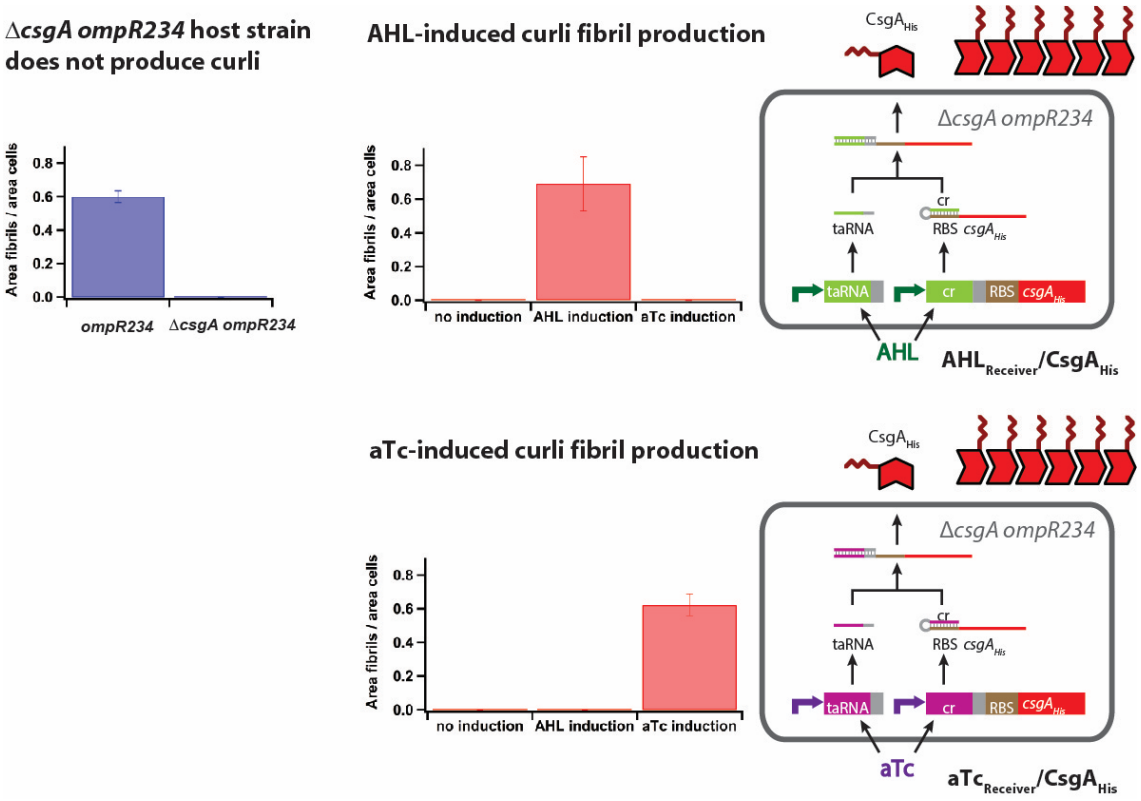

Supplementary Figure A-8 | Engineered *E. coli* only produce curli fibrils when induced by the correct inducer. The curli knockout host strain used to create engineered inducer-responsive strains, *E. coli* MG1655 *PRO ΔcsgA ompR234* ("*ΔcsgA ompR234*"), does not produce curli fibrils. In contrast, the *E. coli* MG1655 *ompR234* ("*ompR234*") strain does. The AHL-responsive engineered strain ($AHL_{Receiver}$/$CsgA_{His}$) only produces curli fibrils when induced by AHL. The aTc-responsive engineered strain ($aTc_{Receiver}$/$CsgA_{His}$) only produces curli fibrils when induced by aTc. Curli fibril production was quantified by taking the ratio of area of fibrils to area of cells in TEM images analysed by ImageJ.

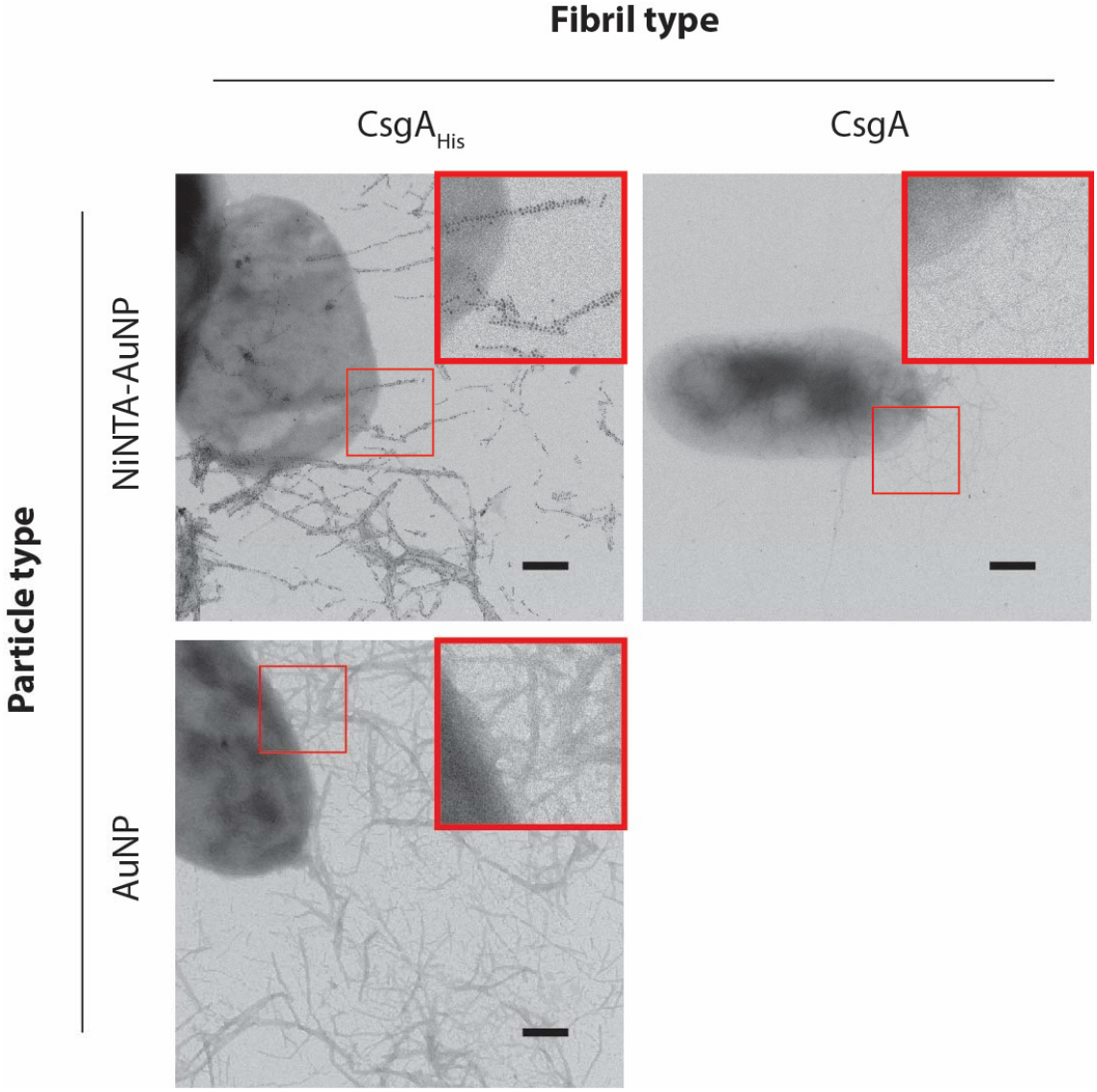

Supplementary Figure A-9 | The interaction between NiNTA-AuNPs and His-tagged curli fibrils is specific. His-tagged CsgA fibrils (CsgA$_{His}$) bound NiNTA-AuNPs but wild-type CsgA fibrils did not, indicating that the His tag was necessary for this interaction. Moreover, gold particles without NiNTA conjugation (AuNP) did not bind His-tagged CsgA fibrils, indicating that NiNTA groups were also required for this interaction. The images outlined by thick red boxes are zoomed-in versions of regions outlined by the smaller red boxes. Scale bars are 200nm.

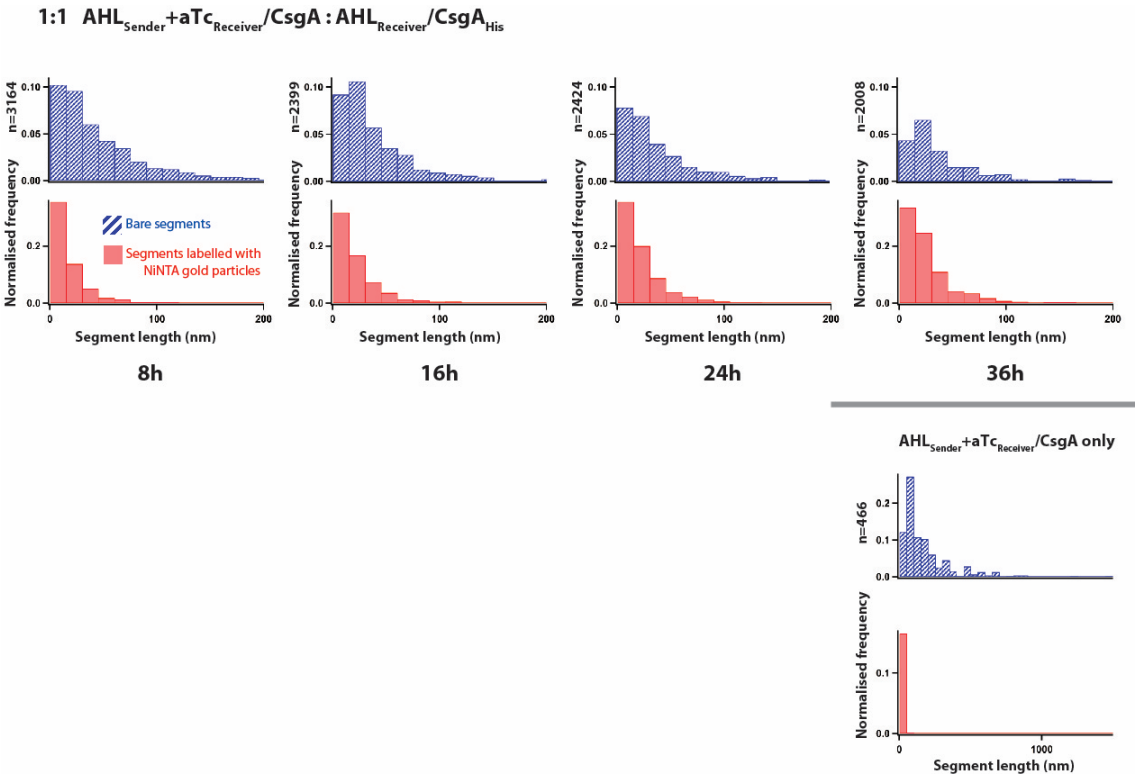

Supplementary Figure A-10 | Histogram data corresponding to the TEM images in Fig. 3b. This data shows that the length distribution of CsgA and CsgA$_{His}$ blocks changed with time when curli synthesis was regulated by autonomous cellular communication circuits. Hashed blue bars indicate bare segments of amyloid fibrils that were unlabelled by NiNTA-AuNPs, while solid red bars indicate amyloid fibril segments labelled with NiNTA-AuNPs.

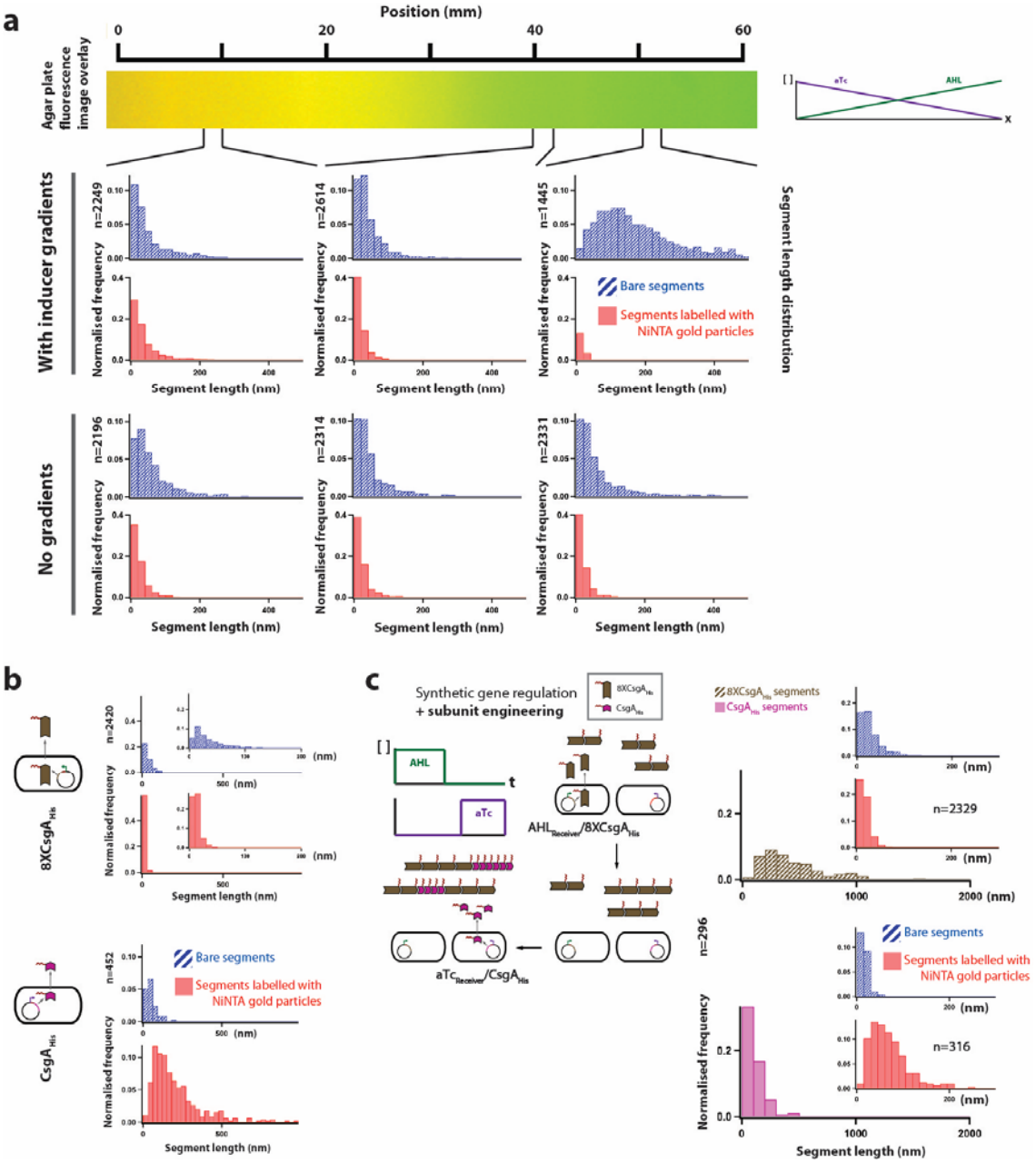

Supplementary Figure A-11 | a, Histogram data corresponding to TEM images in Fig. 4b. This data shows that the length distribution of CsgA and CsgA$_{His}$ blocks changed across the agar plate when inducer concentration gradients were present, but not in the absence of gradients. Hashed blue bars indicate bare segments of amyloid fibrils that were unlabelled by NiNTA-AuNPs, while solid red bars indicate amyloid fibril segments labelled with NiNTA-AuNPs. **b,** Histogram data corresponding to TEM images in Fig. 4c.

Supplementary Figure A-11 (Continued)

This data shows that $CsgA_{His}$ and $8XCsgA_{His}$ fibrils organized NiNTA-AuNPs in different distributions. Hashed blue bars indicate bare segments of amyloid fibrils that were unlabelled by NiNTA-AuNPs, while solid red bars indicate amyloid fibril segments labelled with NiNTA-AuNPs. **c,** Histogram data corresponding to TEM images in Fig. 4d. The length distributions of $8XCsgA_{His}$ segments and $CsgA_{His}$ segments are shown in histograms with hashed brown bars and solid amethyst bars, respectively. Inset histograms show the length distributions of unlabelled segments (hashed blue bars) and segments labelled with NiNTA-AuNPs (solid red bars) for both the $8XCsgA_{His}$ segments and the $CsgA_{His}$ segments.

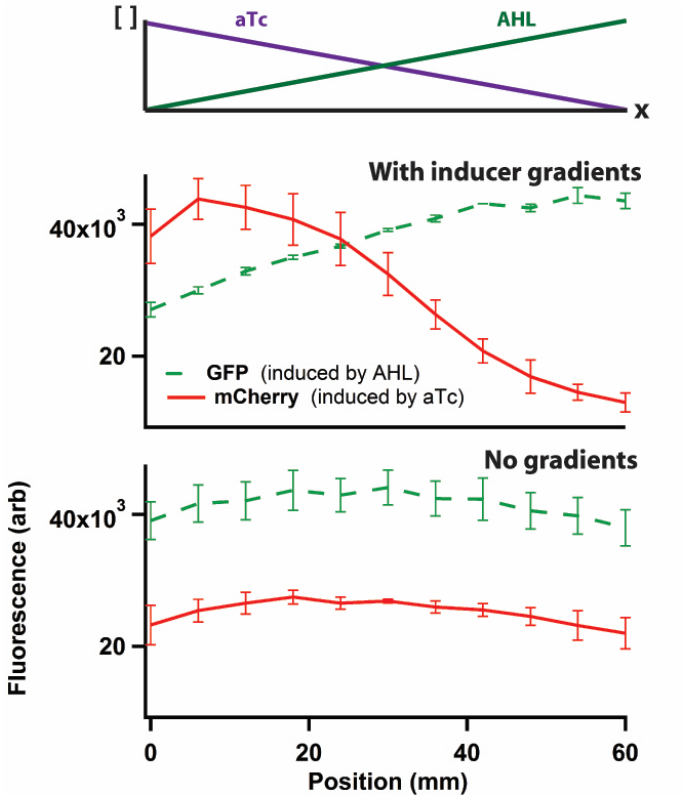

Supplementary Figure A-12 | Inducer gradient visualization for agar plates described in Fig. 4a and Fig. 4b. Top-agar-embedded $AHL_{Receiver}$/GFP reporter cells (dashed green lines) and $aTc_{Receiver}$/mCherry reporter cells (solid red lines) enabled the visualization of inducer concentration gradients across the agar plate.

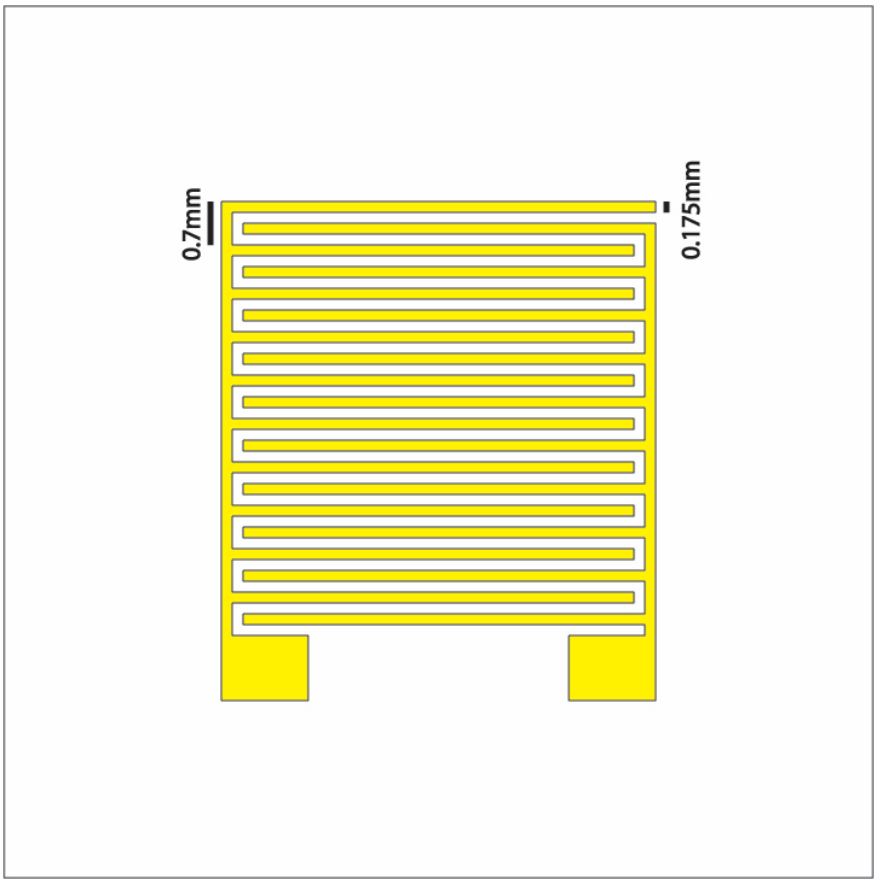

Supplementary Figure A-13 | Shadowing mask used to make interdigitated electrodes. The two continuous yellow regions represent holes in the mask through which gold was shadowed to create the electrodes.

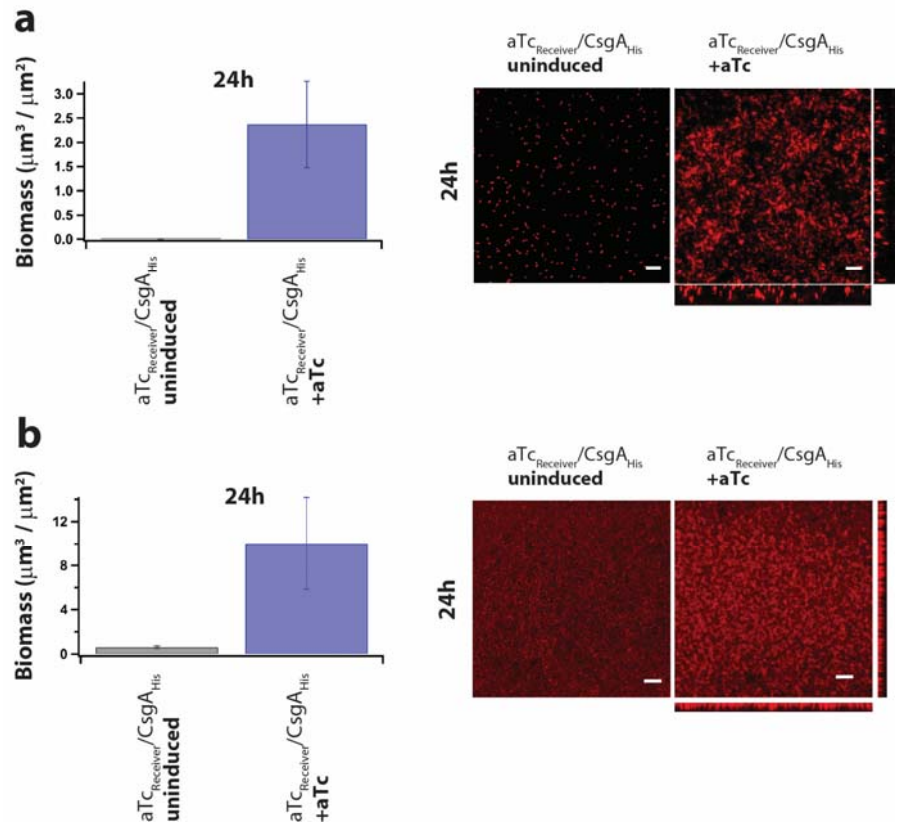

Supplementary Figure A-14 | a, Confocal microscopy and biomass quantification revealed thick biofilms formed by aTc-induced $aTc_{Receiver}/CsgA_{His}$ cells by 24 hours when grown with 100nM NiNTA-AuNP in liquid M63 media containing glucose, under static culture conditions. To enable visualization, we transformed a constitutive mCherry-expressing plasmid into this strain (see Supplementary Methods). **b,** The same was observed under flow conditions. Scale bars are 50μm.

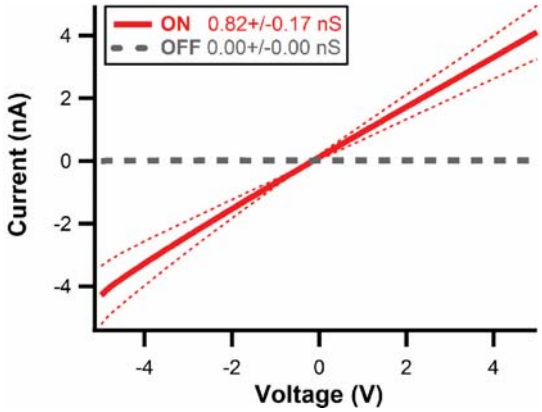

Supplementary Figure A-15 | The aTc-induced 'ON' state for $aTc_{Receiver}/CsgA_{His}$ biofilms exhibited a conductance of 0.82±0.17 (s.e.m.) nS (solid red line), while the 'OFF' state had no measureable conductance (dashed grey line).

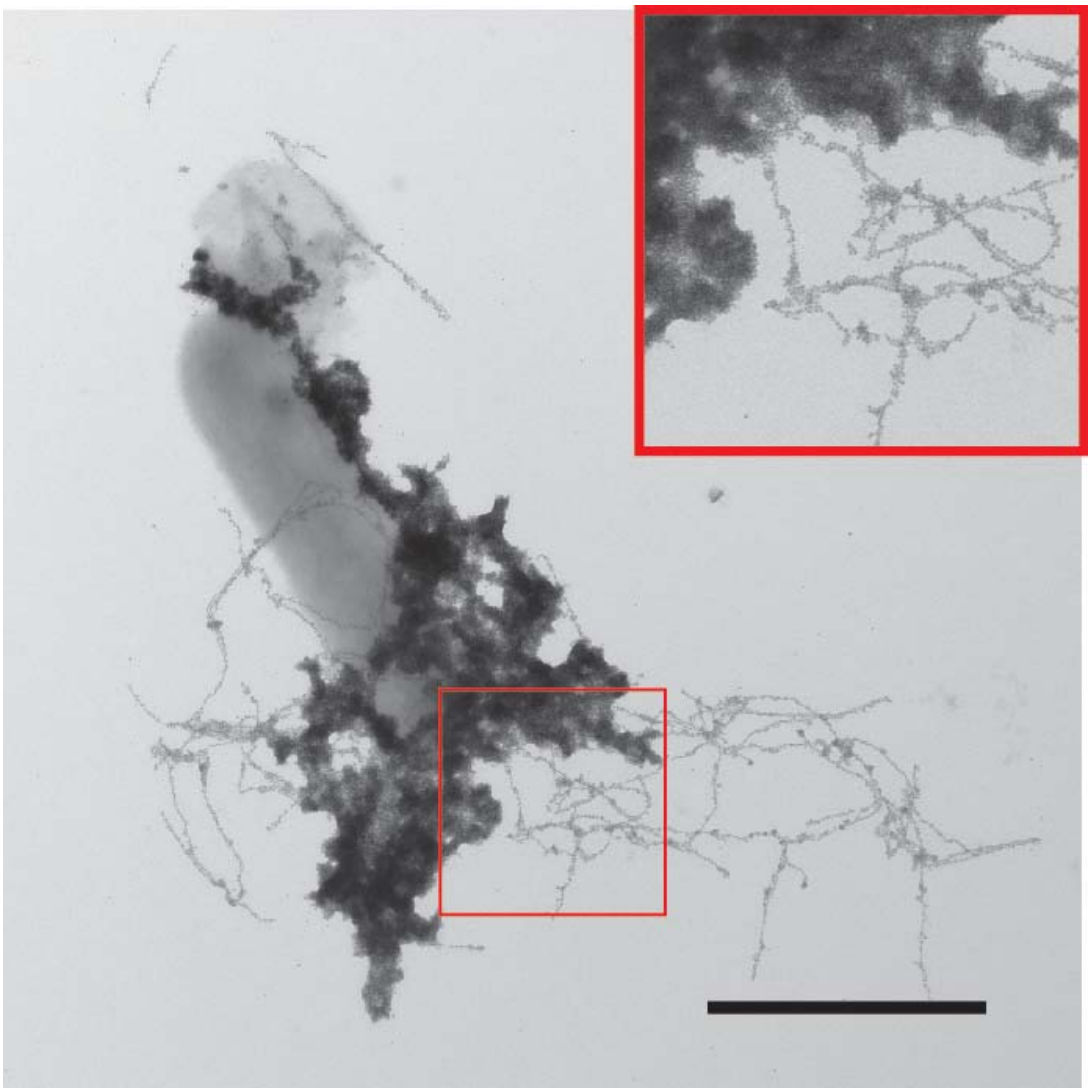

Supplementary Figure A-16 | TEM shows that aTc-induced $aTc_{Receiver}$/$CsgA_{His}$ cells produced curli fibrils that organized NiNTA-AuNPs into dense networks (the 'ON' state). This is complementary data to TEM images show in Fig. 5b. The image outlined by the thick red box is a zoomed-in version of the region outlined by the small red box. Scale bar is 1 m.

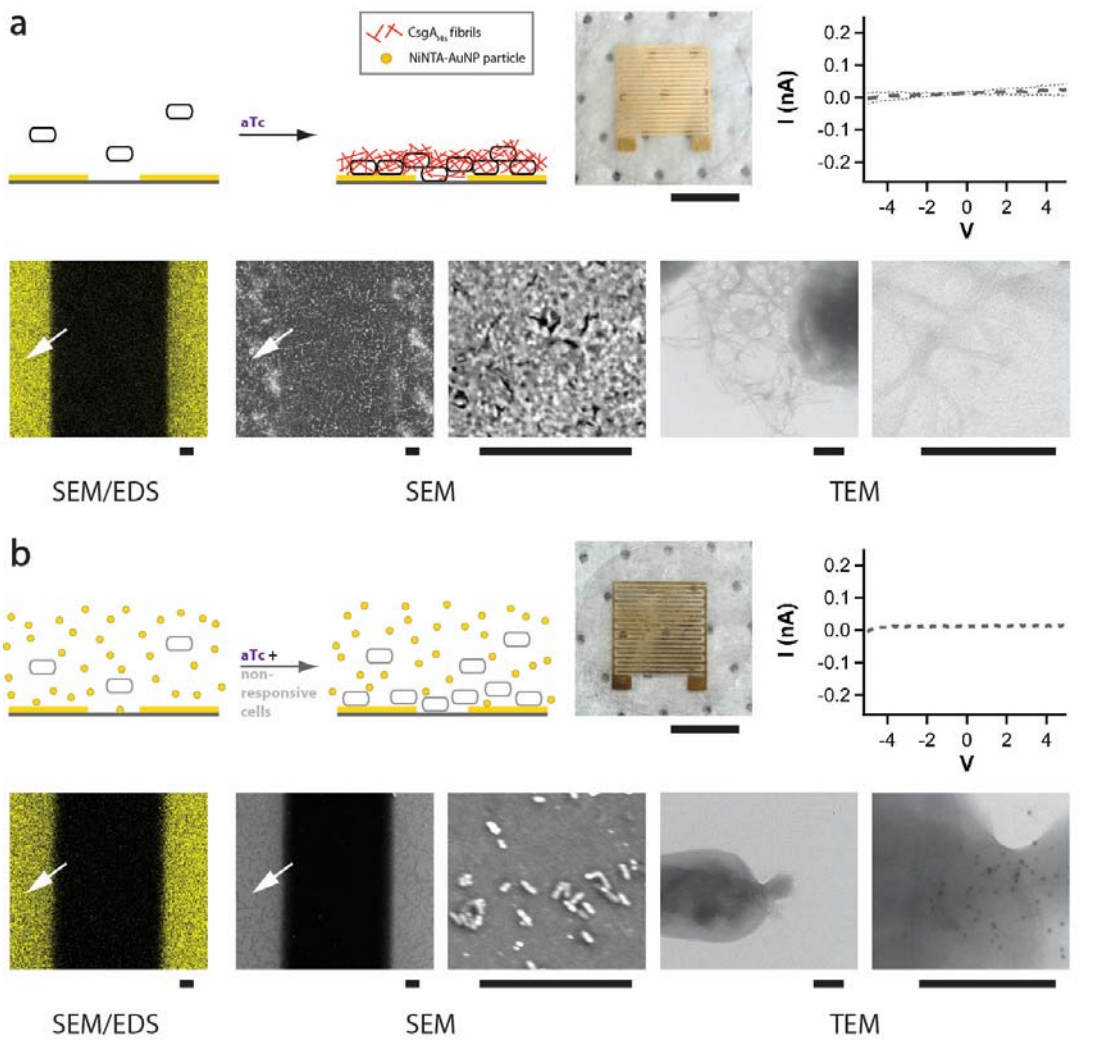

Supplementary Figure A-17 | Additional negative controls for chemical-inducer-switchable conductive biofilms show in Figure 5. **a,** When aTc$_{Receiver}$/CsgA$_{His}$ biofilms were grown with aTc induction but without NiNTA-AuNPs, conductance was 2.4±3.5 (s.e.m.) pS. SEM/EDS showed no gold networks connecting electrodes (white arrows) even though SEM imaging showed that thick biofilms spanned electrodes. TEM imaging showed that curli fibrils were present, but without gold particles. **b,** Populations of cells which do not respond to aTc (AHL$_{Receiver}$/CsgA$_{His}$) were not conductive in the presence of aTc and NiNTA-AuNPs. SEM/EDS showed no gold networks connecting electrodes and SEM imaging showed only scattered cells in the gap between electrodes. TEM

Supplementary Figure A-17 (Continued)

imaging showed no curli fibrils and only scattered, isolated gold particles. Scale bars of digital photographs are 5mm, scale bars of scanning electron micrographs are 20□m, and scale bars of transmission electron micrographs are 200nm.

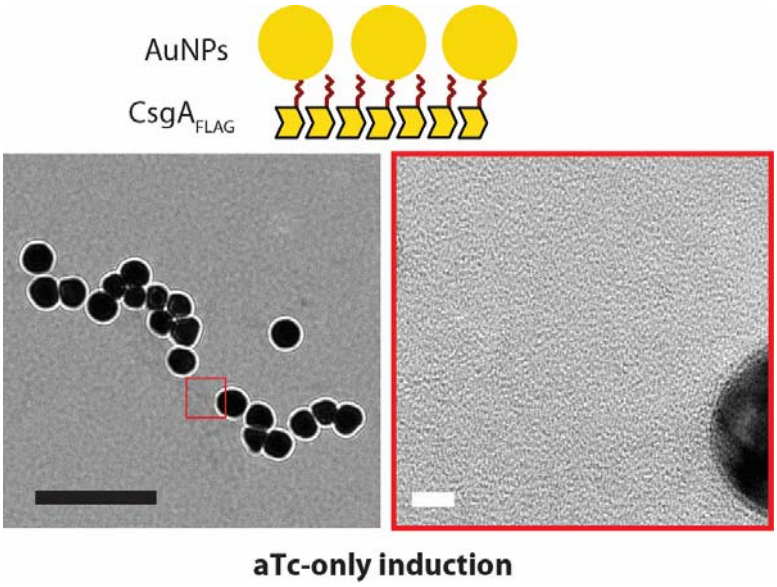

Supplementary Figure A-18 | A mixed population of aTc$_{Receiver}$/CsgA$_{FLAG}$ and AHL$_{Receiver}$/CsgA$_{SpyTag}$ cells produced curli templates for AuNP-only assemblies (CsgA$_{FLAG}$ fibrils) when induced by aTc only. FLAG tags displayed on fibrils specifically bound anti-FLAG antibodies which were in turn bound by AuNPs conjugated to secondary antibodies. The image on the right is the zoomed-in version of the inset red box on the left. Black scale bars are 200nm and white scale bars are 5nm.

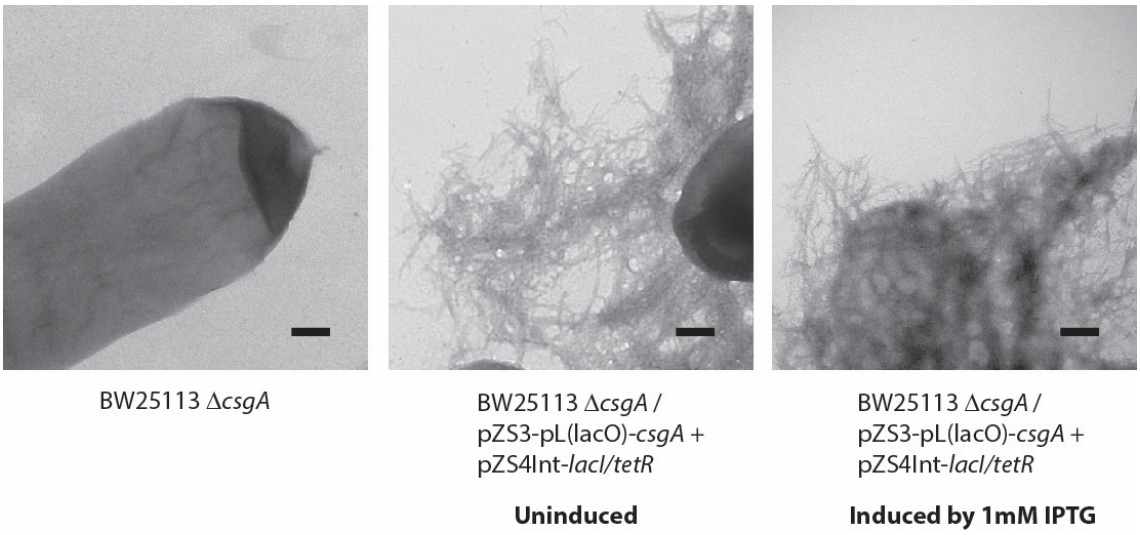

Supplementary Figure A-19 | Synthetic riboregulators enable tight regulation of curli subunit expression, which is important for patterning (Figs. 2-4). When the only means of control of *csgA* gene expression was a pL(lacO) promoter controlling the downstream *csgA* gene (with no riboregulators) in cells expressing the LacI repressor (BW25113 Δ*csgA* / pZS3-pL(lacO)-*csgA* + pZS4Int-*lacI/tetR*), curli fibrils were seen in the absence as well as in the presence of IPTG inducer, making such a system not suitable for patterning. Scale bars are 200nm.

Supplementary Figure A-20 | Sequencing results of the PCR product from the *csgBAC* operon of *E. coli* MG1655 *PRO ΔcsgA ompR234* show that *csgA* was deleted and replaced by a scar sequence, while *csgB* and *csgC* are intact. Moreover, the promoter for *csgB* is present. **a,** The zoomed-out sequencing results showing an overview of the sequenced operon. **b,** The zoomed-in sequencing results showing the underlying DNA sequences. The consensus sequence obtained from integrating three sequencing reactions is the sequence above the green bar. The sequence just below the green bar represents the reference sequence, which is further annotated with yellow, grey, and green arrows representing genes, FRT sites, and promoter elements, respectively. The green bar below the consensus sequence indicates that the sequencing results match the reference sequence.

a

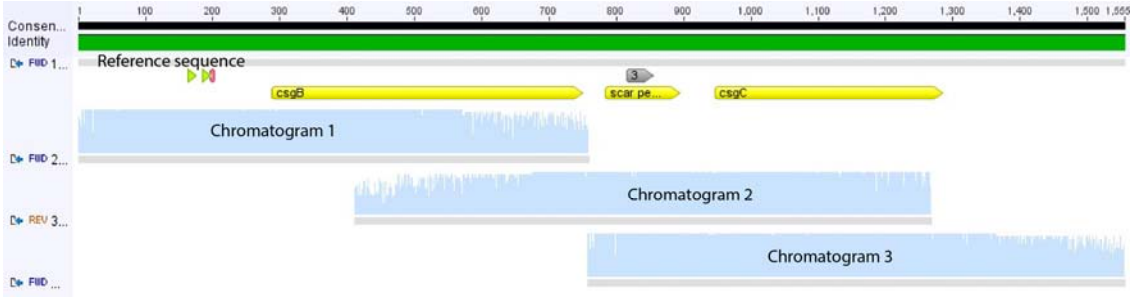

b

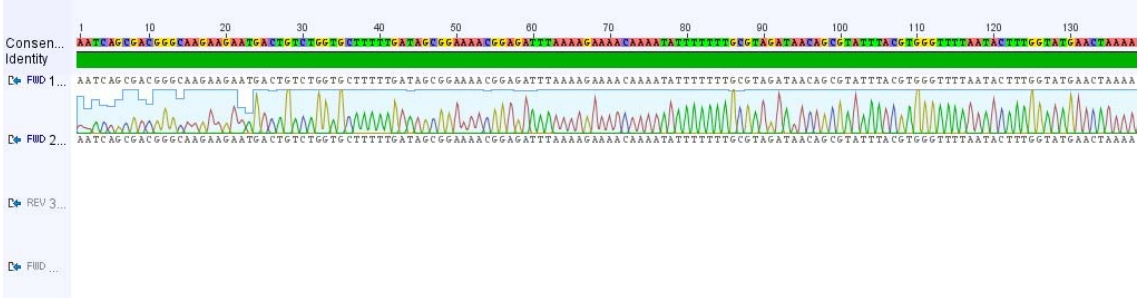

Supplementary Figure A-20 (Continued)

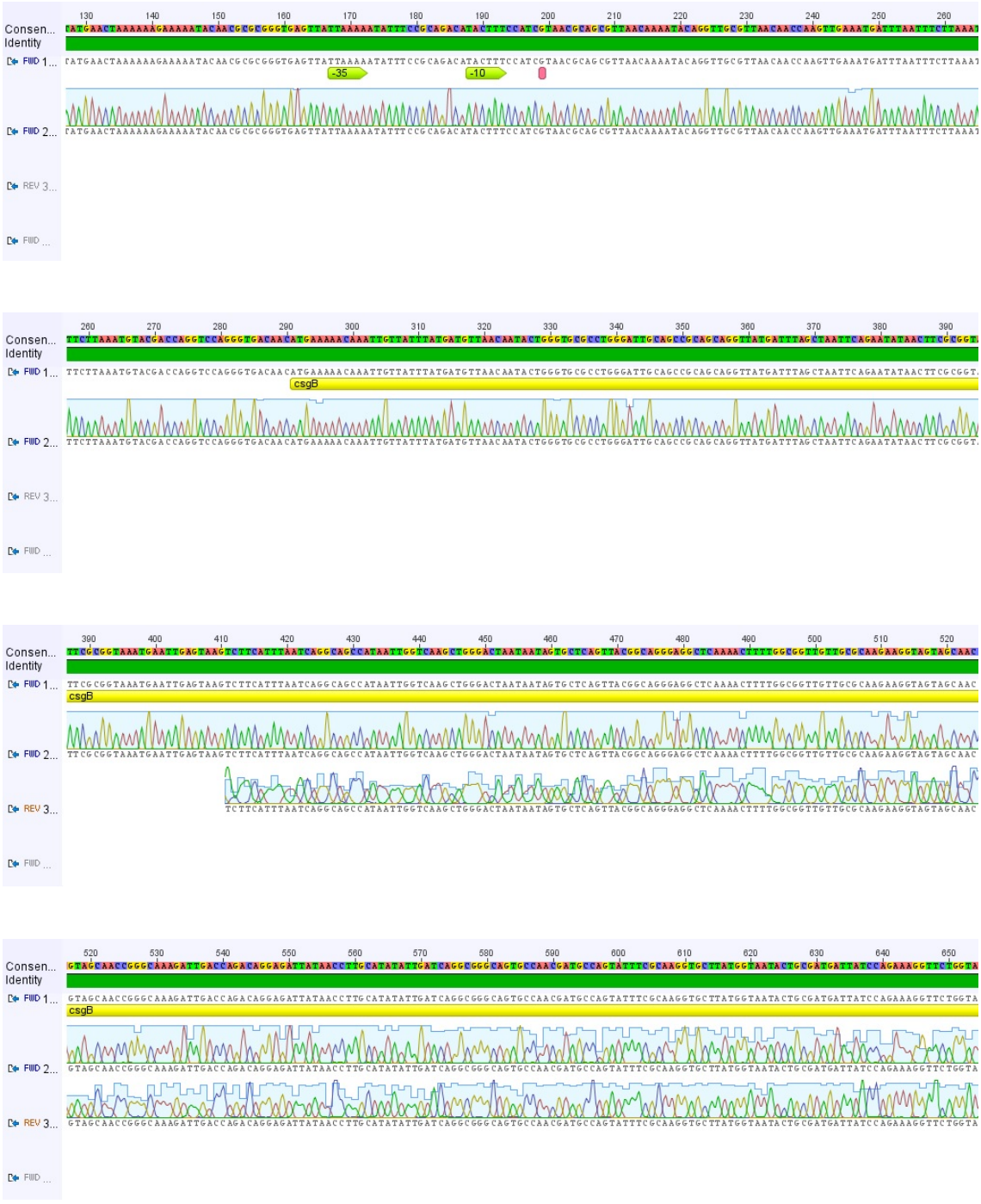

Supplementary Figure A-20 (Continued)

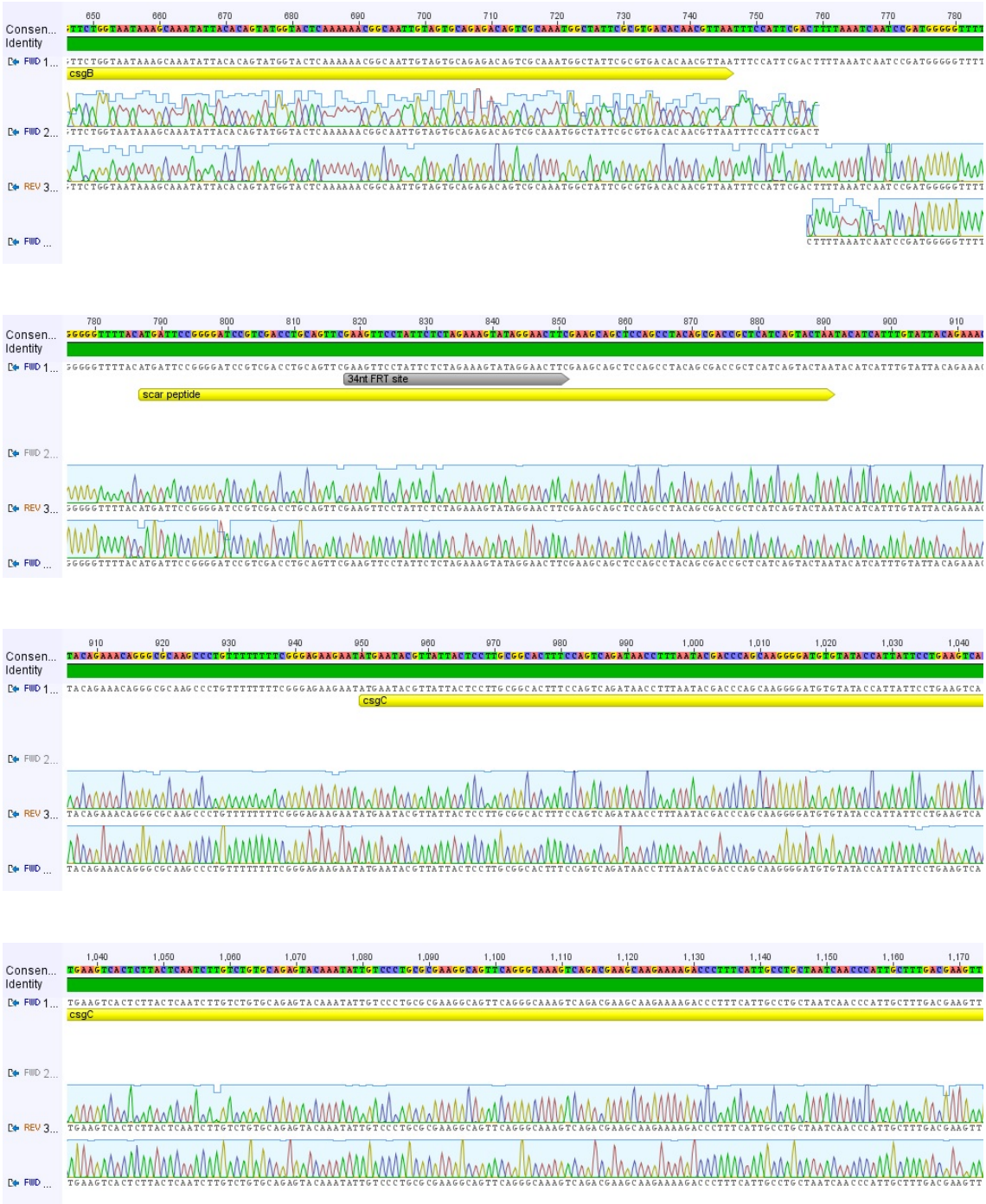

Supplementary Figure A-20 (Continued)

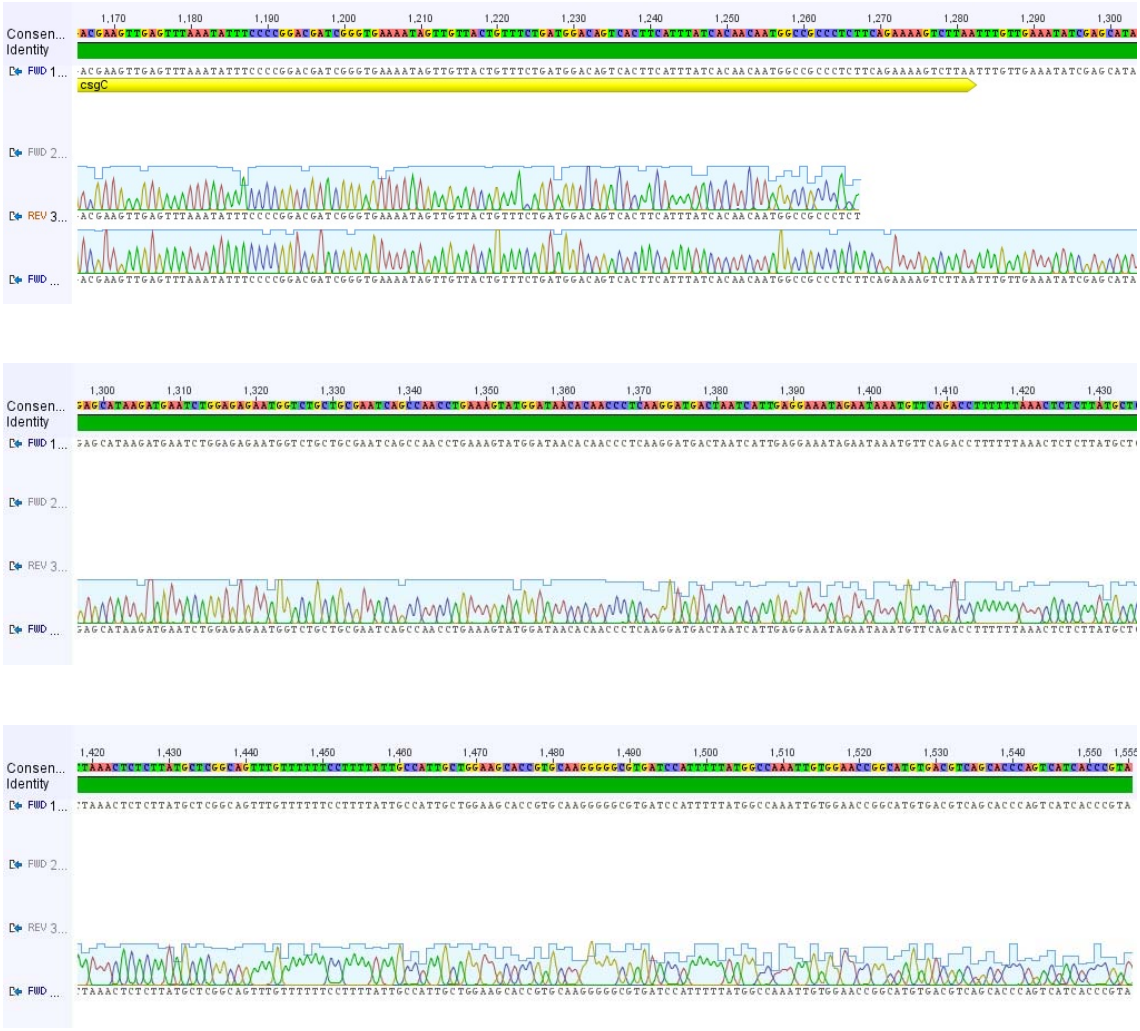

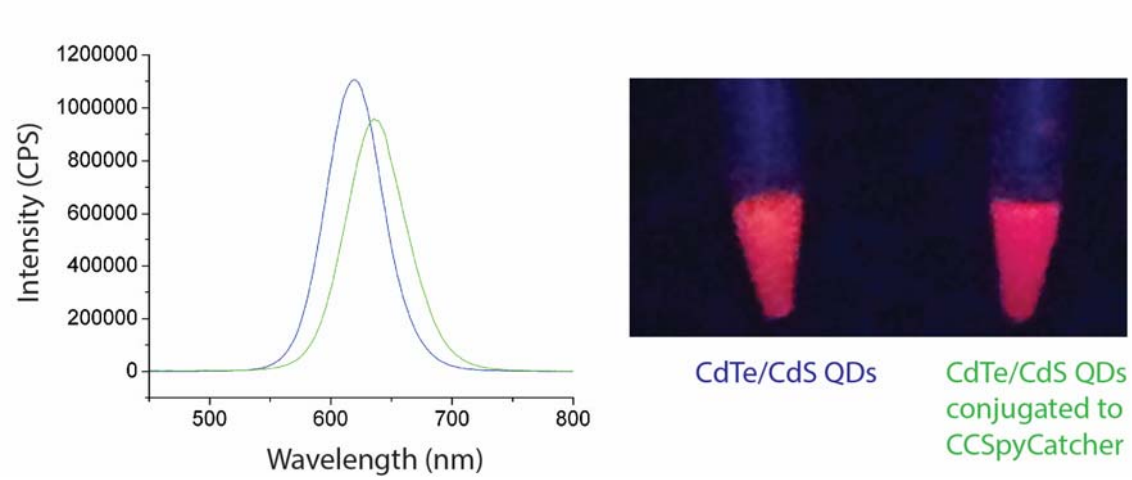

Supplementary Figure A-21 | Photoluminescence spectra and real-color pictures of CdTe/CdS quantum dots before (left blue curve, emission peak at 620nm) and after (right green curve, emission peak at 638nm) conjugation with CCSpyCatcher protein show that CdTe/CdS QDs remained highly fluorescent after conjugation. Photoluminescence spectra were obtained under excitation at 450nm (NanoLog Spectrometer, HORIBA Jobin Yvon). Real-color pictures were obtained under excitation at 365nm (UV lamp).

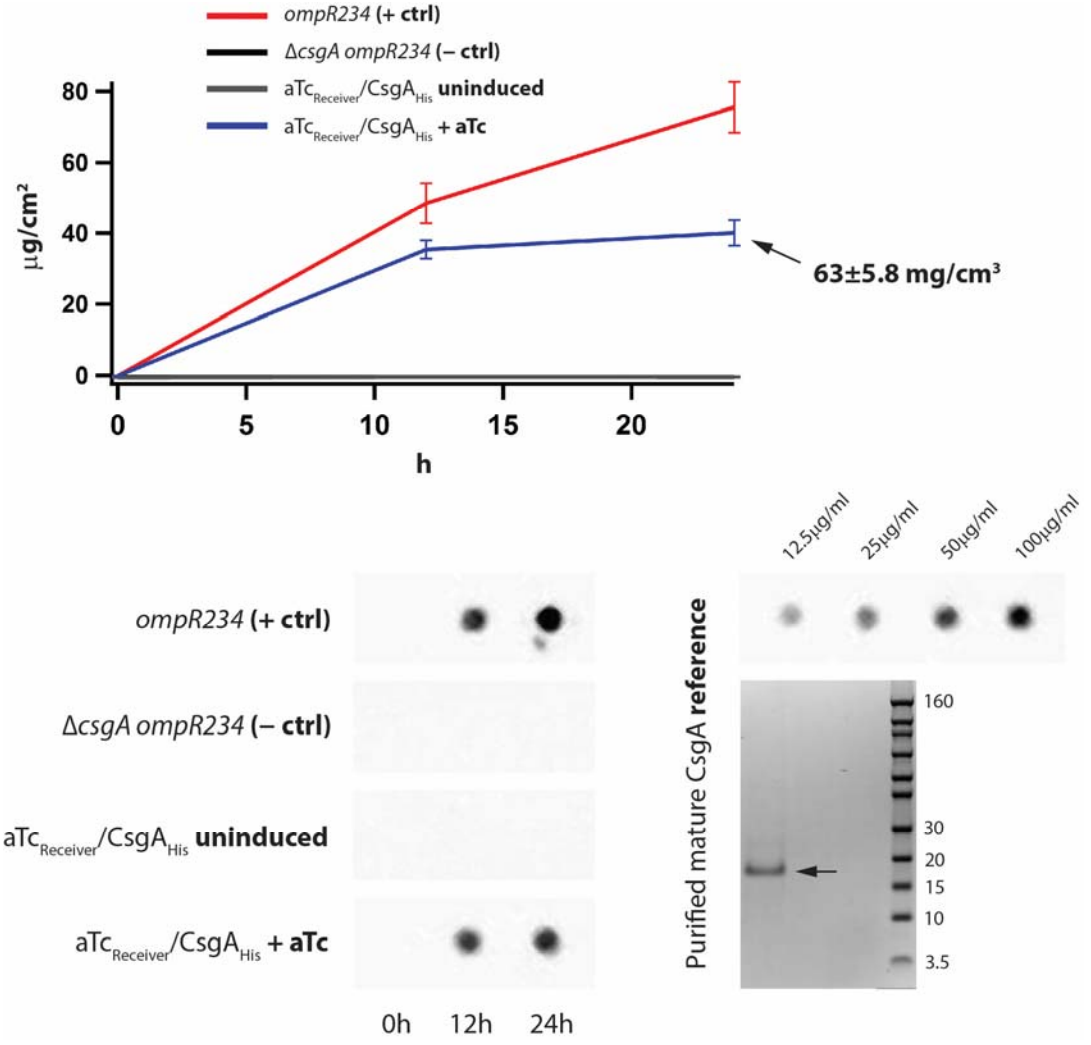

Supplementary Figure A-22 | Dot blot quantitation of CsgA production in biofilms. We quantitated CsgA with anti-CsgA antibody and found no signal from cultures of MG1655 *PRO* Δ*csgA ompR234* cells ("– ctrl") or uninduced $aTc_{Receiver}/CsgA_{His}$ cells. In contrast, $aTc_{Receiver}/CsgA_{His}$ cells induced with 250ng/ml aTc gave no signal at 0h, but at later timepoints gave signal corresponding to 30-40□g of CsgA per cm^2 of biofilm (solid blue line). Similarly, positive control MG1655 *ompR234* cells ("+ ctrl") gave no signal at 0h, but at later timepoints gave signal corresponding to 40-80□g of CsgA per cm^2 of biofilm. At the 24h timepoint, we were also able to use biofilm volume as determined by confocal microscopy (Fig. 1c) to calculate 63±5.8 (s.e.m.) mg of CsgA per cm^3 of biofilm

Supplementary Figure A-22 (Continued)

generated by the aTc-induced $aTc_{Receiver}$/$CsgA_{His}$ cells. For calculation of protein concentration in samples, a reference curve was constructed using serial dilutions of purified mature CsgA without the Sec signal sequence that is cleaved off during secretion. Mature CsgA was checked for purity by running on a SDS-PAGE gel with Coomassie staining. The purified CsgA monomer migrates at a higher apparent MW on the gel, at ~17.5kDa, even though the actual MW is 14.2kDa; this is consistent with results reported in the literature[1].

Supplementary Figure A-23 | Plasmid maps

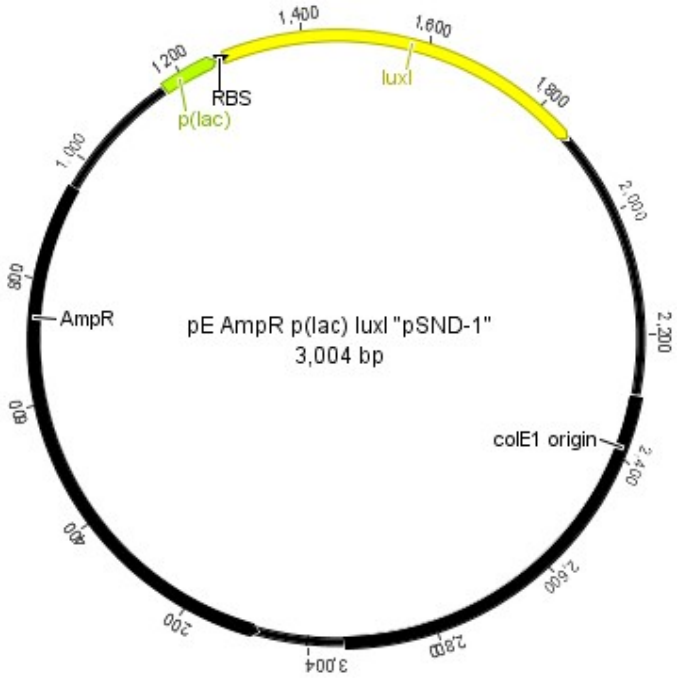

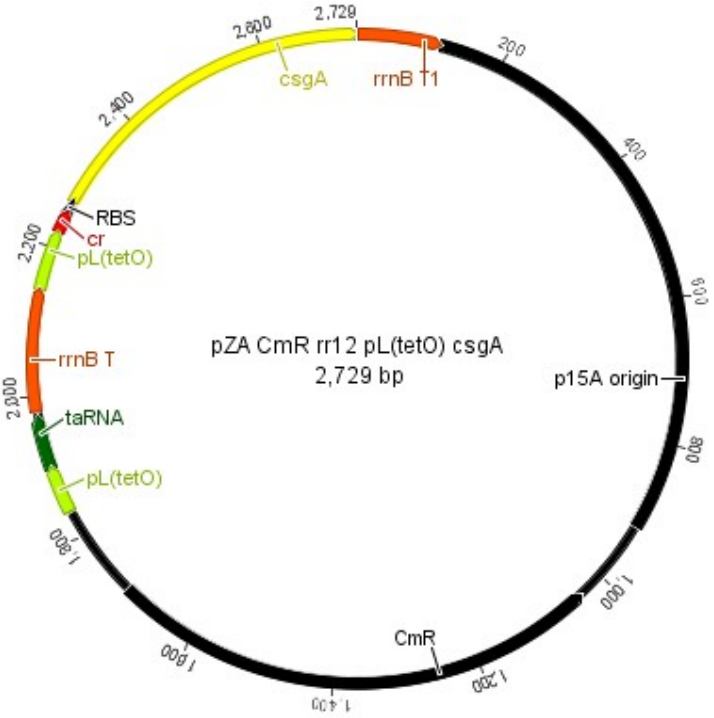

Supplementary Figure A-23 (Continued)

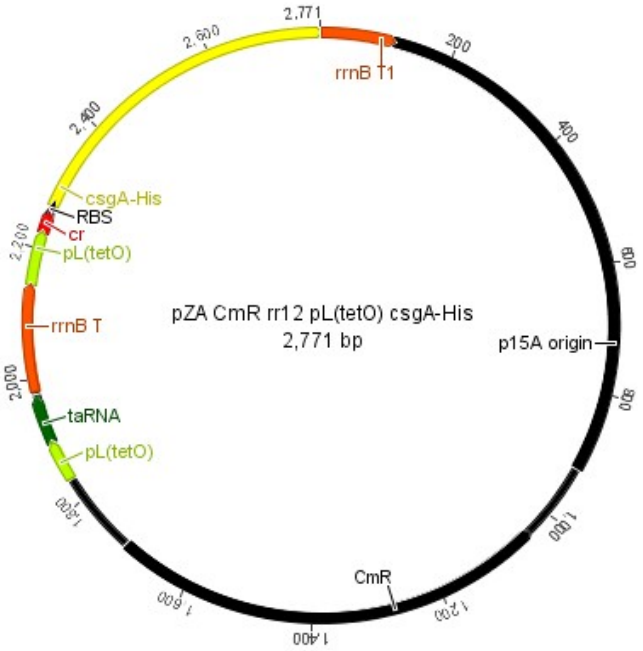

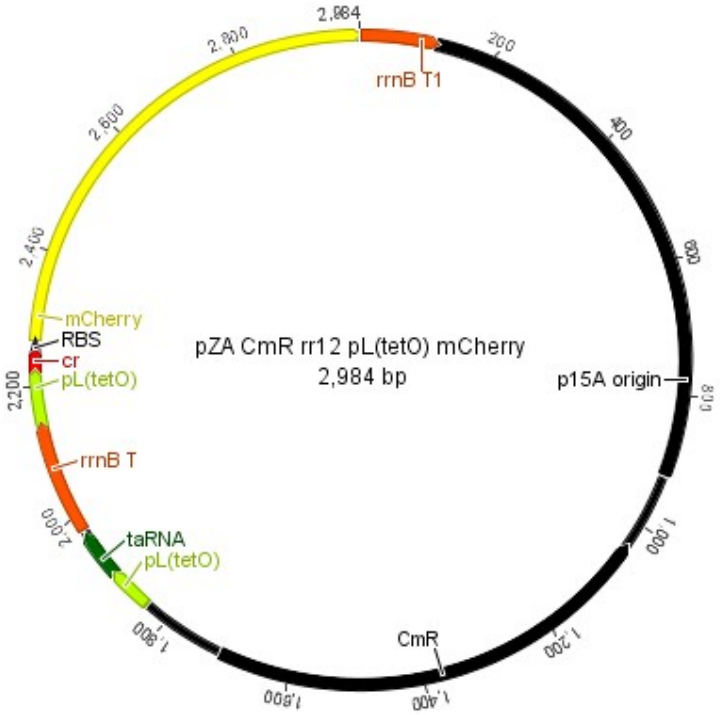

Supplementary Figure A-23 (Continued)

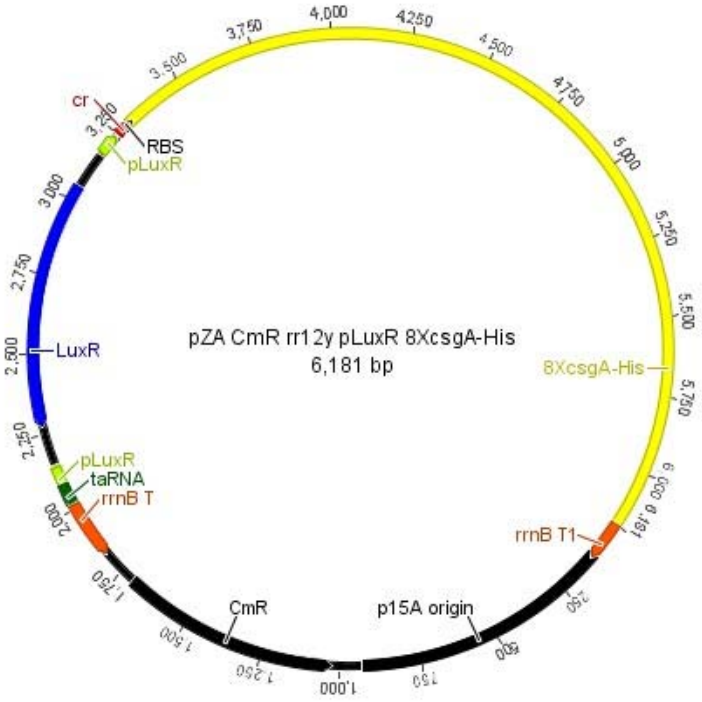

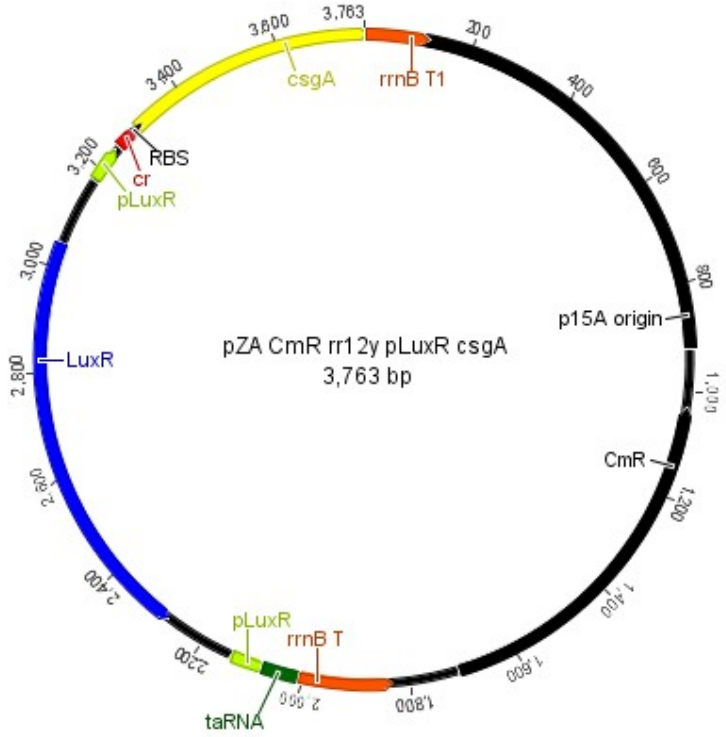

Supplementary Figure A-23 (Continued)

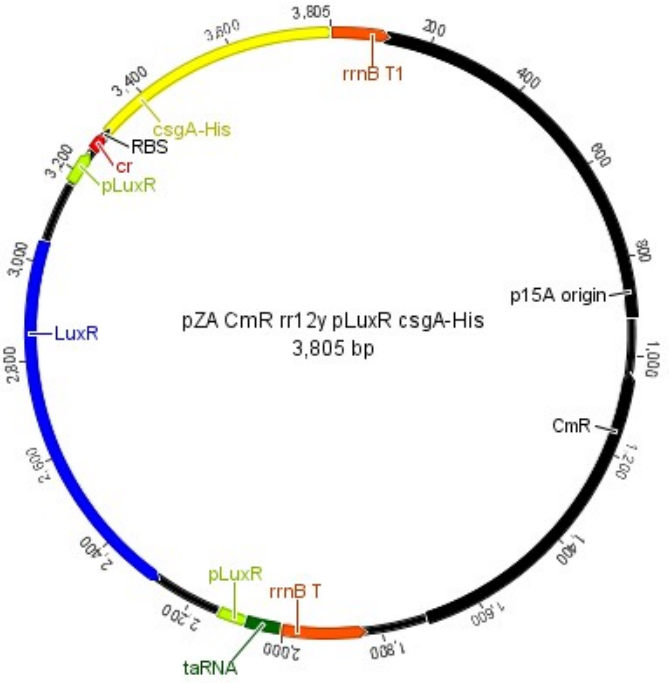

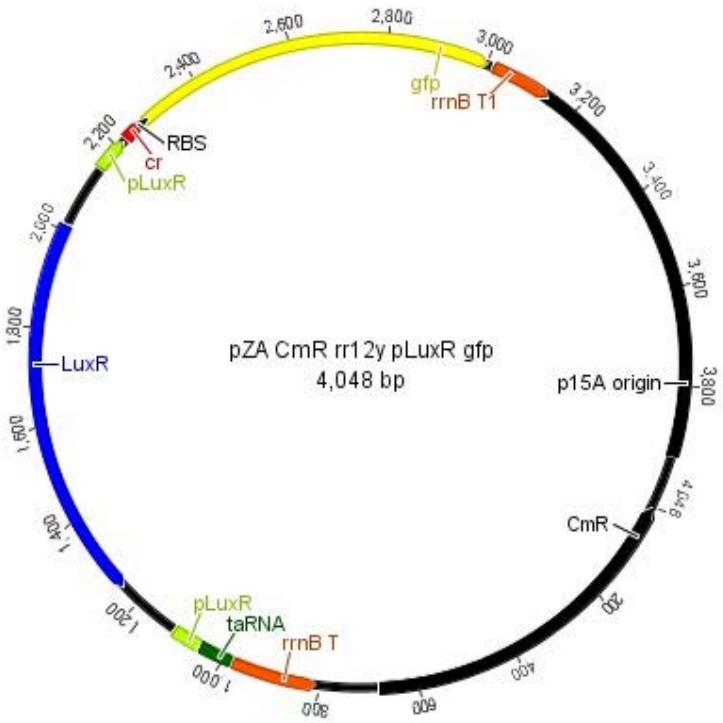

Supplementary Figure A-23 (Continued)

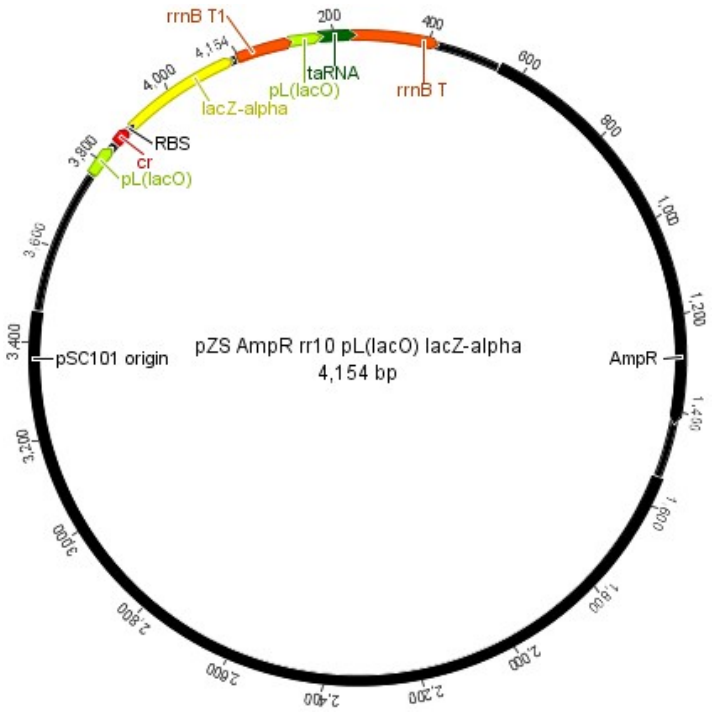

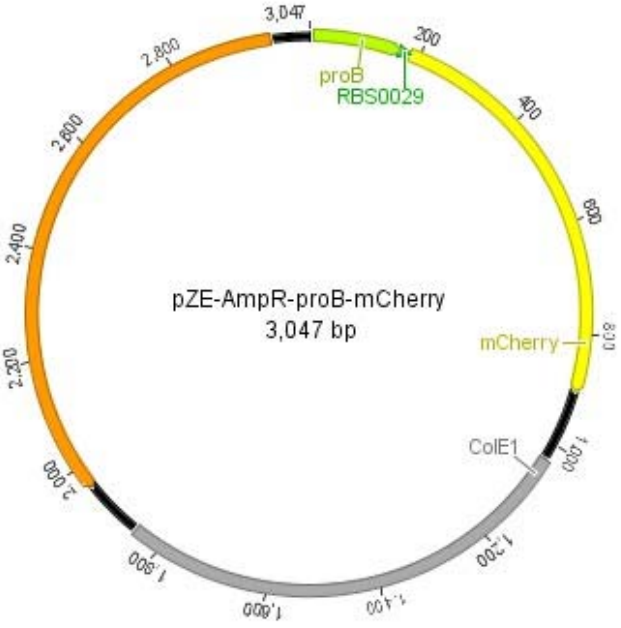

Supplementary Figure A-23 (Continued)

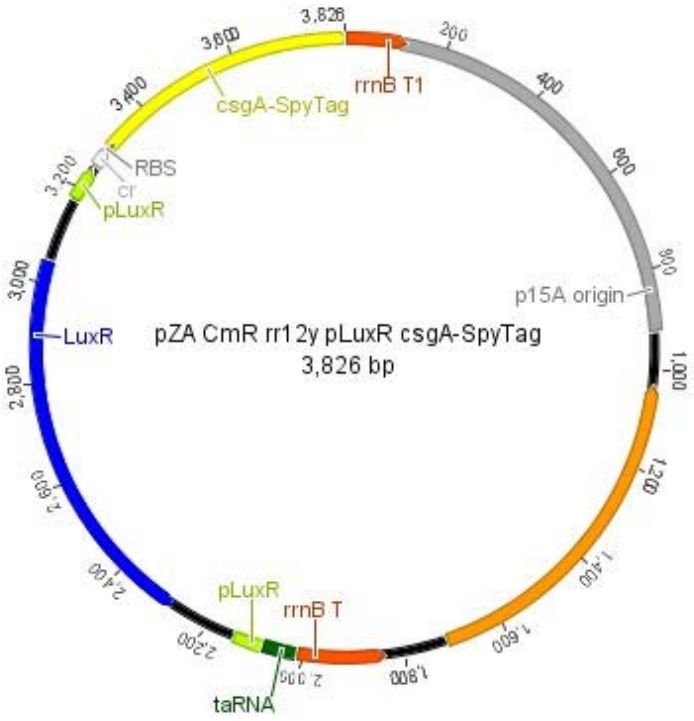

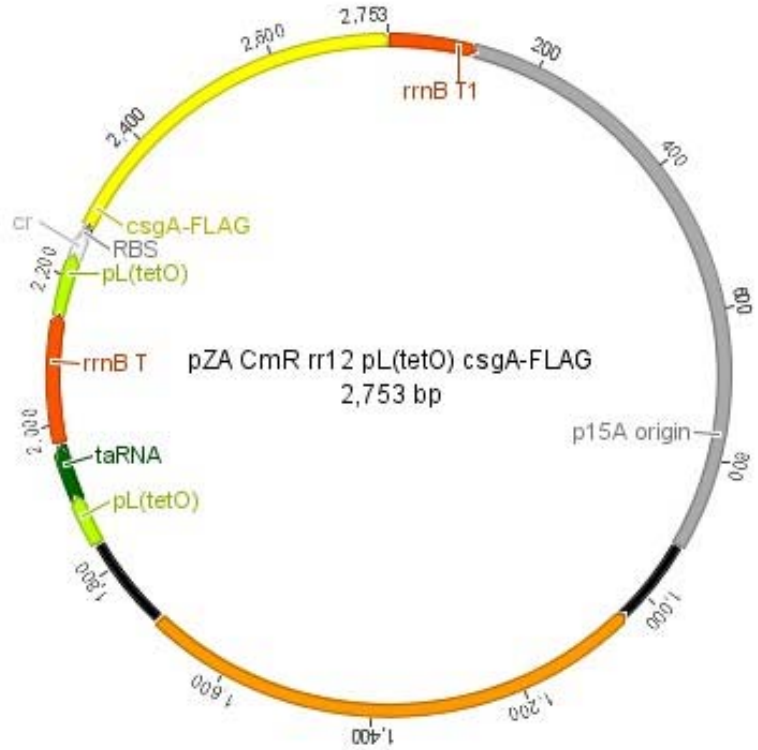

Supplementary Figure A-23 (Continued)

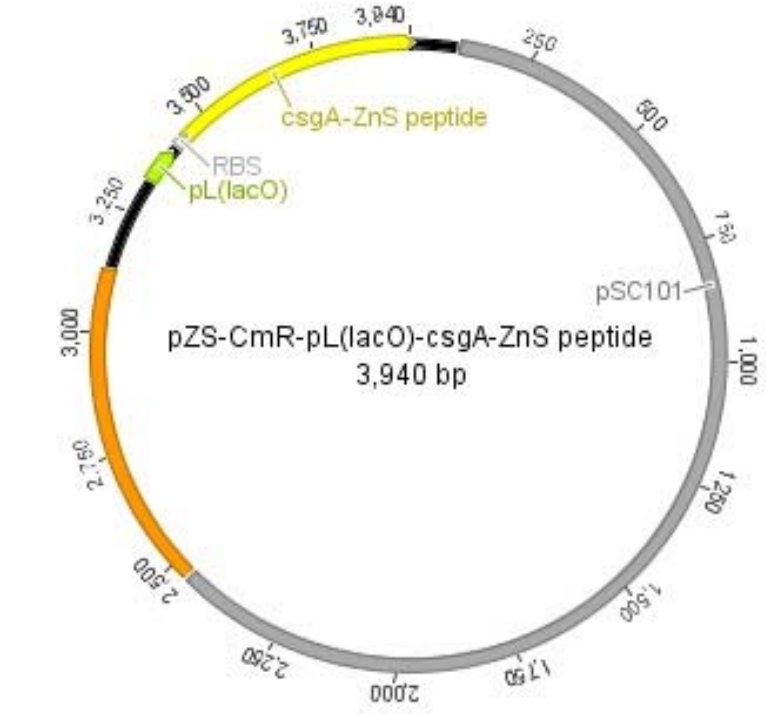

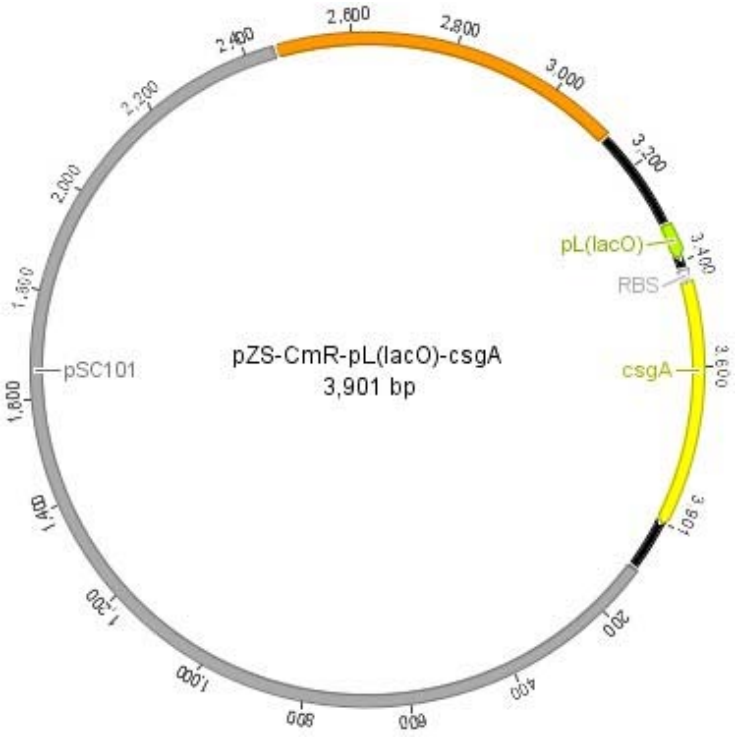

Supplementary Figure A-23 (Continued)

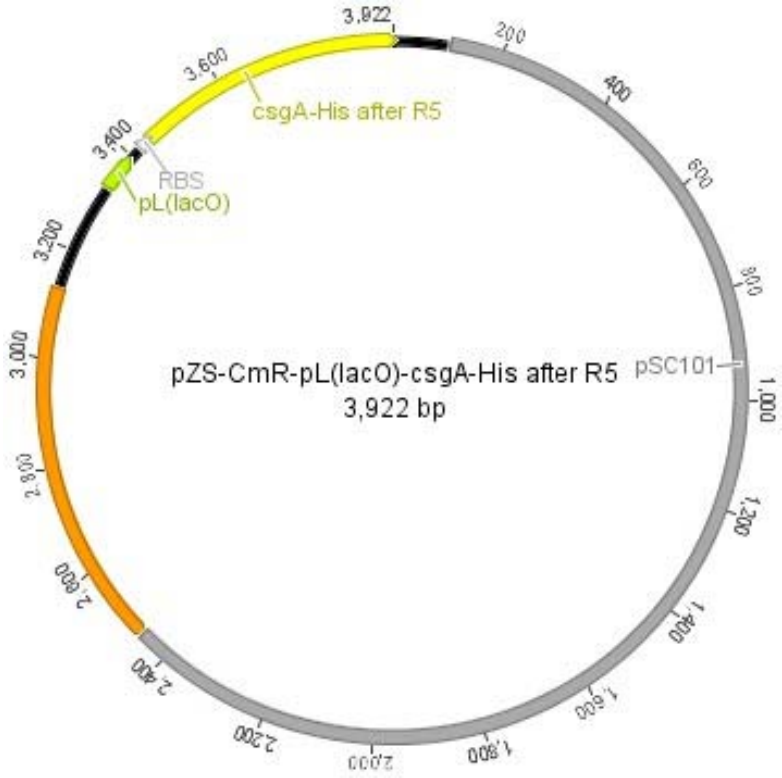

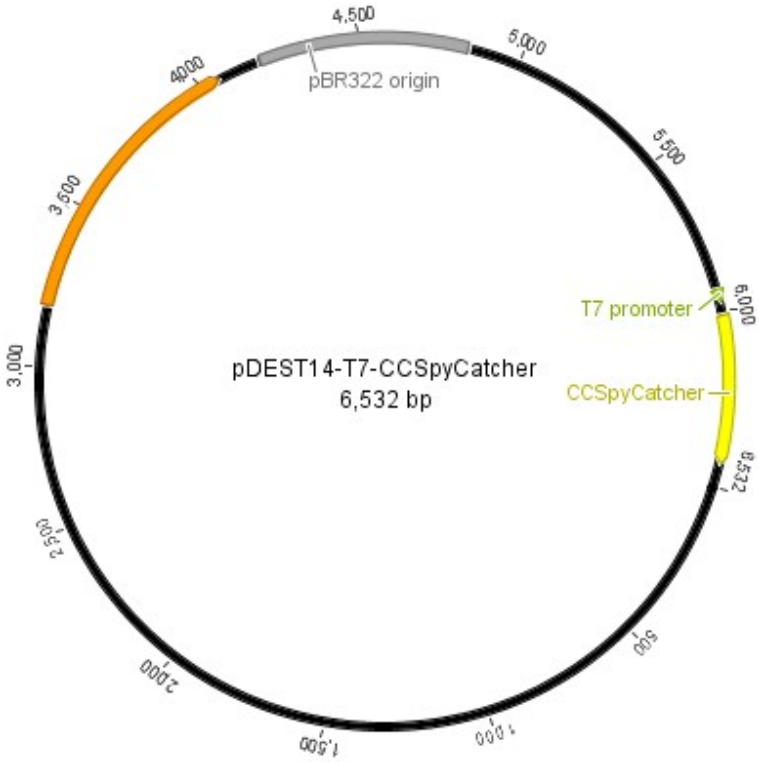

Supplementary Figure A-23 (Continued)

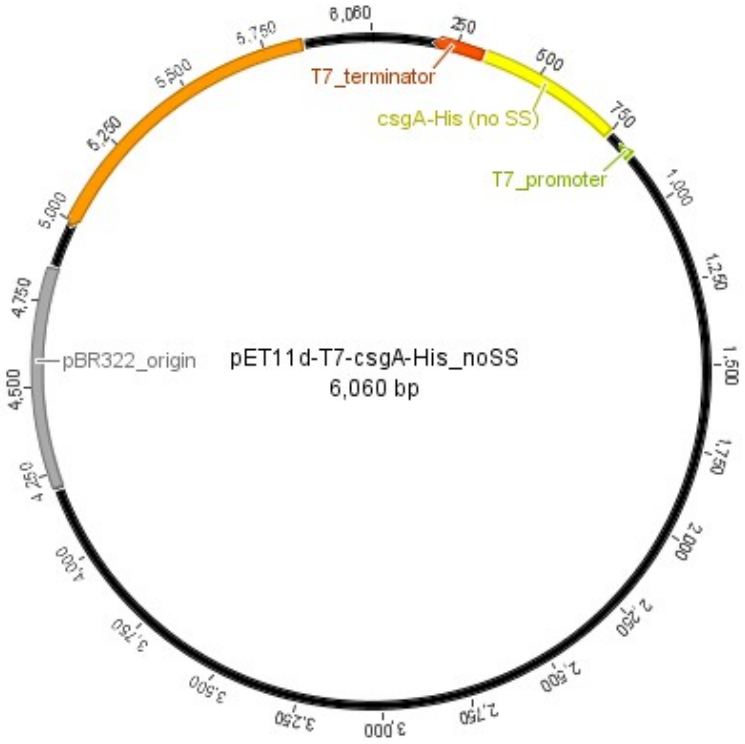

Supplementary Methods

Plasmid construction. The plasmids used in this study were constructed with standard molecular cloning techniques[2] using New England Biolabs (NEB) restriction endonucleases, T4 DNA Ligase, and Phusion PCR kits. A Bio-Rad S1000 Thermal Cycler with Dual 48/48 Fast Reaction Modules (Bio-Rad) was used to perform PCRs, ligations, and restriction digests. Gel extractions were carried out with QIAquick Gel Extraction Kits (Qiagen). Custom oligonucleotide primers were obtained from Integrated DNA Technologies (Coralville, IA).

All ligations for plasmid construction were transformed into *E. coli* strain DH5αPRO with standard protocols[2]. Isolated colonies were inoculated into Luria-Bertani (LB)-Miller medium (Fisher), which is LB medium with 10g/L NaCl[2], using antibiotics corresponding to antibiotic-selection markers within the plasmids (Supplementary Tables 1, 2) at the following concentrations: carbenicillin at 50μg/ml, chloramphenicol at 25μg/ml, kanamycin at 30μg/ml, and spectinomycin at 100μg/ml. DNA was extracted with Qiagen QIAprep Spin Miniprep Kits. Plasmid construct sequences were confirmed by restriction digest and sequencing was performed by Genewiz (Cambridge, MA).

The parts that constitute the plasmids used in this work are described in Supplementary Table 1, and plasmids are described in Supplementary Table 2. To create constructs for the expression of output genes under tight regulation by an aTc-inducible riboregulator, pZE-AmpR-rr12-pL(tetO)-*gfp* was used as a starting point[3]. The AmpR cassette of pZE-AmpR-rr12-pL(tetO)-*gfp* was replaced by the CmR cassette from

pZS-CmR-pL(lacO)-*gfp* by using SacI-HF/AatII digestion and T4 ligation to create pZE-CmR-rr12-pL(tetO)-*gfp*. Then, the ColE1 origin of pZE-CmR-rr12-pL(tetO)-*gfp* was replaced by the p15A origin from pZA-AmpR-pL(tetO)-*gfp* by using SacI-HF/AvrII excision and T4 ligation to create pZA-CmR-rr12-pL(tetO)-*gfp*. The *gfp* gene was excised using KpnI/MluI digest to create the vector pZA-CmR-rr12-pL(tetO)-. The genes *csgA*, $csgA_{His}$, *mCherry*, and $csgA_{FLAG}$ with KpnI and MluI sticky ends were generated by PCR and KpnI/MluI digest; these fragments were ligated with pZA-CmR-rr12-pL(tetO)- to create pZA-CmR-rr12-pL(tetO)-*csgA*, pZA-CmR-rr12-pL(tetO)-$csgA_{His}$, pZA-CmR-rr12-pL(tetO)-*mCherry*, and pZA-CmR-rr12-pL(tetO)-$csgA_{FLAG}$ plasmids, respectively.

To create constructs for the expression of output genes under tight regulation by an AHL-inducible riboregulator, pZE-KanR-rr12y-pLuxR-*gfp* was used as a starting point[3]. The KanR cassette of pZE-KanR-rr12y-pLuxR-*gfp* was replaced by the CmR cassette from pZS-CmR-pL(lacO)-*gfp* by using SacI-HF/AatII digestion and T4 ligation to create pZE-CmR-rr12y-pLuxR-*gfp*. Then, the ColE1 origin of pZE-CmR-rr12y-pLuxR-*gfp* was replaced by the p15A origin from pZA-AmpR-pL(tetO)-*gfp* by using SacI-HF/AvrII excision and T4 ligation to create pZA-CmR-rr12y-pLuxR-*gfp*. The *gfp* gene was excised using KpnI/MluI digest to create the vector pZA-CmR-rr12y-pLuxR-. A codon-optimized gene encoding a CsgA variant consisting of eight tandem repeats of CsgA with a histidine tag at the C-terminus ($8XcsgA_{His}$), and flanked by KpnI and MluI sites, was designed and custom synthesized by GenScript (Piscataway, NJ). The gene $8XcsgA_{His}$ with sticky ends was generated by KpnI/MluI digest and ligated with pZA-CmR-rr12y-pLuxR- to create pZA-CmR-rr12y-pLuxR-$8XcsgA_{His}$. The genes *csgA*, $csgA_{His}$, and $csgA_{SpyTag}$, also with KpnI and MluI sticky ends, were ligated with the vector to create pZA-CmR-rr12y-pLuxR-

csgA, pZA-CmR-rr12y-pLuxR-$csgA_{His}$, and pZA-CmR-rr12y-pLuxR-$csgA_{SpyTag}$, respectively.

A plasmid with an AmpR resistance marker was also created for use in co-culture experiments (Fig. 3). This plasmid had a low-copy origin and an output gene ($lacZ_{alpha}$) under tight repression by a riboregulator to ensure minimal effects on the host cell apart from conferring ampicillin resistance. The plasmid pZE-KanR-rr10-pL(lacO)-*mCherry* was used as a starting point[3]. The KanR cassette of pZE-KanR-rr10-pL(lacO)-*mCherry* was replaced by the AmpR cassette from pZA-AmpR-pL(tetO)-*gfp* by using SacI-HF/AatII digestion and T4 ligation to create pZE-AmpR-rr10-pL(lacO)-*mCherry*. Then, the ColE1 origin of pZE-AmpR-rr10-pL(lacO)-*mCherry* was replaced by the pSC101 origin from pZS-CmR-pL(lacO)-*gfp* by using SacI-HF/AvrII excision and T4 ligation to create pZS-AmpR-rr10-pL(lacO)-*mCherry*. The *mCherry* gene of pZSAmpR-rr10-pL(lacO)-*mCherry* was replaced by the $lacZ_{alpha}$ gene from pZE-AmpR-pLuxR-$lacZ_{alpha}$ using KpnI/MluI excision and T4 ligation to create pZS-AmpR-rr10-pL(lacO)-$lacZ_{alpha}$.

Plasmids for expressing genes from the pL(lacO) promoter were constructed by using pZS-CmR-pL(lacO)-*gfp*[4] as a starting point. The *gfp* gene was excised by digestion with KpnI/MluI to create vector pZS-CmR-pL(lacO)-. This vector was ligated, using T4 ligase, with digested PCR fragments that had KpnI and MluI sticky ends. These fragments encoded *csgA*, $csgA_{His\ after\ C\text{-}terminus}$, or $csgA_{ZnS\ peptide}$. This created pZS-CmR-pL(lacO)-*csgA*, pZS-CmR-pL(lacO)-$csgA_{His\ after\ C\text{-}terminus}$, and pZS-CmR-pL(lacO)-$csgA_{ZnS\ peptide}$ plasmids.

The pDEST14-T7-*CCSpyCatcher* plasmid for the expression of CCSpyCatcher was created from pDEST14-T7-*SpyCatcher*[5] using the QuikChange Lightning Kit (Agilent) to

add codons encoding two cysteines immediately after the start codon. The thiol groups on cysteines were used to conjugate SpyCatcher to QDs as described below.

Strain construction. To create the *E. coli* MG1655 *PRO ΔcsgA ompR234* strain used in this study, we sequentially generated *E. coli* MG1655 *PRO ΔcsgA::aph*, *E. coli* MG1655 *PRO ΔcsgA*, and *E. coli* MG1655 *PRO ΔcsgA ompR234*. The PRO cassette (P_{laci^q}/*lacI*, P_{N25}/*tetR*, $Spec^R$) has a spectinomycin resistance marker and expresses *lacI* and *tetR* at high constitutive levels[4].

E. coli MG1655 *PRO ΔcsgA::aph* was generated via P1 transduction of the *ΔcsgA::aph* mutation from donor strain JW1025-1 of the Keio collection[6] into recipient *E. coli* MG1655 *PRO*[3], as previously described[2]. To prepare P1 lysate, 100µl overnight culture of donor strain was incubated with 100µl P1 phage in 10ml LB + 7mM $CaCl_2$ + 12mM $MgSO_4$ for 20min without shaking at 37°C, then for 2h with shaking at 37°C. To produce more P1 lysate, 300µl more of donor strain was added, the culture incubated for 20min without shaking at 37°C, then for 2h with shaking at 37°C. The culture was transferred to a 50ml Falcon tube, 2ml of chloroform was added, and the mixture was vortexed and centrifuged for 15min at 3000rpm. The supernatant, containing the P1 lysate, was transferred to Eppendorf tubes and centrifuged for 5min at 14000rpm to pellet remaining debris. For transduction, the P1 lysate was diluted 60-fold into 1ml LB + 7mM $CaCl_2$ + 12mM $MgSO_4$ in an Eppendorf tube, 100µl overnight culture of recipient strain was added, and the tube was incubated for 1h with shaking at 37°C. This culture was then plated onto LB kanamycin agar with 25mM sodium citrate to select for recipients successfully transduced with the *ΔcsgA::aph* mutation. Transformants were restreaked onto LB kanamycin agar for re-isolation.

E. coli MG1655 *PRO ΔcsgA* was generated by removing the kanamycin resistance cassette as previously described[7] (in order to free this antibiotic selection marker for subsequent usage). Briefly, MG1655 *PRO ΔcsgA::aph* was transformed with pCP20[8] carrying the gene for FLP recombinase and selected on LB ampicillin agar at 30°C. Transformants were restreaked onto non-selective LB and grown overnight at 42°C to cure the temperature-sensitive pCP20. Isolates were patched onto LB agar containing either kanamycin or ampicillin to confirm the loss of the FRT-flanked kanamycin cassette and pCP20, respectively.

Finally, *E. coli* MG1655 *PRO ΔcsgA ompR234* was generated via P1 transduction of the *ompR234* mutation (linked to a kanamycin resistance marker) from donor *E. coli* MG1655 *ompR234*[9] into recipient *E. coli* MG1655 *PRO ΔcsgA* with the same protocol as above. The final strain was verified via PCR amplicon size using check primers for each locus. The *ompR234* mutation was verified via sequencing of both strands of the amplicon. We also used sequencing to verify that the *csgBAC* locus in MG1655 *PRO ΔcsgA ompR234* perfectly matched the predicted sequence for the *csgA* knockout, with an intact *csgB* gene, as constructed in the Keio collection[6] (Supplementary Fig. 20).

Finally, cell strains used in patterning experiments in this study were created by transforming plasmids constructed above into MG1655 *PRO ΔcsgA ompR234*, and are described in Supplementary Table 3.

Culture conditions. Seed cultures were inoculated from frozen glycerol stocks and grown in LB-Miller medium using antibiotics corresponding to the plasmids in the cells (Supplementary Table 3) at the following concentrations: carbenicillin at 50μg/ml, chloramphenicol at 25μg/ml, kanamycin at 30μg/ml, and spectinomycin at 100μg/ml. Seed cultures were grown for 12h at 37°C in 14-ml culture tubes (Falcon), with shaking

at 300rpm. Experimental cultures were grown in M63 minimal medium (Amresco) supplemented with 1mM $MgSO_4$ and with 0.2% w/v glucose or 0.2% w/v glycerol (hereafter referred to as glucose-supplemented M63 or glycerol-supplemented M63, respectively); all liquid experimental cultures were grown in 24-well plate wells at 30°C with no shaking[10]. For inducing conditions, inducers used were anhydrotetracycline (Sigma) at concentrations of 1-250ng/ml and N-(β-ketocaproyl)-L-homoserine lactone (Sigma) at concentrations of 1-1000nM. All experiments reporting standard-error-of-the-mean (s.e.m.) error bars were performed in triplicate.

For experiments to show inducible biofilm formation and inducible curli production (Fig. 1; Supplementary Figs. 1, 3, 8), the following strains and growth conditions were used: $aTc_{Receiver}/CsgA_{His}$ at an initial seeding density of $5X10^7$ cells/ml was grown on Thermanox or polystyrene or embedded in 0.7% M63 agar, for 24h in the case of liquid media and 48h in the case of agar, with glucose or glycerol-supplemented M63, with no aTc or with 250ng/ml aTc. Positive control strain MG1655 *ompR234* and negative control strain MG1655 *PRO csgA ompR234* were similarly cultured in M63 media, without inducer.

For experiments to show inducible biofilm formation by confocal microscopy (Fig. 1; Supplementary Figs. 2, 14), the same conditions were used as above, with the cell strains used possessing an additional constitutive mCherry-expressing plasmid, and using Thermanox coverslips. The inducible strain used was $aTc_{Receiver}/CsgA_{His}$ with the addition of pZE-AmpR-proB-*mCherry*, the positive control strain used was MG1655 *ompR234* / pZE-AmpR-proB-*mCherry*, and the negative control strain used was MG1655 *PRO csgA ompR234* / pZE-AmpR-proB-*mCherry*. Cultures were grown for 4-48h.

Biofilms in flow cells (Fig. 1; Supplementary Fig. 2). PDMS (Polydimethylsiloxane; Sylgard 184; Dow Corning, MI, USA) flow devices were molded from a polystyrene master yielding a negative imprint of 4 straight channels (2mm deep/2mm wide/350mm long) and then bonded with silicone adhesive to Thermanox coverslips (Nunc). For each strain and experimental condition tested, a bacterial suspension of $5X10^7$ cells/ml in glucose or glycerol supplemented M63 was introduced into flow cells under continuous flow driven by syringe pumps (PHD Ultra, Harvard Apparatus, MA, USA) at a flow rate of 0.5µl/min. Devices were placed on an inverted Zeiss 510 Meta confocal laser-scanning microscope for the duration of the experiments. Fluorescence images were recorded across the channels at 4, 10, 24, and 48 hours using a 10x/0.45 n.a. objective. The total biomass for each experiment was calculated in ImageJ[11] for 2 dimensional surface coverage (xy) and by COMSTAT for MATLAB[12] for biofilm formation (xyz image series). For each data point, 3 z-stacks per sample were analysed across 3 samples.

Static culture biofilms (Fig. 1; Supplementary Fig. 2). Biofilm formation in static culture was quantified on Thermanox coverslips at 4 and 24 hours. Each sample was rinsed in 1XPBS to remove unattached cells, placed on a No. 1 coverslip and imaged with an inverted Zeiss 510 Meta confocal laser-scanning microscope using a 100x/1.4 n.a. oil immersion objective. Fluorescence images were recorded at multiple locations across the substrate to quantify the average biomass coverage for each substrate. Biomass was quantified as described for flow cell experiments. For each data point, 3 z-stacks per sample were analysed across 3 samples.

Transmission electron microscopy. For transmission electron microscopy (TEM), a 20µl droplet of sample was placed on parafilm (Pechiney), and a 200-mesh

formvar/carbon coated nickel TEM grid (Electron Microscopy Sciences) was placed with coated side face-down on the droplet for 30-60s. In all protocols requiring incubation for greater than 10min, samples were covered with petri dish lids to minimize evaporation. The grid was then rinsed with ddH_2O by placing the grid face-down in a 30µl droplet of ddH_2O and wicking off on filter paper (Whatman), and placed face-down for 15-30s on a droplet of 2% uranyl acetate (UA) (Electron Microscopy Sciences) filtered through 0.22µm syringe filter (Whatman). Excess uranyl acetate was wicked off and the grid was allowed to air dry. TEM images were obtained on a FEI Tecnai Spirit transmission electron microscope operated at 80kV accelerating voltage. High-resolution transmission electron microscopy (HRTEM) and energy-dispersive X-ray spectroscopy (EDS) were performed on a JEOL 2010F electron microscope operating at 200 kV.

Scanning electron microscopy. For scanning electron microscopy (SEM), biofilm samples on coverslips were coated with carbon sputtered to ~10nm with a Desk II Sputter Coater (Denton Vacuum). The samples were then imaged with a JEOL JSM-6010LA scanning electron microscope operated at 10kV accelerating voltage. Images were obtained in secondary electron imaging (SEI) mode, and elemental mapping was performed with energy-dispersive X-ray spectroscopy (EDS).

Fluorescence microscopy. Fluorescence-lifetime imaging microscopy (FLIM) was performed with a Zeiss 710 NLO multiphoton microscope with 20X objective and connected to a time-correlated single-photon counting system (Becker & Hickl). The excitation source was a 2-photon laser (Coherent Chameleon Vision II) tuned to 800nm, and emission was detected through a 590-650nm bandpass filter. FLIM decays were fit using SPCImage software (Becker and Hickl, Germany).

Lambda scan analysis of fluorescent ZnS nanocrystals was performed with a Zeiss LSM 710 NLO Laser Scanning Confocal with 10X objective and 405nm excitation laser.

Anti-CsgA immuno-labelling assay (Fig. 1, Supplementary Fig. 1). We optimized antibody concentrations and based our protocol on that used in Collinson *et al.*[13]. TEM grids (Electron Microscopy Sciences) were placed with coated side face-down on 20µl droplets of samples on parafilm for 2min. The side of the TEM grids with sample was rinsed with a 30µl droplet of ddH_2O, then placed on a 50µl droplet of Blocking Buffer (10mM Tris (pH 8.0)-0.15M NaCl-1% skim milk) for 30min, followed by transfer to a 50µl droplet of Binding Buffer (10mM Tris (pH 8.0)-0.15M NaCl-0.1% skim milk) with 1:1000 dilution of rabbit anti-CsgA antibody (M. Chapman, University of Michigan[14,15]), where it was incubated for 1h at room temperature (RT). The grid was then rinsed four times in 50µl droplets of Wash Buffer (10mM Tris (pH 8.0)-0.15M NaCl), and subsequently transferred to a 50µl droplet of Binding Buffer with 1:10 dilution of goat anti-rabbit antibody conjugated to 10nm gold particles (Sigma), where it was incubated for 1h at RT. The grid was then rinsed four times in 50µl droplets of Wash Buffer, followed by four rinses in 30µl droplets of ddH_2O. The thoroughly washed grid was placed face-down on a droplet of filtered 2% uranyl acetate for 15-30s to negative stain the sample. Excess uranyl acetate was wicked off with filter paper and the grid was allowed to air dry. All sample preparation steps were done at RT.

NiNTA-AuNP labelling assay. For nickel nitrilotriacetic acid gold nanoparticle (NiNTA-AuNP) labelling of histidine tags displayed on CsgA, 200-mesh formvar/carbon-coated nickel TEM grids (Electron Microscopy Sciences) were placed with coated side face-down on 20µl droplets of samples on parafilm for 2min. The side of the TEM grid with

sample was rinsed with a 30µl droplet of ddH_2O, then with selective binding buffer (1XPBS with 0.487M NaCl, 80mM imidazole, and 0.2v/v% Tween20), and placed face-down in a 60µl droplet of selective binding buffer with 10nM 5nm NiNTA-AuNP particles (Nanoprobes). The TEM grid and droplet on parafilm was covered with a petri dish to minimize evaporation and allowed to incubate for 90min. The grid was then washed 5 times with selective binding buffer without NiNTA-AuNP particles, then twice with 1XPBS and twice with ddH_2O. The thoroughly washed grid was placed face-down on a droplet of filtered 2% uranyl acetate for 15-30s to negative stain the sample. Excess uranyl acetate was wicked off with filter paper and grid allowed to air dry. All sample preparation steps were done at RT. Images were obtained on a FEI Tecnai Spirit transmission electron microscope operated at 80kV accelerating voltage.

AuNP binding assay. This assay was performed identically to the NiNTA-AuNP labelling assay with tannic-acid-capped 5nm AuNP (Ted Pella) in place of NiNTA-AuNP.

Verifying the specificity of the histidine-tag-NiNTA interaction (Supplementary Fig. 9). Strain $aTc_{Receiver}/CsgA_{His}$ was used to produce $CsgA_{His}$ fibrils and strain $aTc_{Receiver}$/CsgA was used to produce CsgA fibrils; cells were seeded at $5X10^7$ cells/ml and cultured in glucose-supplemented M63 media with 50ng/ml aTc for 24h at 30°C. $CsgA_{His}$ fibrils and CsgA fibrils were labelled with the NiNTA-AuNP labelling assay; additionally $CsgA_{His}$ fibrils were labelled with the AuNP particle binding assay.

Strain verification experiments (Supplementary Figs. 5, 8). For strain verification experiments, all cultures had an initial seeding concentration of $5X10^7$ cells/ml and were grown in M63 medium supplemented with 0.2%w/v glucose as a carbon source. For experiments to verify that the fibrils seen on TEM were self-assembled from CsgA, MG1655 *ompR234* was grown for 24h, $aTc_{Receiver}$/CsgA was grown for 14h with

62.5ng/ml aTc, and aTc$_{Receiver}$/CsgA$_{His}$ was grown for 14h with 62.5ng/ml aTc. Biofilms resulting from aTc$_{Receiver}$/CsgA and aTc$_{Receiver}$/CsgA$_{His}$ cultures were resuspended in 1XPBS and the NiNTA-AuNP particle labelling assay (above) was performed to characterize curli fibrils. For experiments to verify that insertion of histidine tags into CsgA still allows curli fibril production (Supplementary Fig. 5), aTc$_{Receiver}$/CsgA was grown for 14h with 250ng/ml aTc, aTc$_{Receiver}$/CsgA$_{His}$ was grown for 14h with 250ng/ml aTc, AHL$_{Receiver}$/CsgA was grown for 14h with 1000nM AHL, and AHL$_{Receiver}$/CsgA$_{His}$ was grown for 14h with 1000nM AHL. The resulting biofilms were resuspended in 1XPBS and TEM imaging was performed.

Experiments were performed to verify that the MG1655 *PRO ΔcsgA ompR234* host strain does not produce curli fibrils, that AHL$_{Receiver}$/CsgA$_{His}$ only produces curli fibrils when induced by AHL, and that aTc$_{Receiver}$/CsgA$_{His}$ only produces curli fibrils when induced by aTc (Supplementary Fig. 8). MG1655 *PRO ΔcsgA ompR234* and MG1655 *ompR234* were grown for 48h. AHL$_{Receiver}$/CsgA$_{His}$ was grown for 48h with no inducer, 1000nM AHL, or 250ng/ml aTc. Similarly, aTc$_{Receiver}$/CsgA$_{His}$ was grown for 48h with no inducer, 1000nM AHL, or 250ng/ml aTc. The resulting biofilms were resuspended in 1XPBS and TEM imaging was performed. ImageJ (NIH) was used to threshold images and calculate area covered by curli fibrils and area covered by cells. The ratio of areas was used to quantify curli fibril production.

Crystal Violet (CV) biofilm assays (Supplementary Fig. 3). Experiments were performed to verify that aTc$_{Receiver}$/CsgA$_{His}$ formed thick adherent biofilms only when induced by aTc, on both Thermanox coverslips (Nunc) and on polystyrene. Thermanox coverslips were placed at the bottom of 24-well plate wells in which aTc$_{Receiver}$/CsgA$_{His}$, at an initial seeding density of $5X10^7$ cells/ml, was grown for 24h in glucose-

supplemented M63 with no aTc or with 250ng/ml aTc, in 24-well plate wells with or without Thermanox coverslips. Positive control strain MG1655 *ompR234* and negative control strain MG1655 *PRO csgA ompR234* were similarly cultured for 24h in glucose-supplemented M63.

Crystal violet staining and quantification was performed following a standard protocol given in O'Toole *et. al.*[16] Thermanox coverslips with biofilm were washed in ddH_2O to remove unattached cells, placed in a clean 24-well plate well with 400µl of 0.1% aqueous crystal violet (Sigma), and incubated at RT for 10-15min, after which the coverslips were washed by immersing 3-4 times in a tub of ddH_2O until no more visible dye was washed off. The Thermanox coverslips were allowed to air dry, placed back into clean 24-well plate wells, and photographs taken with a ChemiDoc MP imaging system (BioRad). For quantification of CV staining, the Thermanox coverslips were placed in 24-well plate wells and 400µl of 30% acetic acid in water was added. The coverslips were incubated for 10-15min at RT to solubilize CV. Subsequently, 125µl of solubilized CV was transferred to a 96-well plate well and absorbance at 550nm was measured, with 30% acetic acid in water as a blank.

For biofilms grown on polystyrene surface of 24-well plate wells, wash steps were performed by repeatedly immersing entire plates in a tub of ddH_2O.

Congo Red assay for quantification of curli fibril production (Supplementary Fig. 4). Cells were grown to saturation at 30°C in liquid YESCA media (10g/L casamino acids, 1g/L yeast extract) and 15µl was drop cast on YESCA agar (10g/L casamino acids, 1g/L yeast extract, and 20g/L agar) in triplicate and grown for 72h at 30°C [17]. Colonies were scraped and resuspended in 700µl 1XPBS; 300µl of cell suspension was used for OD600 cell number normalization, and the remaining 400µl combined with 5X Congo

Red (CR) for a final concentration of 20μg/ml CR, and incubated for 5min at RT. The cells and curli with bound CR were spun down at 15,000 x g for 5min, and 300μl supernatant was removed for CR quantification. Concentration of CR in supernatant was quantified by absorbance at 480nm. The amount of CR bound by cells and curli were quantified by subtracting the Ab_{480nm} of supernatant from Ab_{480nm} of 20μg/ml CR [18].

For growth of BW25113 Δ*csgA*, kanamycin at 30μg/ml was added to YESCA. For growth of BW25113 Δ*csgA* / pZS3-pL(lacO)-*csgA* and BW25113 Δ*csgA* / pZS3-pL(lacO)-$csgA_{His\ after\ C\text{-}terminus}$, chloramphenicol at 25μg/ml and kanamycin at 30μg/ml were added to YESCA.

Evaluating pL(lacO) for regulation of curli production (Supplementary Fig. 19). Cells grown to saturation at 30°C in liquid YESCA media were drop cast onto YESCA agar and grown for 48h at 30°C [17]. For growth of BW25113 Δ*csgA*, kanamycin at 30μg/ml was added to YESCA. For growth of BW25113 Δ*csgA* / pZS3-pL(lacO)-*csgA* + pZS4Int-*lacI/tetR*, chloramphenicol at 25μg/ml, spectinomycin at 100μg/ml, and kanamycin at 30μg/ml were added to YESCA. For isopropyl β-D-1-thiogalactopyranoside (IPTG) induction, 1mM IPTG was added to YESCA agar.

Patterning experiments (Figs. 2-4; Supplementary Figs. 6, 7, 10-12). In all cases, cultures were grown at 30°C with no shaking. After patterning, the resulting cell populations were resuspended in 1XPBS and the NiNTA-AuNP labelling assay and TEM imaging were performed to characterize the resulting amyloid fibrils. ImageJ (NIH) was used to measure the length of unlabelled and NiNTA-AuNP labelled fibril segments.

For tunable patterning based on changing induction time (Fig. 2a, b), $AHL_{Receiver}$/CsgA at an initial seeding density of $5X10^6$ cells/ml and $aTc_{Receiver}$/$CsgA_{His}$ at

an initial seeding density of $5X10^5$ cells/ml were co-cultured in 24-well plate wells with a 12mm glass coverslip (Ted Pella) placed at the bottom. Cells were cultured in glycerol-supplemented M63 media. The cells were first co-cultured in the presence of 50nM N-(β-ketocaproyl)-L-homoserine lactone (AHL) inducer for 18-48h. The media was then removed and the resulting cells were incubated with no-inducer media for 6h. The no-inducer media was then removed and replaced with media with 50ng/ml aTc inducer. The cells were resuspended and the cultures incubated for 16h. The resulting cells were resuspended and the NiNTA-AuNP labelling assay was performed to characterize curli fibrils. For the control experiment to produce fibrils when CsgA and $CsgA_{His}$ were secreted slowly and simultaneously without temporal separation, $AHL_{Receiver}$/CsgA and $aTc_{Receiver}$/$CsgA_{His}$ were co-cultured for 24h in glycerol-supplemented M63 media with induction by 50nM AHL and 50ng/ml aTc simultaneously.

For tunable patterning based on varying inducer concentration (Fig. 2c, d), $AHL_{Receiver}$/CsgA and $aTc_{Receiver}$/$CsgA_{His}$, each at an initial seeding density of $5X10^7$ cells/ml, were co-cultured in glucose-supplemented M63 media with AHL inducer at 0-1000nM and aTc inducer at 0-250ng/ml, for 18h.

For production of a dynamic material whose composition changes with time (Fig. 3), a cellular communication system consisting of AHL_{Sender}+$aTc_{Receiver}$/CsgA and $AHL_{Receiver}$/$CsgA_{His}$ was used. The two cell strains were co-cultured, with AHL_{Sender}+$aTc_{Receiver}$/CsgA at an initial seeding density of $5X10^6$ cells/ml and $AHL_{Receiver}$/$CsgA_{His}$ at an initial seeding density of $5X10^7$, $5X10^6$, or $5X10^5$ cells/ml. The cells were co-cultured in glucose-supplemented M63 media with 50ng/ml aTc for 4-36h. The resulting cells were resuspended and the NiNTA-AuNP labelling assay was performed to characterize curli fibrils. For controls, AHL_{Sender}+$aTc_{Receiver}$/CsgA and

$AHL_{Receiver}$/$CsgA_{His}$ were grown separately. In each case, the cells were grown for 16h with 50ng/ml aTc induction, with an initial seeding density of $5X10^6$ cells/ml.

For patterning at two different length scales by combining genetic regulation of subunit expression with spatial inducer gradients (Fig. 4a, b), inducer-responsive cells were grown in solid phase on agar with opposing AHL and aTc inducer gradients. Inducer gradient agar plates were prepared by a two-step process[19]. A 100mmX100mm square petri dish (Ted Pella) was elevated at one end by 1cm. It was first filled by 20ml of 1.5% agar glucose-supplemented M63 with 50nM AHL and was allowed to harden into an agar wedge. The plate was then laid flat and filled with 20ml of 1.5% agar glucose-supplemented M63 with 50ng/ml aTc. The plates were left for 12h to allow diffusion of inducers to set up a concentration gradient. The surface of the agar was then overlaid with 5ml of 0.7% agar glucose-supplemented M63 (top-agar) embedded with four cell strains – $AHL_{Receiver}$/CsgA, $aTc_{Receiver}$/$CsgA_{His}$, $AHL_{Receiver}$/GFP, and $aTc_{Receiver}$/mCherry – each at a cell density of $3.33X10^8$ cells/ml. The top-agar with embedded cells was allowed to harden, and the plate was incubated at 30°C for 40h. Fluorescence was imaged with a ChemiDoc MP imaging system (BioRad) and fluorescence intensity values extracted with ImageJ (NIH). Top agar was sampled and resuspended in 1XPBS, and the NiNTA-AuNP labelling assay was performed to characterize curli fibrils. For the control condition with no inducer gradients, the same procedure was carried out but the petri dish was not elevated at one end to create agar wedges.

For patterning by protein-level engineering (Fig. 4c), $AHL_{Receiver}$/8X$CsgA_{His}$ cells, at an initial seeding density of $5X10^6$ cells/ml, were cultured in glucose-supplemented M63 with 10nM AHL inducer for 28h. The resulting cells were resuspended and the

NiNTA-AuNP labelling assay was performed to characterize curli fibrils. For the control experiment, $aTc_{Receiver}/CsgA_{His}$ at an initial seeding density of $1.5X10^6$ cells/ml was cultured in glucose-supplemented M63 with 10ng/ml aTc inducer for 28h.

For patterning at two different length scales by combining genetic regulation of subunit expression with subunit-level protein engineering (Fig. 4d), $AHL_{Receiver}/8XCsgA_{His}$ at an initial seeding density of $5X10^7$ cells/ml and $aTc_{Receiver}/CsgA_{His}$ at an initial seeding density of $5X10^5$ cells/ml were first co-cultured in glucose-supplemented M63 media with 4nM AHL inducer for 36h. The media was then removed and the resulting cells incubated with no-inducer glucose-supplemented M63 media for 6h. The no-inducer media was then removed and replaced with glucose-supplemented M63 media with 1ng/ml aTc inducer. The cells were resuspended and the cultures were incubated for 18h.

Conductive biofilm demonstration (Fig. 5, Supplementary Figs. 13-17). To create interdigitated electrodes (IDEs) for measurement of biofilm conductance, custom shadowing masks (Tech-Etch) with holes of the appropriate dimensions (Supplementary Fig. 13) were placed over Thermanox coverslips. Gold was sputtered to a thickness of ~200nm with a Desk II Sputter Coater (Denton Vacuum) and the resulting IDEs were tested with a Keithley 4200 picoammeter with two-point probe to confirm the absence of short circuits.

IDEs were placed at the bottom of 24-well plate wells and covered with glucose-supplemented M63 media with 250ng/ml anhydrotetracycline (aTc), $aTc_{Receiver}/CsgA_{His}$ cells at $1X10^8$ cells/ml, and 100nM NiNTA-AuNP particles. The cultures were incubated at 30°C with no shaking for 24h. For control experiments, either aTc was excluded, $AHL_{Receiver}/CsgA_{His}$ cells were used in place of $aTc_{Receiver}/CsgA_{His}$ cells, or NiNTA-AuNP

particles were excluded (Fig. 5, Supplementary Fig. 17). $aTc_{Receiver}/CsgA_{His}$ with the addition of pZE-AmpR-proB-*mCherry* was used to show by confocal microscopy that biofilm formation is induced by aTc in presence of 100nM NiNTA-AuNP, with images taken at 4h and 24h timepoints (Supplementary Fig. 14). Please see above for details of confocal microscopy methods.

To obtain samples of biofilms for TEM, a small amount of biofilm was scraped from the IDE substrate and resuspended in 1XPBS. IDEs were washed by repeatedly immersing in ddH_2O, laid on a flat surface, and allowed to air dry for three days. A Keithley 4200 picoammeter with two-point probe was used to carry out a voltage sweep; a voltage difference was applied across the two probes and the current measured. Resulting I-V curves were fitted to simple linear regression lines and conductance of the biofilm was obtained from the slope (Supplementary Fig. 15). SEM imaging was then performed to characterize intact biofilms; SEM imaging was performed after conductance measurements because the samples were coated with a conductive carbon layer to facilitate imaging (Fig. 5b).

Gold nanowire and nanorod synthesis (Fig. 5c). Strains $aTc_{Receiver}/CsgA_{His}$ and $AHL_{Receiver}/CsgA$ were seeded each at a concentration of $5X10^7$ cells/ml into glucose-supplemented M63, and grown for 24h at 30°C in 24-well plates. The cells were induced with 50ng/ml aTc alone, 100nM AHL alone, or both simultaneously. The resulting cells with curli fibrils were resuspended in 1XPBS, deposited on TEM grids, and labelled with 5nm NiNTA-AuNP using the specific NiNTA-AuNP binding protocol above. Gold was specifically deposited on NiNTA-AuNP chains using the GoldEnhance™ EM kit (Nanoprobes). Gold enhancement was performed for 2min following kit instructions, resulting in gold nanowires and nanorods.

Expression and purification of SpyCatcher protein. *E. coli* BL21 DE3 pLysS / pDEST14-T7-*CCSpyCatcher* (Supplementary Table 3) was grown for 12-16h at 37°C in LB-Miller with 50µg/ml carbenicillin and 0.4mM IPTG[5]. The His-tagged SpyCatcher protein with two N-terminal cyteines was purified with Ni-NTA Spin Columns (Qiagen) following the native protein purification protocol described in the Ni-NTA Spin Kit Handbook. The buffer of the elution fraction was exchanged for 1XPBS using 0.5ml Amicon filter columns (MWCO 3kDa).

Synthesis of QDs and conjugation to SpyCatcher. CdTe/CdS QDs with a photoluminescence emission peak at 620nm were synthesized following the method described in Deng *et al.*[20]. The QDs were purified by adding isopropyl alcohol, followed by centrifugation at 15000rpm for 15min and subsequent resuspension in ddH_2O. The concentration of the CdTe/CdS QDs and the amount of additional shell precursors needed to obtain specific shell thicknesses were calculated by following the method described in Deng *et al.*: 5µl $Cd(NO_3)_2$ (as Cd^{2+} source) stock solution (25mM) and 10µl 3-mercaptopropionic acid stock solution (25mM) were combined with the CdTe/CdS QDs dispersed in 100µl ddH_2O, vortexed, and gently sonicated in a 1.5ml Eppendorf. Next, 20µl of 2mg/ml of CCSpyCatcher protein was added and gently vortexed. The pH was tuned to 12.2 by adding NaOH (1M). The reaction mixture was placed on a heating block at 90°C for 30min, and then cooled down by submerging the tube in an ice water bath. The reacted solution was loaded into a 0.5ml Amicon filter (MWCO 30kDa, EMD Millipore), 250µl 1XPBS buffer was added to the filter, and the sample was subjected to centrifugation at 7000rpm for 5min. The washing (each wash was performed with 350µl of 1XPBS buffer) and centrifugation (7000rpm for 5min) steps were repeated three times. The final product was re-dispersed in 100µl 1XPBS. The diameter of the

CdTe/CdS quantum dots was ~4nm. We measured the emission spectrum of CCSpyCatcher conjugated CdTe/CdS QDs with a NanoLog Spectrometer (HORIBA Jobin Yvon) and found an emission peak at 638nm when excited at 450nm. The particles were also visibly highly fluorescent when illuminated by a UV lamp at 365nm (Supplementary Fig. 21).

Specific binding of QD-SpyCatcher to curli fibrils (Fig. 6a). Curli fibrils deposited on TEM grids were floated on 50µl of SpyCatcher Binding Buffer (1X PBS + 350mM NaCl + 0.3v/v% Tween20) for 5min and subsequently transferred to 50µl SpyCatcher Binding Buffer with 1:333 dilution of QD-SpyCatcher, followed by incubation at RT for 45min. The grid was subsequently washed four times with 50µl droplets of SpyCatcher Binding Buffer, then washed four times with 30µl droplets of ddH_2O, followed by negative staining with UA if no subsequent AuNP binding was performed. Strain $AHL_{Receiver}/CsgA_{SpyTag}$ was used to produce $CsgA_{SpyTag}$ fibrils and strain $AHL_{Receiver}$/CsgA was used to produce CsgA fibrils; cells were seeded at $5X10^7$ cells/ml and cultured in glucose-supplemented M63 media with 100nM AHL for 12h at 30°C.

Specific binding of 40nm-AuNP-antibody conjugates to curli fibrils (Fig. 6a). Curli fibrils deposited on TEM grids were floated on a 50µl droplet of Blocking Buffer (10mM Tris (pH 8.0)-0.15M NaCl-1% skim milk) for 30min, followed by transfer to a 50µl droplet of Binding Buffer (10mM Tris (pH 8.0)-0.15M NaCl-0.1% skim milk) with 1:250 dilution of rabbit anti-FLAG antibody (Sigma), where it was incubated for 1h at RT. The grid was then rinsed four times in 50µl droplets of Wash Buffer (10mM Tris (pH 8.0)-0.15M NaCl), and subsequently transferred to a 50µl droplet of Binding Buffer with 1:10 dilution of goat anti-rabbit antibodies conjugated to 40nm AuNPs (Abcam), where it was incubated for 3 hours at RT. The grid was then rinsed four times in 50µl droplets of

Wash Buffer, followed by four rinses in 30µl droplets of ddH_2O and negative staining with UA. Strain $aTc_{Receiver}/CsgA_{FLAG}$ was used to produce $CsgA_{FLAG}$ fibrils and strain $aTc_{Receiver}$/CsgA was used to produce CsgA fibrils; cells were seeded at $5X10^7$ cells/ml and cultured in glucose-supplemented M63 media with 50ng/ml aTc for 12h at 30°C.

Co-docking of QD and AuNP to curli fibrils (Fig. 6b-c). Strains $AHL_{Receiver}/CsgA_{SpyTag}$ and $aTc_{Receiver}/CsgA_{FLAG}$ were seeded each at a concentration of $5X10^7$ cells/ml into glucose-supplemented M63 media, and grown with 12mm glass coverslips (Ted Pella) for 12h at 30°C. The cells were induced with 100nM AHL alone, 50ng/ml aTc alone, or both simultaneously. Curli was resuspended in 1XPBS, deposited on TEM grids, and the specific QD-SpyCatcher binding protocol was performed, followed by the specific AuNP-antibody binding protocol and negative staining with UA. For FLIM characterization, the QD-binding protocol followed by the AuNP-binding protocol was performed directly on rinsed coverslips with attached cells and curli fibrils, sans negative staining.

Zinc sulphide nanocrystal synthesis (Fig. 6d-e). Cells were grown for 12h in LB-Miller, washed in 1XPBS, and resuspended to a concentration of 10^{10} cells/ml. 5µl of cell suspension was drop cast on YESCA agar and grown for 30h at 30°C. For culturing BW25113 Δ*csgA* / pZS3-pL(lacO)-*csgA* and BW25113 Δ*csgA* / pZS3-pL(lacO)-$csgA_{ZnS\ peptide}$ strains, chloramphenicol at 25µg/ml was added to YESCA agar. The colony was then resuspended in 30µl ddH_2O. We used a ZnS synthesis protocol based on that given in Mao *et. al.*[21] Specifically, 10µl of cell and curli suspension was added to 1ml of 1µM $ZnCl_2$ and incubated at RT for 12h. Then, 1µM Na_2S was added, and samples were incubated at 0°C for 24h by packing in ice and placing in a 4°C room. Samples were subsequently allowed to age for 12h at RT before being deposited on TEM grids for HRTEM and glass coverslips for fluorescence characterization.

Expression and purification of mature CsgA$_{His}$noSS (Supplementary Fig. 22). For the concentration reference standard for quantitating CsgA production in biofilms by dot blot, we use purified CsgA$_{His}$noSS, which is the mature form of CsgA protein without the secretion signal sequence that is cleaved during secretion. We followed the protocol described in Zhong *et al.*[22].

In summary, the pET11d-T7 vector (Novagen) was digested at BamHI and NcoI restriction sites, and the *csgA$_{His}$noSS* gene (Supplementary Table 1) was amplified by PCR with introduction of compatible overhangs for Gibson assembly. To create the pET11d-T7-*csgA$_{His}$noSS* plasmid (Supplementary Table 2), the digested vector and *csgA$_{His}$noSS* PCR product were incubated with Gibson Assembly Master Mix (NEB) at 50°C for 1h, then transformed into *E. coli* DH5□. The sequence-verified pET11d-T7-*csgA$_{His}$noSS* plasmid was then transformed into *E. coli* BL21 T7 Express *I^{q}* (NEB) to create the BL21 T7 Express *I^{q}* / pET11d-T7-*csgA$_{His}$noSS* strain (Supplementary Table 3) for protein expression.

BL21 T7 Express *I^{q}* / pET11d-T7-*csgA$_{His}$noSS* was grown to OD600 ~0.9 in LB-Miller containing 50□g/ml carbenicillin at 37° C. Protein expression was induced with 0.5mM IPTG at 37° C for 1h. Cells were collected by centrifugation and the pellets stored at −80° C. The cells were subsequently resuspended and lysed with Extraction Buffer (8M guanidine hydrochloride (GdnHCl), 300mM NaCl, 50mM K_2HPO_4/KH_2PO_4, pH 7.2). A total of 50ml of Extraction Buffer was used for each cell pellet from a 1.5 litre culture. Lysates were incubated at 4°C for 24h. The insoluble portions of the lysates were removed by centrifugation at 10,000 x g. 6ml of TALON cobalt resin (Clontech) was washed with Equilibration Buffer (300mM NaCl, 50mM K_2HPO_4/KH_2PO_4, pH 7.2) and the supernatant was incubated with equilibrated TALON cobalt resin for 2h at RT.

Resin binding the His-tagged $CsgA_{His}$noSS was spun down, washed twice with 20ml Equilibration Buffer, and loaded into HisTALON™ Gravity Columns (Clontech). The resin was further washed with 12ml of Equilibration Buffer passed through columns. Subsequently, Wash Buffer (40mM imidazole, 300mM NaCl, 50mM K_2HPO_4/KH_2PO_4, pH 7.2) was passed through columns in 5 consecutive wash steps, using 6ml in each wash. Then Elution Buffer (300mM imidazole, 300mM NaCl, 50mM K_2HPO_4/KH_2PO_4, pH 7.2) was passed through columns to elute $CsgA_{His}$noSS in 3 consecutive elution steps, using 6ml in each elution. Fractions from wash and elution steps were then mixed with loading sample buffer (Novex 4X LDS Sample Buffer, NuPAGE) in a 3:1 ratio and heated at 90°C for 10min. The samples were then loaded into a Novex 4-12% Bis-Tris gel (NuPAGE) and ran at 165V for 35min in MES Buffer (NuPAGE). The gel was then stained with Coomassie Blue G-250 (0.1% in 7/50/43 acetic acid/methanol/ddH_2O) by incubating at RT for 30min, followed by 3 consecutive wash steps with incubation in 25ml destaining solution (10/40/50 acetic acid/methanol/ddH_2O) for 30min at RT, followed by incubation in 25ml ddH_2O overnight at RT. The destained gel was then imaged with a Gel Doc™ XR+ System with Image Lab™ Software (Bio-rad).

Dot blot quantitation of curli production (Supplementary Fig. 22). Strains MG1655 *ompR234*, MG1655 *PRO ΔcsgA ompR234*, and $aTc_{Receiver}/CsgA_{His}$ were cultured in M63 glucose at 30°C in 24-well plate wells, without shaking, for 0, 12, and 24h. $aTc_{Receiver}/CsgA_{His}$ cells were grown either in the presence or absence of 250ng/ml aTc. At each timepoint, culture supernatant was removed without disturbing biomass at the bottom of wells, and biomass at the bottom of wells was resuspended in 1ml ddH_2O. $CsgA_{His}$ was quantified by a standard dot blot protocol, following references in which dot blots were used to quantitate the concentrations of CsgA and other amyloid

proteins[23-25]. Briefly, 2□l of samples were spotted onto Protran BA83 nitrocellulose membranes (Whatman) with a dot blot manifold (Schleicher & Schuell Minifold-I Dot-Blot System). The membrane was blocked in TBST + 5% skim milk for 30min at RT, followed by incubation in TBST + 0.1% skim milk with a 1:10000 dilution of rabbit anti-CsgA antibody (M. Chapman, University of Michigan[14,15]) for 1h at RT. The membrane was then washed three times in TBST (incubating at RT for 5min), followed by incubation in TBST + 0.1% skim milk with a 1:5000 dilution of HRP-conjugated goat anti-rabbit IgG antibody (Abcam) for 30min at RT. Subsequently, the membrane was washed three times in TBST (incubating at RT for 15min, then 2 X 5min), followed by one wash in TBS (incubating at RT for 5min). The washed membrane was incubated with SuperSignal West Pico (Thermo) chemiluminescent substrate following kit instructions, and imaged with a ChemiDoc MP imaging system (BioRad), with quantitation of spot luminescence signal intensity by Quantity One (BioRad) software. Protein concentrations were calculated from a reference curve established by serial dilutions of fibrils of purified mature $CsgA_{His}$noSS protein, which lacks the CsgA secretion signal sequence cleaved off during secretion[26]. The purified protein was incubated at RT for ~12h to allow for fibrillization. We accounted for the difference in molecular weights between secreted $CsgA_{His}$ (15kDa) and purified $CsgA_{His}$noSS (14.2kDa), since the former has an additional His tag. The amount of $CsgA_{His}$ protein per biofilm sample grown in 24-well plate wells was divided by the 1.9cm^2 surface area of the wells to obtain □g of $CsgA_{His}$ per cm^2 of biofilm. For the 24h timepoint, for which the volume per unit area of biofilm was measured by confocal microscopy, we also calculated mg of $CsgA_{His}$ per cm^3 of biofilm.

Supplementary Tables

Supplementary Table A-1 | Synthetic parts used in this work.

Part Name	**Part Type**	**Sequence**	**Source**
pL(tetO)	Promoter	TCCCTATCAGTGATAGAGATTGACATCCCTATCAGTGATAGAGATACTGAGCACATCAGCAGGACGCACTGACC	[4]
pLuxR *Designated "pLuxI" in* [3]	Promoter	ACCTGTAGGATCGTACAGGTTTACGCAAGAAAATGGTTTGTTATAGTCGAATA	[3]
pL(lacO)	Promoter	AATTGTGAGCGGATAACAATTGACATTGTGAGCGGATAACAAGATACTGAGCACA	[4]
P(lac)	Promoter	CCGGTTAGCGCTCTCATTAGGCACCCCAGGCTTGACACTTTATGCTTCCGGCTCGTATAATGACTGCATTTATTGGTAC	[27]
cr_rr10	Riboregulator *cis* repressor sequence	TACCTATCTGCTCTTGAATTTGGGT	[3]
cr_rr12	Riboregulato	TACCATTCACCTCTTGGATTTGGGT	[3]

	r *cis* repressor sequence		
cr_rr12y	Riboregulator *cis* repressor sequence	TACCATTCACCTCTTGGATTTAGCT	[3]
taRNA_rr10	Riboregulator *trans* activator sequence	ACCCAAATTCATGAGCAGATTGGTAGTGGTGGTT AATGAAAATTAACTTACTACTACCTTTC	[3]
taRNA_rr12	Riboregulator *trans* activator sequence	ACCCAAATCCAGGAGGTGATTGGTAGTGGTGGTT AATGAAAATTAACTTACTACTACCATATATC	[3]
taRNA_rr12y	Riboregulator *trans* activator sequence	AGCTAAATCCAGGAGGTGATTGGTAGTGGTGGTT AATGAAAATTAACTTACTACTACCATATATC	[3]
rrnB T1	Terminator	GGCATCAAATAAAACGAAAGGCTCAGTCGAAAGA CTGGGCCTTTCGTTTTATCTGTTGTTTGTCGGTGA ACGCTCTCCTGAGTAGGACAAATCCGCCGCCCTAG	[3]

		A	
rrnB T	Terminator (double terminator from rrnB)	TGCCTGGCGGCAGTAGCGCGGTGGTCCCACCTGAC CCCATGCCGAACTCAGAAGTGAAACGCCGTAGCGC CGATGGTAGTGTGGGGTCTCCCCATGCGAGAGTA GGGAACTGCCAGGCATCAAATAAAACGAAAGGCT CAGTCGAAAGACTGGGCCTT	[28]
luxR	Repressor	ATGAAAAACATAAATGCCGACGACACATACAGAA TAATTAATAAAATTAAAGCTTGTAGAAGCAATAA TGATATTAATCAATGCTTATCTGATATGACTAAA ATGGTACATTGTGAATATTATTTACTCGCGATCA TTTATCCTCATTCTATGGTTAAATCTGATATTTC AATTCTAGATAATTACCCTAAAAAATGGAGGCAA TATTATGATGACGCTAATTTAATAAAATATGATC CTATAGTAGATTATTCTAACTCCAATCATTCACC AATTAATTGGAATATATTTGAAAACAATGCTGTA AATAAAAAATCTCCAAATGTAATTAAAGAAGCGA AAACATCAGGTCTTATCACTGGGTTTAGTTTCCC TATTCATACGGCTAACAATGGCTTCGGAATGCTT AGTTTTGCACATTCAGAAAAAGACAACTATATAG ATAGTTTATTTTTACATGCGTGTATGAACATACC ATTAATTGTTCCTTCTCTAGTTGATAATTATCGA AAAATAAATATAGCAAATAATAAATCAAACAACG ATTTAACCAAAAGAGAAAAAGAATGTTTAGCGTG GGCATGCGAAGGAAAAAGCTCTTGGGATATTTCA	[3]

		AAAATATTAGGCTGCAGTGAGCGTACTGTCACTT TCCATTTAACCAATGCGCAAATGAAACTCAATAC AACAAACCGCTGCCAAAGTATTTCTAAAGCAATT TTAACAGGAGCAATTGATTGCCCATACTTTAAAA ATTAA	
luxI	AHL signalling molecule generator	ATGACTATAATGATAAAAAAATCGGATTTTTTGG CAATTCCATCGGAGGAGTATAAAGGTATTCTAAG TCTTCGTTATCAAGTGTTTAAGCAAAGACTTGAG TGGGACTTAGTTGTAGAAAATAACCTTGAATCAG ATGAGTATGATAACTCAAATGCAGAATATATTTA TGCTTGTGATGATACTGAAAATGTAAGTGGATGC TGGCGTTTATTACCTACAACAGGTGATTATATGC TGAAAAGTGTTTTTCCTGAATTGCTTGGTCAACA GAGTGCTCCCAAAGATCCTAATATAGTCGAATTA AGTCGTTTTGCTGTAGGTAAAAATAGCTCAAAGA TAAATAACTCTGCTAGTGAAATTACAATGAAACT ATTTGAAGCTATATATAAACACGCTGTTAGTCAA GGTATTACAGAATATGTAACAGTAACATCAACAG CAATAGAGCGATTTTTAAAGCGTATTAAAGTTCC TTGTCATCGTATTGGAGACAAAGAAATTCATGTA TTAGGTGATACTAAATCGGTTGTATTGTCTATGC CTATTAATGAACAGTTTAAAAAAGCAGTCTTAAA TTAA	[27]

csgA	Curli amyloid material subunit	ATGAAACTTTTAAAAGTAGCAGCAATTGCAGCAA TCGTATTCTCCGGTAGCGCTCTGGCAGGTGTTGTT CCTCAGTACGGCGGCGGCGGTAACCACGGTGGTG GCGGTAATAATAGCGGCCCAAATTCTGAGCTGAA CATTTACCAGTACGGTGGCGGTAACTCTGCACTTG CTCTGCAAACTGATGCCCGTAACTCTGACTTGACT ATTACCCAGCATGGCGGCGGTAATGGTGCAGATG TTGGTCAGGGCTCAGATGACAGCTCAATCGATCT GACCCAACGTGGCTTCGGTAACAGCGCTACTCTTG ATCAGTGGAACGGCAAAAATTCTGAAATGACGGT TAAACAGTTCGGTGGTGGCAACGGTGCTGCAGTT GACCAGACTGCATCTAACTCCTCCGTCAACGTGAC TCAGGTTGGCTTTGGTAACAACGCGACCGCTCATC AGTACTAA	[1]
csgA$_{His}$	Curli amyloid material subunit	ATGAAACTTTTAAAAGTAGCAGCAATTGCAGCAA TCGTATTCTCCGGTAGCGCTCTGGCAGGTGTTGTT CCTCAGTACGGCGGCGGCGGTAACCACGGTGGTG GCGGTAATAATAGCGGCCCAAATCACCATCACCA TCACCACCATTCTGAGCTGAACATTTACCAGTACG GTGGCGGTAACTCTGCACTTGCTCTGCAAACTGAT GCCCGTAACTCTGACTTGACTATTACCCAGCATGG CGGCGGTAATGGTGCAGATGTTGGTCAGGGCTCA GATGACAGCTCAATCGATCTGACCCAACGTGGCT TCGGTAACAGCGCTACTCTTGATCAGTGGAACGG	This work

		CAAAAATTCTGAAATGACGGTTAAACAGTTCGGT GGTGGCAACGGTGCTGCAGTTGACCAGACTGCAT CTAACTCCTCCGTCAACGTGACTCAGGTTGGCTTT GGTAACAACGCGACCGCTCATCAGTACCACCATCA CCATCACCACCATTAA	
8XcsgA$_{His}$	Curli amyloid material subunit	ATGAAGCTGCTGAAGGTGGCTGCTATCGCTGCTA TCGTGTTTTCCGGTTCGGCACTGGCTGGTGTCGTC CCGCAATACGGTGGCGGTGGCAACCATGGCGGTG GCGGTAACAATAGTGGTCCGAACTCCGAACTGAA TATTTATCAGTACGGCGGTGGCAACAGCGCACTG GCACTGCAAACGGATGCACGTAATTCTGACCTGA CCATTACGCAGCATGGTGGCGGTAACGGCGCTGA TGTGGGCCAAGGTAGTGATGACAGCTCTATCGAC CTGACCCAGCGCGGCTTTGGTAATAGTGCAACGCT GGATCAATGGAACGGCAAAAATTCCGAAATGACC GTTAAGCAGTTCGGCGGTGGCAATGGTGCGGCCG TCGATCAAACCGCGTCCAACAGTTCCGTGAATGTT ACGCAGGTTGGCTTTGGTAACAATGCAACCGCTC ATCAATATAACGGCAAAAATGGATCCTCGGAACT GAACATCTATCAGTACGGTGGCGGTAATTCAGCG CTGGCCCTGCAAACCGATGCGCGTAACTCGGATCT GACGATTACGCAGCATGGCGGTGGCAACGGTGCC GATGTCGGTCAGGGCAGCGACGATTCTAGCATCG ACCTGACGCAACGTGGCTTTGGTAACAGCGCCACC	This work

		CTGGACCAGTGGAATGGTAAAAATTCTGAAATGA CCGTGAAGCAGTTCGGTGGCGGTAATGGTGCAGC TGTTGATCAAACGGCAAGCAACAGTTCCGTCAAT GTGACCCAAGTGGGCTTCGGTAACAATGCAACGG CTCATCAATACAATGGTAAGAACGGATCCTCGGA ACTGAACATTTACCAATACGGCGGTGGCAATAGT GCCCTGGCGCTGCAAACCGATGCACGTAACTCCGA TCTGACGATCACGCAGCACGGTGGCGGTAACGGT GCTGATGTTGGCCAAGGTTCAGACGATTCTTCCA TTGATCTGACGCAACGCGGCTTTGGTAACTCAGC GACCCTGGACCAATGGAATGGTAAGAACTCGGAA ATGACCGTCAAACAATTTGGCGGTGGCAACGGGG CGGCCGTGGATCAAACCGCCTCTAACAGTTCCGTT AATGTCACGCAAGTGGGTTTCGGCAATAACGCCA CGGCCCACCAGTACAATGGTAAGAATGGATCCAG CGAACTGAATATCTACCAATATGGTGGCGGTAAT AGCGCCCTGGCTCTGCAGACGGATGCGCGTAACAG CGATCTGACCATCACCCAGCACGGCGGTGGCAACG GCGCAGACGTGGGTCAGGGCAGCGATGATTCTTC TATCGACCTGACGCAGCGTGGTTTTGGTAACAGT GCAACCCTGGATCAGTGGAATGGCAAGAACAGCG AAATGACGGTTAAACAATTTGGTGGCGGTAACGG GGCAGCTGTCGATCAAACGGCCAGTAATAGTTCC GTGAACGTGACGCAAGTTGGTTTTGGCAATAACG	

		CGACCGCCCATCAATACAATGGCAAGAACGGATC CAGCGAACTGAACATTTATCAATATGGCGGTGGC AACTCTGCCCTGGCTCTGCAAACGGACGCCCGTAA CTCGGACCTGACGATCACCCAACATGGTGGCGGTA ATGGTGCCGACGTTGGCCAAGGTAGCGACGATTC CAGCATTGATCTGACCCAACGTGGTTTCGGTAAC AGCGCGACCCTGGATCAATGGAATGGCAAGAATA GCGAAATGACGGTCAAACAATTCGGCGGTGGCAA CGGAGCGGCCGTTGATCAAACCGCCAGTAACAGT TCCGTCAACGTGACGCAAGTGGGTTTTGGCAATA ATGCCACGGCCCACCAATACAATGGTAAAAACGG ATCCTCTGAACTGAATATTTACCAGTATGGTGGC GGTAACAGTGCCCTGGCACTGCAGACGGACGCGC GTAACTCCGACCTGACGATCACGCAACATGGCGGT GGCAATGGCGCCGATGTTGGCCAGGGTAGCGACG ATAGTAGCATTGATTTAACCCAGCGTGGTTTCGG CAATAGCGCCACGCTGGATCAGTGGAACGGTAAG AATTCAGAAATGACGGTCAAGCAATTTGGTGGCG GTAATGGGGCAGCTGTGGATCAGACGGCCAGCAA TAGTTCCGTTAACGTCACCCAAGTGGGTTTCGGT AACAACGCCACGGCTCATCAGTACAATGGTAAAA ATGGATCCTCCGAGTTAAACATCTACCAGTATGG CGGTGGCAATTCTGCCCTGGCCCTGCAAACGGACG CGCGCAATAGCGATCTGACCATTACCCAACACGGT	

		GGCGGTAATGGCGCCGACGTGGGCCAGGGTAGCG ATGATAGTTCCATTGACCTGACGCAACGCGGTTT CGGCAACAGTGCGACGCTGGACCAATGGAACGGT AAGAACTCTGAAATGACGGTGAAACAGTTTGGCG GTGGCAATGGGGCGGCCGTCGATCAGACCGCGTCT AACAGTTCCGTGAACGTGACACAGGTCGGTTTCG GCAATAATGCCACCGCCCATCAGTACAATGGCAA GAATGGATCCCAATACGGTGGCGGTAACTCGGCA CTGGCACTGCAGACCGATGCACGTAATAGCGACCT GACGATTACCCAACACGGCGGTGGCAATGGAGCA GATGTGGGCCAGGGTTCTGATGACTCATCGATTG ATCTGACGCAGCGTGGCTTCGGTAATTCAGCCACG CTGGACCAGTGGAACGGTAAAAACAGCGAGATGA CCGTTAAGCAATTCGGTGGCGGTAACGGAGCAGC TGTTGATCAGACGGCGAGCAACAGCTCTGTCAAT GTGACCCAGGTCGGTTTCGGTAATAATGCTACGG CACATCAGTATCACCACCACCATCATCATCACTAA	
gfp	Fluorescent reporter	ATGAGTAAAGGAGAAGAACTTTTCACTGGAGTTG TCCCAATTCTTGTTGAATTAGATGGTGATGTTAA TGGGCACAAATTTTCTGTCAGTGGAGAGGGTGAA GGTGATGCAACATACGGAAAACTTACCCTTAAAT TTATTTGCACTACTGGAAAACTACCTGTTCCATG GCCAACACTTGTCACTACTTTCGGTTATGGTGTTC AATGCTTTGCGAGATACCCAGATCATATGAAACA	[3]

		GCATGACTTTTTCAAGAGTGCCATGCCCGAAGGT TATGTACAGGAAAGAACTATATTTTTCAAAGATG ACGGGAACTACAAGACACGTGCTGAAGTCAAGTT TGAAGGTGATACCCTTGTTAATAGAATCGAGTTA AAAGGTATTGATTTTAAAGAAGATGGAAACATTC TTGGACACAAATTGGAATACAACTATAACTCACA CAATGTATACATCATGGCAGACAAACAAAAGAAT GGAATCAAAGTTAACTTCAAAATTAGACACAACA TTGAAGATGGAAGCGTTCAACTAGCAGACCATTA TCAACAAAATACTCCAATTGGCGATGGCCCTGTCC TTTTACCAGACAACCATTACCTGTCCACACAATCT GCCCTTTCGAAAGATCCCAACGAAAAGAGAGACC ACATGGTCCTTCTTGAGTTTGTAACAGCTGCTGG GATTACACATGGCATGGATGAACTATACAAATAA	
mCherry	Fluorescent reporter	ATGGTGAGCAAGGGCGAAGAAGATAACATGGCCA TCATCAAGGAGTTCATGCGCTTCAAGGTGCACAT GGAGGGCTCCGTGAACGGCCACGAGTTCGAGATC GAGGGCGAGGGCGAGGGCCGCCCCTACGAGGGCA CCCAGACCGCCAAGCTGAAGGTGACCAAGGGTGG CCCCCTGCCCTTCGCCTGGGACATCCTGTCCCCTC AGTTCATGTACGGCTCCAAGGCCTACGTGAAGCA CCCCGCCGACATCCCCGACTACTTGAAGCTGTCCT TCCCCGAGGGCTTCAAGTGGGAGCGCGTGATGAA CTTCGAGGACGGCGGCGTGGTGACCGTGACCCAG	[3]

		GACTCCTCCCTGCAGGACGGCGAGTTCATCTACAA GGTGAAGCTGCGCGGCACCAACTTCCCCTCCGACG GCCCCGTAATGCAGAAGAAGACCATGGGCTGGGA GGCCTCCTCCGAGCGGATGTACCCCGAGGACGGCG CCCTGAAGGGCGAGATCAAGCAGAGGCTGAAGCT GAAGGACGGCGGCCACTACGACGCTGAGGTCAAG ACCACCTACAAGGCCAAGAAGCCCGTGCAGCTGCC CGGCGCCTACAACGTCAACATCAAGTTGGACATC ACCTCCCACAACGAGGACTACACCATCGTGGAACA GTACGAACGCGCCGAGGGCCGCCACTCCACCGGCG GCATGGACGAGCTGTACAAGTAA	
csgA$_{SpyTag}$	Curli amyloid material subunit	ATGAAACTTTTAAAAGTAGCAGCAATTGCAGCAA TCGTATTCTCCGGTAGCGCTCTGGCAGGTGTTGTT CCTCAGTACGGCGGCGGCGGTAACCACGGTGGTG GCGGTAATAATAGCGGCCCAAATTCTGAGCTGAA CATTTACCAGTACGGTGGCGGTAACTCTGCACTTG CTCTGCAAACTGATGCCCGTAACTCTGACTTGACT ATTACCCAGCATGGCGGCGGTAATGGTGCAGATG TTGGTCAGGGCTCAGATGACAGCTCAATCGATCT GACCCAACGTGGCTTCGGTAACAGCGCTACTCTTG ATCAGTGGAACGGCAAAAATTCTGAAATGACGGT TAAACAGTTCGGTGGTGGCAACGGTGCTGCAGTT GACCAGACTGCATCTAACTCCTCCGTCAACGTGAC TCAGGTTGGCTTTGGTAACAACGCGACCGCTCATC	This work

		AGTACGGCGGGGGCTCCGGCGGGGGCTCCGCGCAC ATCGTTATGGTCGATGCATATAAACCCACCAAAT AA	
csgA$_{FLAG}$	Curli amyloid material subunit	ATGAAACTTTTAAAAGTAGCAGCAATTGCAGCAA TCGTATTCTCCGGTAGCGCTCTGGCAGGTGTTGTT CCTCAGTACGGCGGCGGCGGTAACCACGGTGGTG GCGGTAATAATAGCGGCCCAAATTCTGAGCTGAA CATTTACCAGTACGGTGGCGGTAACTCTGCACTTG CTCTGCAAACTGATGCCCGTAACTCTGACTTGACT ATTACCCAGCATGGCGGCGGTAATGGTGCAGATG TTGGTCAGGGCTCAGATGACAGCTCAATCGATCT GACCCAACGTGGCTTCGGTAACAGCGCTACTCTTG ATCAGTGGAACGGCAAAAATTCTGAAATGACGGT TAAACAGTTCGGTGGTGGCAACGGTGCTGCAGTT GACCAGACTGCATCTAACTCCTCCGTCAACGTGAC TCAGGTTGGCTTTGGTAACAACGCGACCGCTCATC AGTACGATTACAAGGATGACGATGACAAGTAA	This work
csgA$_{ZnS\ peptide}$	Curli amyloid material subunit	ATGAAACTTTTAAAAGTAGCAGCAATTGCAGCAA TCGTATTCTCCGGTAGCGCTCTGGCAGGTGTTGTT CCTCAGTACGGCGGCGGCGGTAACCACGGTGGTG GCGGTAATAATAGCGGCCCAAATTCTGAGCTGAA CATTTACCAGTACGGTGGCGGTAACTCTGCACTTG CTCTGCAAACTGATGCCCGTAACTCTGACTTGACT ATTACCCAGCATGGCGGCGGTAATGGTGCAGATG	This work

		TTGGTCAGGGCTCAGATGACAGCTCAATCGATCT GACCCAACGTGGCTTCGGTAACAGCGCTACTCTTG ATCAGTGGAACGGCAAAAATTCTGAAATGACGGT TAAACAGTTCGGTGGTGGCAACGGTGCTGCAGTT GACCAGACTGCATCTAACTCCTCCGTCAACGTGAC TCAGGTTGGCTTTGGTAACAACGCGACCGCTCATC AGTACGGTGGTGGTTCTTGCAACAACCCGATGCA CCAGAACTGCTAA	
csgA$_{His\ after\ C\text{-}terminus}$	Curli amyloid material subunit	ATGAAACTTTTAAAAGTAGCAGCAATTGCAGCAA TCGTATTCTCCGGTAGCGCTCTGGCAGGTGTTGTT CCTCAGTACGGCGGCGGCGGTAACCACGGTGGTG GCGGTAATAATAGCGGCCCAAATTCTGAGCTGAA CATTTACCAGTACGGTGGCGGTAACTCTGCACTTG CTCTGCAAACTGATGCCCGTAACTCTGACTTGACT ATTACCCAGCATGGCGGCGGTAATGGTGCAGATG TTGGTCAGGGCTCAGATGACAGCTCAATCGATCT GACCCAACGTGGCTTCGGTAACAGCGCTACTCTTG ATCAGTGGAACGGCAAAAATTCTGAAATGACGGT TAAACAGTTCGGTGGTGGCAACGGTGCTGCAGTT GACCAGACTGCATCTAACTCCTCCGTCAACGTGAC TCAGGTTGGCTTTGGTAACAACGCGACCGCTCATC AGTACCACCATCACCATCACCACCATTAA	This work
CCSpyCatche	Gene encoding the	ATGTGTTGTTCGTACTACCATCACCATCACCATCA CGATTACGACATCCCAACGACCGAAAACCTGTAT	[5]

r	SpyCatcher protein with two N-terminal cysteines for conjugation to CdTe/CdS QDs	TTTCAGGGCGCCATGGTTGATACCTTATCAGGTT TATCAAGTGAGCAAGGTCAGTCCGGTGATATGAC AATTGAAGAAGATAGTGCTACCCATATTAAATTC TCAAAACGTGATGAGGACGGCAAAGAGTTAGCTG GTGCAACTATGGAGTTGCGTGATTCATCTGGTAA AACTATTAGTACATGGATTTCAGATGGACAAGTG AAAGATTTCTACCTGTATCCAGGAAAATATACAT TTGTCGAAACCGCAGCACCAGACGGTTATGAGGT AGCAACTGCTATTACCTTTACAGTTAATGAGCAA GGTCAGGTTACTGTAAATGGCAAAGCAACTAAAG GTGACGCTCATATTTAA	
csgA$_{His}$noSS	Gene encoding the mature form of CsgA protein without the secretion signal, with a His tag at C-terminus; purified as a reference standard for	ATGGGTGTTGTTCCTCAGTACGGCGGCGGCGGTA ACCACGGTGGTGGCGGTAATAATAGCGGCCCAAA TTCTGAGCTGAACATTTACCAGTACGGTGGCGGT AACTCTGCACTTGCTCTGCAAACTGATGCCCGTAA CTCTGACTTGACTATTACCCAGCATGGCGGCGGTA ATGGTGCAGATGTTGGTCAGGGCTCAGATGACAG CTCAATCGATCTGACCCAACGTGGCTTCGGTAACA GCGCTACTCTTGATCAGTGGAACGGCAAAAATTC TGAAATGACGGTTAAACAGTTCGGTGGTGGCAAC GGTGCTGCAGTTGACCAGACTGCATCTAACTCCTC CGTCAACGTGACTCAGGTTGGCTTTGGTAACAAC GCGACCGCTCATCAGTACCATCACCATCACCATCA CCACTAA	22

	quantitating CsgA production in biofilms via dot blot		
ampR	AmpR	ATGAGTATTCAACATTTCCGTGTCGCCCTTATTCC CTTTTTTGCGGCATTTTGCCTTCCTGTTTTTGCTC ACCCAGAAACGCTGGTGAAAGTAAAAGATGCTGA AGATCAGTTGGGTGCACGAGTGGGTTACATCGAA CTGGATCTCAACAGCGGTAAGATCCTTGAGAGTT TTCGCCCCGAAGAACGTTTTCCAATGATGAGCACT TTTAAAGTTCTGCTATGTGGCGCGGTATTATCCC GTATTGACGCCGGGCAAGAGCAACTCGGTCGCCGC ATACACTATTCTCAGAATGACTTGGTTGAGTACT CACCAGTCACAGAAAAGCATCTTACGGATGGCAT GACAGTAAGAGAATTATGCAGTGCTGCCATAACC ATGAGTGATAACACTGCGGCCAACTTACTTCTGA CAACGATCGGAGGACCGAAGGAGCTAACCGCTTT TTTGCACAACATGGGGGATCATGTAACTCGCCTT GATCGTTGGGAACCGGAGCTGAATGAAGCCATAC CAAACGACGAGCGTGACACCACGATGCCTGTAGC AATGGCAACAACGTTGCGCAAACTATTAACTGGC GAACTACTTACTCTAGCTTCCCGGCAACAATTAAT AGACTGGATGGAGGCGGATAAAGTTGCAGGACCA	[4]

		CTTCTGCGCTCGGCCCTTCCGGCTGGCTGGTTTAT TGCTGATAAATCTGGAGCCGGTGAGCGTGGGTCT CGCGGTATCATTGCAGCACTGGGGCCAGATGGTA AGCCCTCCCGTATCGTAGTTATCTACACGACGGGG AGTCAGGCAACTATGGATGAACGAAATAGACAGA TCGCTGAGATAGGTGCCTCACTGATTAAGCATTG GTAA	
cmR	CmR	ATGGAGAAAAAAATCACTGGATATACCACCGTTG ATATATCCCAATGGCATCGTAAAGAACATTTTGA GGCATTTCAGTCAGTTGCTCAATGTACCTATAAC CAGACCGTTCAGCTGGATATTACGGCCTTTTTAA AGACCGTAAAGAAAAATAAGCACAAGTTTTATCC GGCCTTTATTCACATTCTTGCCCGCCTGATGAATG CTCATCCGGAATTCCGTATGGCAATGAAAGACGG TGAGCTGGTGATATGGGATAGTGTTCACCCTTGT TACACCGTTTTCCATGAGCAAACTGAAACGTTTT CATCGCTCTGGAGTGAATACCACGACGATTTCCGG CAGTTTCTACACATATATTCGCAAGATGTGGCGT GTTACGGTGAAAACCTGGCCTATTTCCCTAAAGG GTTTATTGAGAATATGTTTTTCGTCTCAGCCAAT CCCTGGGTGAGTTTCACCAGTTTTGATTTAAACG TGGCCAATATGGACAACTTCTTCGCCCCCGTTTTC ACCATGGGCAAATATTATACGCAAGGCGACAAGG TGCTGATGCCGCTGGCGATTCAGGTTCATCATGCC	[4]

		GTCTGTGATGGCTTCCATGTCGGCAGAATGCTTA ATGAATTACAACAGTACTGCGATGAGTGGCAGGG CGGGGCGTAA	
kanR	KanR	CTCGAACCCCAGAGTCCCGCTCAGAAGAACTCGTC AAGAAGGCGATAGAAGGCGATGCGCTGCGAATCG GGAGCGGCGATACCGTAAAGCACGAGGAAGCGGT CAGCCCATTCGCCGCCAAGCTCTTCAGCAATATCA CGGGTAGCCAACGCTATGTCCTGATAGCGGTCCGC CACACCCAGCCGGCCACAGTCGATGAATCCAGAAA AGCGGCCATTTTCCACCATGATATTCGGCAAGCA GGCATCGCCATGGGTCACGACGAGATCCTCGCCGT CGGGCATGCGCGCCTTGAGCCTGGCGAACAGTTCG GCTGGCGCGAGCCCCTGATGCTCTTCGTCCAGATC ATCCTGATCGACAAGACCGGCTTCCATCCGAGTAC GTGCTCGCTCGATGCGATGTTTCGCTTGGTGGTCG AATGGGCAGGTAGCCGGATCAAGCGTATGCAGCC GCCGCATTGCATCAGCCATGATGGATACTTTCTCG GCAGGAGCAAGGTGAGATGACAGGAGATCCTGCC CCGGCACTTCGCCCAATAGCAGCCAGTCCCTTCCC GCTTCAGTGACAACGTCGAGCACAGCTGCGCAAG GAACGCCCGTCGTGGCCAGCCACGATAGCCGCGCT GCCTCGTCCTGCAGTTCATTCAGGGCACCGGACAG GTCGGTCTTGACAAAAAGAACCGGGCGCCCCTGC GCTGACAGCCGGAACACGGCGGCATCAGAGCAGC	[4]

		CGATTGTCTGTTGTGCCCAGTCATAGCCGAATAGC CTCTCCACCCAAGCGGCCGGAGAACCTGCGTGCAA TCCATCTTGTTCAATCATGCGAAACGATCCTCATC CTGTCTCTTGATCAGATCTTGATCCCCTGCGCCAT CAGATCCTTGGCGGCAAGAAAGCCATCCAGTTTA CTTTGCAGGGCTTCCCAACCTTACCAGAGGGCGCC CCAGCTGGCAATTCCG	
specR	SpecR	ATGCGCTCACGCAACTGGTCCAGAACCTTGACCGA ACGCAGCGGTGGTAACGGCGCAGTGGCGGTTTTC ATGGCTTGTTATGACTGTTTTTTTGGGGTACAGT CTATGCCTCGGGCATCCAAGCAGCAAGCGCGTTAC GCCGTGGGTCGATGTTTGATGTTATGGAGCAGCA ACGATGTTACGCAGCAGGGCAGTCGCCCTAAAAC AAAGTTAAACATCATGAGGGAAGCGGTGATCGCC GAAGTATCGACTCAACTATCAGAGGTAGTTGGCG TCATCGAGCGCCATCTCGAACCGACGTTGCTGGCC GTACATTTGTACGGCTCCGCAGTGGATGGCGGCCT GAAGCCACACAGTGATATTGATTTGCTGGTTACG GTGACCGTAAGGCTTGATGAAACAACGCGGCGAG CTTTGATCAACGACCTTTTGGAAACTTCGGCTTCC CCTGGAGAGAGCGAGATTCTCCGCGCTGTAGAAG TCACCATTGTTGTGCACGACGACATCATTCCGTGG CGTTATCCAGCTAAGCGCGAACTGCAATTTGGAG AATGGCAGCGCAATGACATTCTTGCAGGTATCTT	[4]

		CGAGCCAGCCACGATCGACATTGATCTGGCTATCT TGCTGACAAAAGCAAGAGAACATAGCGTTGCCTT GGTAGGTCCAGCGGCGGAGGAACTCTTTGATCCG GTTCCTGAACAGGATCTATTTGAGGCGCTAAATG AAACCTTAACGCTATGGAACTCGCCGCCCGACTGG GCTGGCGATGAGCGAAATGTAGTGCTTACGTTGT CCCGCATTTGGTACAGCGCAGTAACCGGCAAAAT CGCGCCGAAGGAGGTCGCTGCCGACTGGGCAATG GAGCGCCTGCCGGCCCAGTATCAGCCCGTCATACG TGAAGCTAGACAGGCTTATCTTGGACAAGAAGAA GATCGCTTGGCCTCGCGCGCAGATCAGTTGGAAG AATTTGTCCACTACGTGAAAGGCGAGATCACCAA GGTAGTCGGCAAATAA	

Supplementary Table A-2 | Plasmids used in this work.

Plasmid name	Plasmid ID	Description	Source
pE-AmpR-p(lac)-*luxI* *Designated "pSND-1" in [27]*	pSND-1	ColE1 origin, Amp resistance, p(lac) promoter, *luxI* output gene	[27]
pZA-AmpR-pL(tetO)-*gfp* *Designated "pZA11G" in [4]*	pZA11G	p15A origin, Amp resistance, pL(tetO) promoter, *gfp* output gene	[4]
pZS-CmR-pL(lacO)-*gfp* *Designated "pZS32G" in [4]*	pZS32G	pSC101 origin, Cm resistance, pL(lacO) promoter, *gfp* output gene	[4]
pZE-AmpR-rr12-pL(tetO)-*gfp*	rrjt12(11)g	ColE1 origin, Amp resistance, rr12 riboregulator, pL(tetO) promoter, *gfp* output gene	[3]

Designated "rrjt12(11)g" in [3]			
pZE-KanR-rr12y-pLuxR-*gfp* *Designated "rr12y(rii)g" in* [3]	rr12y(rii)g	ColE1 origin, Kan resistance, rr12y riboregulator, pLuxR promoter, *gfp* output gene	[3]
pZE-KanR-rr10-pL(lacO)-*mCherry* *Designated "rrjc10(22)mc" in* [3]	rrjc10(22)mc	ColE1 origin, Kan resistance, rr10 riboregulator, pL(lacO) promoter, *mCherry* output gene	[3]
pZE-AmpR-pLuxR-*lacZalpha*	pAYC001	ColE1 origin, Amp resistance, pLuxR promoter, $lacZ_{alpha}$ output gene	Gift of Jacob Rubens, Lu Lab
pZA-CmR-rr12-pL(tetO)-*csgA*	pAYC002	p15A origin, Cm resistance, rr12 riboregulator, pL(tetO) promoter, *csgA* output gene	This work

pZA-CmR-rr12-pL(tetO)-*csgA$_{His}$*	pAYC003	p15A origin, Cm resistance, rr12 riboregulator, pL(tetO) promoter, *csgA$_{His}$* output gene	This work
pZA-CmR-rr12-pL(tetO)-*mCherry*	pAYC004	p15A origin, Cm resistance, rr12 riboregulator, pL(tetO) promoter, *mCherry* output gene	This work
pZA-CmR-rr12y-pLuxR-*8XcsgA$_{His}$*	pAYC005	p15A origin, Cm resistance, rr12y riboregulator, pLuxR promoter, *8XcsgA$_{His}$* output gene	This work
pZA-CmR-rr12y-pLuxR-*csgA*	pAYC006	p15A origin, Cm resistance, rr12y riboregulator, pLuxR promoter, *csgA* output gene	This work
pZA-CmR-rr12y-pLuxR-*csgA$_{His}$*	pAYC007	p15A origin, Cm resistance, rr12y riboregulator, pLuxR promoter, *csgA$_{His}$* output gene	This work
pZA-CmR-rr12y-pLuxR-*gfp*	pAYC008	p15A origin, Cm resistance, rr12y riboregulator, pLuxR promoter, *gfp* output gene	This work
pZS-AmpR-rr10-pL(lacO)-*lacZ$_{alpha}$*	pAYC009	pSC101 origin, Cm resistance, rr12y riboregulator, pL(lacO) promoter, *lacZ$_{alpha}$* output gene	This work

pZE-AmpR-proB-*mCherry*	pAYC010	ColE1 origin, Amp resistance, proB promoter, *mCherry* output gene	Gift of Tomi Jun, Lu Lab
pZA-CmR-rr12y-pLuxR-$csgA_{SpyTag}$	pAYC011	p15A origin, Cm resistance, rr12y riboregulator, pLuxR promoter, $csgA_{SpyTag}$ output gene	This work
pZA-CmR-rr12-pL(tetO)-$csgA_{FLAG}$	pAYC012	p15A origin, Cm resistance, rr12 riboregulator, pL(tetO) promoter, $csgA_{FLAG}$ output gene	This work
pZS-CmR-pL(lacO)-$csgA_{ZnS\ peptide}$	pAYC013	pSC101 origin, Cm resistance, pL(lacO) promoter, $csgA_{ZnS\ peptide}$ output gene	This work
pZS-CmR-pL(lacO)-*csgA*	pAYC014	pSC101 origin, Cm resistance, pL(lacO) promoter, $csgA_{ZnS}$ output gene	This work
pZS-CmR-pL(lacO)-$csgA_{His\ after\ C\text{-}terminus}$	pAYC015	pSC101 origin, Cm resistance, pL(lacO) promoter, $csgA_{His\ after\ R5}$ output gene	This work
pDEST14-T7-*CCSpyCatcher*	pAYC016	pBR322 origin, Amp resistance, T7 promoter, *CCSpyCatcher* output gene	This work
pET11d-T7-	pAYC017	pBR322 origin, Amp resistance, T7	Gift of Chao

c*sgA$_{His}$noSS*		promoter, *csgA$_{His}$noSS* output gene	Zhong, Lu Lab
pZS4Int-*lacI/tetR*	pAYC018	pSC101 origin, PRO cassette (P_{laci^q}/*lacI*, P_{N25}/*tetR*, $Spec^R$)	Expressys

Supplementary Table A-3 | Cell strains used in this work.

Strain name	Strain ID	Description	Antibiotic resistance*	Source
MG1655 *ompR234* *Referred to as "ompR234" in figures*	MG1655 *ompR234*	*E. coli* strain with *ompR234* mutation that confers ability to produce curli fibrils in liquid M63 minimal media.	Kan	[9]
BW25113 *ΔcsgA::aph*	BW25113 *ΔcsgA::aph*	*E. coli* strain with *csgA* knock-out achieved by replacement with kanamycin resistance cassette (*aph*).	Kan	[6]
BW25113 *ΔcsgA*	fAYC001	*E. coli* strain with *csgA* knocked out	N/A	This work
BL21 DE3 pLysS	BL21 DE3 *pLysS*	*E.coli* strain for inducible protein expression	Cm	Stratagene
MG1655 *PRO ΔcsgA ompR234* *Referred to as "ΔcsgA*	fAYC002	*E. coli* strain with constitutive high level expression of *tetR* and	Spec, Kan	This work

* Kanamycin (Kan), Spectinomycin (Spec), Chloramphenicol (Cm), Ampicillin (Amp)

ompR234" in figures		*lacI* from *PRO* cassette derived from pZS4Int-*lacI/tetR*, with *csgA* knocked out, and with *ompR234* mutation that confers ability to produce curli fibrils in liquid M63 minimal media.		
$aTc_{Receiver}$/$CsgA_{His}$	fAYC003	*E. coli* strain that expresses $CsgA_{His}$ under tight regulation by an anhydrotetracycline (aTc) inducer-responsive riboregulator. Made by transforming pZA-CmR-rr12-pL(tetO)-$csgA_{His}$ plasmid into MG1655 *PRO ΔcsgA ompR234*.	Spec, Kan, Cm	This work
$AHL_{Receiver}$/CsgA	fAYC004	*E. coli* strain that expresses CsgA under tight regulation by an acyl-homoserine lactone	Spec, Kan, Cm	This work

		(AHL) inducer-responsive riboregulator. Made by transforming pZA-CmR-rr12y-pLuxR-*csgA* plasmid into MG1655 *PRO ΔcsgA ompR234*.		
AHL_{Sender} + $aTc_{Receiver}$/CsgA	fAYC005	*E. coli* strain that constitutively produces AHL at a low basal level and inducibly expresses CsgA under tight regulation by an aTc inducer-responsive riboregulator. Made by co-transforming pZA-CmR-rr12-pL(tetO)-*csgA* and pE-AmpR-p(lac)-*luxI* into MG1655 *PRO ΔcsgA ompR234*.	Spec, Kan, Cm, Amp	This work
$AHL_{Receiver}$/$CsgA_{His}$	fAYC006	*E. coli* strain that expresses $CsgA_{His}$ under tight regulation by an AHL inducer-responsive	Spec, Kan, Cm, Amp	This work

		riboregulator. Made by co-transforming pZA-CmR-rr12y-pLuxR-*csgA*$_{His}$ and pZS-AmpR-rr10-pL(lacO)-*lacZ*$_{alpha}$ into MG1655 *PRO ΔcsgA ompR234*.		
AHL$_{Receiver}$/8XCsgA$_{His}$	fAYC007	*E. coli* strain that expresses 8XCsgA$_{His}$ under tight regulation by an AHL inducer-responsive riboregulator. Made by transforming pZA-CmR-rr12y-pLuxR-*8XcsgA*$_{His}$ into MG1655 *PRO ΔcsgA ompR234*.	Spec, Kan, Cm	This work
aTc$_{CReceiver}$/CsgA	fAYC008	*E. coli* strain that expresses CsgA under tight regulation by an anhydrotetracycline (aTc) inducer-responsive riboregulator. Made by	Spec, Kan, Cm	This work

		transforming pZA-CmR-rr12-pL(tetO)-*csgA* plasmid into MG1655 *PRO ΔcsgA ompR234*.		
aTc$_{Receiver}$/mCherry	fAYC009	*E. coli* strain that expresses mCherry under tight regulation by an anhydrotetracycline (aTc) inducer-responsive riboregulator. Made by transforming pZA-CmR-rr12-pL(tetO)-*mCherry* plasmid into MG1655 *PRO ΔcsgA ompR234*.	Spec, Kan, Cm	This work
AHL$_{Receiver}$/GFP	fAYC010	*E. coli* strain that expresses GFP under tight regulation by an acyl-homoserine lactone (AHL) inducer-responsive riboregulator. Made by transforming pZA-CmR-rr12y-pLuxR-*gfp*	Spec, Kan, Cm	This work

		plasmid into MG1655 *PRO ΔcsgA ompR234*.		
mCherry+ $aTc_{Receiver}/CsgA_{His}$	fAYC011	*E. coli* strain that expresses $CsgA_{His}$ under tight regulation by an anhydrotetracycline (aTc) inducer-responsive riboregulator, and constitutively expresses mCherry. Made by co-transforming pZE-AmpR-proB-*mCherry* and pZA-CmR-rr12-pL(tetO)-$csgA_{His}$ into MG1655 *PRO ΔcsgA ompR234*.	Spec, Kan, Cm, Amp	This work
MG1655 *ompR234* / pZE-AmpR-proB-*mCherry*	fAYC012	*E. coli* strain that expresses CsgA under control of native curli operon, and constitutively expresses mCherry. Made by transforming pZE-	Spec, Kan, Amp	This work

		AmpR-proB-*mCherry* plasmid into MG1655 *ompR234*.		
MG1655 PRO Δ*csgA ompR234* / pZE-AmpR-proB-*mCherry*	fAYC013	*E. coli* strain that constitutively expresses mCherry. Made by transforming pZE-AmpR-proB-*mCherry* plasmid into MG1655 *PRO ΔcsgA ompR234*.	Spec, Kan, Amp	This work
$AHL_{Receiver}$/$CsgA_{SpyTag}$	fAYC014	*E. coli* strain that expresses $CsgA_{SpyTag}$ under tight regulation by an AHL inducer-responsive riboregulator. Made by transforming pZA-CmR-rr12y-pLuxR-$csgA_{SpyTag}$ into MG1655 *PRO ΔcsgA ompR234*.	Spec, Kan, Cm	This work
$aTc_{Receiver}$/$CsgA_{FLAG}$	fAYC015	*E. coli* strain that expresses $CsgA_{FLAG}$ under tight regulation by	Spec, Kan, Cm	This work

		an anhydrotetracycline (aTc) inducer-responsive riboregulator. Made by transforming pZA-CmR-rr12-pL(tetO)-*csgA*$_{FLAG}$ plasmid into MG1655 *PRO ΔcsgA ompR234*.		
BL21 DE3 pLysS / pDEST14-T7-*CCSpyCatcher*	fAYC016	*E. coli* strain that expresses CCSpyCatcher when induced by IPTG. Made by transforming pDEST14-T7-*CCSpyCatcher* into BL21 DE3 pLysS.	Cm, Amp	This work
BL21 T7 Express I^q / pET11d-T7-*csgA*$_{His}$*noSS*	fAYC017	*E. coli* strain that expresses CsgA$_{His}$noSS when induced by IPTG. Made by transforming pET11d-T7-*csgA*$_{His}$*noSS* into BL21 T7 Express I^q.	Cm, Amp	Gift of Chao Zhong, Lu Lab
BW25113 *ΔcsgA* / pZS-CmR-pL(lacO)-	fAYC018	*E. coli* strain that expresses CsgA under	Kan, Cm, Spec	This work

csgA + pZS4Int-*lacI/tetR*		control of pL(lacO) promoter, along with constitutive expression of lacI and tetR. Made by co-transforming pZS-CmR-pL(lacO)-*csgA* and pZS4Int-*lacI/tetR* into BW25113 *ΔcsgA*.		
BW25113 *ΔcsgA* / pZS-CmR-pL(lacO)-$csgA_{ZnS\ peptide}$ (also referred to as "*csgA*/$CsgA_{ZnS\ peptide}$")	fAYC019	*E. coli* strain that expresses $CsgA_{ZnS\ peptide}$ under control of pL(lacO) promoter. Made by transforming pZS-CmR-pL(lacO)-$csgA_{ZnS\ peptide}$ into BW25113 *ΔcsgA*.	Kan, Cm	This work

BW25113 *ΔcsgA* / pZS-CmR-pL(lacO)-*csgA* (also referred to as "*csgA*/CsgA")	fAYC020	*E. coli* strain that expresses CsgA under control of pL(lacO) promoter. Made by transforming pZS-CmR-pL(lacO)-*csgA* into BW25113 *ΔcsgA*.	Kan, Cm	This work
BW25113 *ΔcsgA* / pZS-CmR-pL(lacO)-$csgA_{His\ after\ C\text{-}terminus}$	fAYC021	*E. coli* strain that expresses $CsgA_{His\ after\ R5}$ under control of pL(lacO) promoter. Made by transforming pZS-CmR-pL(lacO)-$csgA_{His\ after\ R5}$ into BW25113 *ΔcsgA*.	Kan, Cm	This work

References

1 Chapman, M. R. *et al.* Role of Escherichia coli curli operons in directing amyloid fiber formation. *Science* **295**, 851-855, doi:10.1126/science.1067484295/5556/851 [pii] (2002).

2 Sambrook, J., Fritsch, E.F. & Maniatis, T. *Molecular cloning: a laboratory manual.*, (Cold Spring Laboratory Press 2, 1989).

3 Callura, J. M., Cantor, C. R. & Collins, J. J. Genetic switchboard for synthetic biology applications. *Proceedings of the National Academy of Sciences of the United States of America* **109**, 5850-5855, doi:10.1073/pnas.1203808109 (2012).

4 Lutz, R. & Bujard, H. Independent and tight regulation of transcriptional units in Escherichia coli via the LacR/O, the TetR/O and AraC/I1-I2 regulatory elements. *Nucleic Acids Res* **25**, 1203-1210, doi:gka167 [pii] (1997).

5 Zakeri, B. *et al.* Peptide tag forming a rapid covalent bond to a protein, through engineering a bacterial adhesin. *Proceedings of the National Academy of Sciences of the United States of America* **109**, E690-697, doi:10.1073/pnas.1115485109 (2012).

6 Baba, T. *et al.* Construction of Escherichia coli K-12 in-frame, single-gene knockout mutants: the Keio collection. *Mol Syst Biol* **2**, 2006 0008, doi:msb4100050 [pii]10.1038/msb4100050 (2006).

7 Datsenko, K. A. & Wanner, B. L. One-step inactivation of chromosomal genes in Escherichia coli K-12 using PCR products. *Proc Natl Acad Sci U S A* **97**, 6640-6645, doi:10.1073/pnas.120163297120163297 [pii] (2000).

8 Cherepanov, P. P. & Wackernagel, W. Gene disruption in Escherichia coli: TcR and KmR cassettes with the option of Flp-catalyzed excision of the antibiotic-resistance determinant. *Gene* **158**, 9-14 (1995).

9 Prigent-Combaret, C. *et al.* Complex regulatory network controls initial adhesion and biofilm formation in Escherichia coli via regulation of the csgD gene. *Journal of bacteriology* **183**, 7213-7223 (2001).

10 Prigent-Combaret, C. *et al.* Developmental pathway for biofilm formation in curli-producing Escherichia coli strains: role of flagella, curli and colanic acid. *Environmental microbiology* **2**, 450-464 (2000).

11 Schneider, C. A., Rasband, W. S. & Eliceiri, K. W. NIH Image to ImageJ: 25 years of image analysis. *Nature methods* **9**, 671-675 (2012).

12 Heydorn, A. *et al.* Quantification of biofilm structures by the novel computer program COMSTAT. *Microbiology* **146 (Pt 10)**, 2395-2407 (2000).

13 Collinson, S. K., Emody, L., Muller, K. H., Trust, T. J. & Kay, W. W. Purification and characterization of thin, aggregative fimbriae from Salmonella enteritidis. *Journal of bacteriology* **173**, 4773-4781 (1991).

14 Hung, C. *et al.* Escherichia coli biofilms have an organized and complex extracellular matrix structure. *mBio* **4**, e00645-00613, doi:10.1128/mBio.00645-13 (2013).

15 Wang, X., Hammer, N. D. & Chapman, M. R. The molecular basis of functional bacterial amyloid polymerization and nucleation. *The Journal of biological chemistry* **283**, 21530-21539, doi:10.1074/jbc.M800466200 (2008).

16 O'Toole, G. A. Microtiter dish biofilm formation assay. *Journal of visualized experiments : JoVE*, doi:10.3791/2437 (2011).

17 Zhou, Y., Smith, D. R., Hufnagel, D. A. & Chapman, M. R. Experimental manipulation of the microbial functional amyloid called curli. *Methods Mol Biol* **966**, 53-75, doi:10.1007/978-1-62703-245-2_4 (2013).

18 Ishiguro, E. E., Ainsworth, T., Trust, T. J. & Kay, W. W. Congo red agar, a differential medium for Aeromonas salmonicida, detects the presence of the cell surface protein array involved in virulence. *Journal of bacteriology* **164**, 1233-1237 (1985).

19 Weinberg, E. D. Double-gradient agar plates. *Science* **125**, 196 (1957).

20 Deng, Z. *et al.* Aqueous synthesis of zinc blende CdTe/CdS magic-core/thick-shell tetrahedral-shaped nanocrystals with emission tunable to near-infrared. *Journal of the American Chemical Society* **132**, 5592-5593, doi:10.1021/ja101476b (2010).

21 Mao, C. *et al.* Viral assembly of oriented quantum dot nanowires. *Proceedings of the National Academy of Sciences of the United States of America* **100**, 6946-6951, doi:10.1073/pnas.0832310100 (2003).

22 Zhong, C., Gurry, T., Cheng, A., Downey, J., Stultz, C.M. & Lu, T.K. Biologically Inspired Engineering of Strong, Self-Assembling, and Multi-Functional Underwater Adhesives with Synthetic Biology. *In review*.

23 Wang, X., Smith, D. R., Jones, J. W. & Chapman, M. R. In vitro polymerization of a functional Escherichia coli amyloid protein. *The Journal of biological chemistry* **282**, 3713-3719, doi:10.1074/jbc.M609228200 (2007).

24 Romero, D., Aguilar, C., Losick, R. & Kolter, R. Amyloid fibers provide structural integrity to Bacillus subtilis biofilms. *Proceedings of the National Academy of Sciences of the United States of America* **107**, 2230-2234, doi:10.1073/pnas.0910560107 (2010).

25 Bieschke, J. *et al.* Small-molecule conversion of toxic oligomers to nontoxic beta-sheet-rich amyloid fibrils. *Nature chemical biology* **8**, 93-101, doi:10.1038/nchembio.719 (2012).

26 Robinson, L. S., Ashman, E. M., Hultgren, S. J. & Chapman, M. R. Secretion of curli fibre subunits is mediated by the outer membrane-localized CsgG protein. *Molecular microbiology* **59**, 870-881, doi:10.1111/j.1365-2958.2005.04997.x (2006).

27 Basu, S., Gerchman, Y., Collins, C. H., Arnold, F. H. & Weiss, R. A synthetic multicellular system for programmed pattern formation. *Nature* **434**, 1130-1134, doi:nature03461 [pii]10.1038/nature03461 (2005).

28 Schweizer, H. P. & Hoang, T. T. An improved system for gene replacement and xylE fusion analysis in Pseudomonas aeruginosa. *Gene* **158**, 15-22 (1995).